

Jet-veto resummation at N^3LL_p +NNLO in boson production processes

John M. Campbell,^a R. Keith Ellis,^b Tobias Neumann,^c Satyajit Seth^d

^a*Fermilab, PO Box 500, Batavia IL 60510-5011, USA*

^b*Institute for Particle Physics Phenomenology, Durham University, Durham, DH1 3LE, UK*

^c*Department of Physics, Brookhaven National Laboratory, Upton, New York 11973, USA*

^d*Physical Research Laboratory, Navrangpura, Ahmedabad - 380009, India*

E-mail: johnmc@fnal.gov, keith.ellis@durham.ac.uk, tneumann@bnl.gov,
seth@prl.res.in

ABSTRACT: Vetoing energetic jet activity is a crucial tool for suppressing backgrounds and enabling new physics searches at the LHC, but the introduction of a veto scale can introduce large logarithms that may need to be resummed. We present an implementation of jet-veto resummation for color-singlet processes at the level of N^3LL_p matched to fixed-order NNLO predictions. Our public code MCFM allows for predictions of a single boson, such as Z/γ^* , W^\pm or H , or with a pair of vector bosons, such as W^+W^- , $W^\pm Z$ or ZZ . The implementation relies on recent calculations of the soft and beam functions in the presence of a jet veto over all rapidities, with jets defined using a sequential recombination algorithm with jet radius R . However one of the ingredients that is required to reach full N^3LL accuracy is only known approximately, hence N^3LL_p . We describe in detail our formalism and compare with previous public codes that operate at the level of NNLL. Our higher-order predictions improve significantly upon NNLL calculations by reducing theoretical uncertainties. We demonstrate this by comparing our predictions with ATLAS and CMS results.

Contents

1	Introduction	1
2	Jet-veto factorization and resummation	2
2.1	The collinear anomaly coefficient and its approximations	5
3	Setup for phenomenology	9
3.1	Input parameters	9
3.2	Uncertainty estimates at fixed order	10
3.3	Uncertainty estimates at the resummed and matched level	11
3.4	Effects of cuts on rapidity at fixed order	13
4	Comparison with JetVHeto	15
5	Phenomenological results	17
5.1	Z and W production	17
5.2	W^+W^- production	21
5.3	$W^\pm Z$ production	24
5.4	ZZ production	25
5.5	Higgs production	27
6	Conclusions	28
A	Reduced beam functions	30
A.1	Structure of the two-loop reduced beam function	32
B	Definition of the beta function and anomalous dimensions	33
B.1	Expansion of β -function	33
B.2	Cusp Anomalous Dimension	35
B.3	Non-cusp anomalous dimension	36
C	Definitions for beam function ingredients	38
C.1	Exponent h	38
C.2	One loop splitting functions	39
C.3	Two loop splitting functions	39
C.4	$P^{(1)} \otimes P^{(1)}$ and $R^{(1)} \otimes P^{(1)}$	42
D	Rapidity anomalous dimension	43
D.1	d_2^{veto} expansion	44
E	Renormalization Group Evolution	45

E.1	Recovery of the double log formula	46
F	The hard function for the Drell-Yan process	47
G	The hard function for Higgs production	49
G.1	Implementation of one-step procedure	49
G.2	Implementation of the two-step procedure	51
G.3	Assessment of the two schemes for the Higgs hard function	53

1 Introduction

Jet vetoing is a crucial technique in particle physics that is used primarily to suppress backgrounds in processes involving the production of W^+W^- final states (e.g. directly or in Higgs decays). By identifying and removing events that contain energetic hadronic jets (vetoing), the impact of the dominant top-quark pair production background is reduced. The concrete jet-veto implementation depends on factors such as the jet algorithm and its parameters, as well as the kinematic selection cuts applied to the identified jets. For LHC analyses, the most common jet vetoing scheme is to impose a maximum transverse momentum cut p_T^{veto} on anti- k_T jets.

The jet veto scale p_T^{veto} can induce large logarithms if it is smaller than the hard process scale Q , which then mandates resummation. In this paper we describe a coherent implementation of jet veto resummation in processes involving the production of a color-singlet boson ($W, Z/\gamma^*$ and H bosons) or a pair of bosons ($ZZ, W^\pm Z$, and W^+W^-). Our resummation operates at the level of N^3LL_p ¹ matched to fixed order NNLO.

We build on the pioneering work of previous studies, which have demonstrated the effectiveness of resummation methods for a jet veto [1–5]. General purpose implementations include a numerical approach to resummation at NNLO+NNLL [6, 7] and an automated approach to jet veto studies at NLO+NNLL [8]. Publicly available codes operating at NNLL and addressing the same issue are, JetVHeto [9], the code MCFM-RE [10] which is derivative of both MCFM and JetVHeto, and MATRIX+RadISH [11]. Both JetVHeto and RadISH implement the same analytic resummation formula of ref. [5].

Our research extends and improves upon these earlier results through detailed phenomenological studies of specific final states, including Higgs boson production [5, 12–14], W^+W^- production [15, 16], and ZZ and $W^\pm Z$ production [17]. Another important aspect of our study is the performance of the resummation at N^3LL_p accuracy, which has not always been the case in

¹The last missing ingredient for N^3LL resummation is the exact d_3^{veto} (the three-loop rapidity anomalous dimension) which we approximate and take into account with an uncertainty estimate. We discuss this in detail in the subsequent section.

previous work. We also describe our approximation of the missing d_3^{veto} that would be necessary to reach full N³LL accuracy. Finally, we include our results in MCFM, a publicly distributed code, which allows users to easily perform studies in practice.

Resummation of jet-veto logarithms has a close relationship with the resummation of transverse momentum logarithms. In the latter, one is interested in transverse momenta all the way down to zero p_T , so the logarithms can be larger than in jet-veto processes where p_T^{veto} in the range 25 to 30 GeV is used experimentally. In this paper we explore which jet-veto processes actually require resummation at these values of p_T^{veto} , supply the best predictions for those processes where it is warranted, and confront our theoretical predictions with experimental data where it is available.

In Section 2 we discuss the jet-veto factorization theorem including its ingredients that result in the resummation. We describe our setup for phenomenology including our uncertainty procedure in Section 3, compare with the public code JetVHeto in Section 4, and study the phenomenological implications for a wide range of processes in Section 5. We conclude in Section 6.

2 Jet-veto factorization and resummation

We consider processes where jets have been defined using sequential recombination jet algorithms [18] with distance measure

$$d_{ij} = \min(k_{Ti}^{2n}, k_{Tj}^{2n}) \frac{\Delta y_{ij}^2 + \Delta \phi_{ij}^2}{R^2}, \quad d_{iB} = k_{Ti}^{2n}, \quad (2.1)$$

where the choice $n = -1$ is the anti- k_T algorithm [19], $n = 0$ is the Cambridge-Aachen algorithm [20, 21], and $n = 1$ is the k_T algorithm [22, 23]. k_{Ti} denotes the transverse momentum of (pseudo-)particle i with respect to the beam direction, and Δy_{ij} and $\Delta \phi_{ij}$ are the rapidity and azimuthal angle differences of (pseudo-)particles i and j .

To describe the resummation method we focus on the simplest case of quark-antiquark induced Drell-Yan production of a lepton pair of invariant mass Q and rapidity y . The case of gluon initiated processes is structurally the same, but with different ingredients that we give below and in the appendices. In the presence of a jet veto over all rapidities we have a factorization formula [3, 12, 13],

$$\begin{aligned} \frac{d^2 \sigma(p_T^{\text{veto}})}{dQ^2 dy} &= \frac{d\sigma_0}{dQ^2} |C^V(-Q^2, \mu)|^2 \\ &\times \left[\mathcal{B}_q(\xi_1, Q, p_T^{\text{veto}}, R, \mu, \nu) \mathcal{B}_{\bar{q}}(\xi_2, Q, p_T^{\text{veto}}, R, \mu, \nu) \mathcal{S}(p_T^{\text{veto}}, R, \mu, \nu) \right] + \mathcal{O}\left(\frac{p_T^{\text{veto}}}{Q}\right) \end{aligned} \quad (2.2)$$

where $\xi_{1,2} = (Q/\sqrt{s}) e^{\pm y}$ and,

$$\frac{d\sigma_0}{dQ^2} = \frac{4\pi\alpha^2}{3N_c Q^2 s}. \quad (2.3)$$

Table 1: Counting of orders in the resummation, adapted from ref. [26]. The second column indicates the nominal order when counting $L_\perp \sim 1/\alpha_s$. The third column states which logarithms are included. The last three columns show the necessary additional anomalous dimensions and hard function corrections in each successive order. The requisite anomalous dimensions are provided in Appendix B.

Approximation	Nominal order	Accuracy $\sim \alpha_s^n L_\perp^k$	Γ_{cusp}	$\gamma_{\text{coll.}}$	H
LL	α_s^{-1}	$2n \geq k \geq n + 1$	Γ_0	tree	tree
NLL+LO	α_s^0	$2n \geq k \geq n$	Γ_1 ,	γ_0	tree
N ² LL+NLO	α_s^1	$2n \geq k \geq \max(n - 1, 0)$	Γ_2	γ_1	1-loop
N ³ LL + NNLO	α_s^2	$2n \geq k \geq \max(n - 2, 0)$	Γ_3	γ_2	2-loop

In this equation C^V is a matching coefficient whose square is the hard coefficient function that corrects the lowest order cross-section, see Eq. (2.3). \mathcal{B}_q and $\mathcal{B}_{\bar{q}}$ are the quark beam functions which describe the emission of radiation collinear to the two beam directions in the presence of a jet veto, and \mathcal{S} describes the emission of soft radiation in the presence of a jet veto. The quantity ν is a supplementary scale necessitated by the rapidity divergences present in beam and soft functions. The main process-independent ingredients are the beam and soft functions for both incoming quarks and gluons which have been published recently at the two-loop level [24, 25]. The hard function is process specific. We have used the existing two-loop fixed order implementations in MCFM.

Overall the factorization theorem achieves a separation of scales. The hard function contains logarithms of the ratio Q^2/μ^2 , which can be minimized by setting $\mu^2 = \mu_h^2 \sim Q^2$. However, inside the beam and soft functions, it is natural to choose $\mu = p_T^{\text{veto}}$ to avoid large logarithms. The resummation of large logarithms is achieved by choosing $\mu \sim Q$ in the hard function and evolving it down to the resummation scale $\mu \sim p_T^{\text{veto}}$ using the renormalization group (RG). For the hard function the evolution is solved analytically, see Appendix E.

In RG-improved power counting the logarithms $L_\perp = 2 \log(\mu_h/p_T^{\text{veto}})$, where μ_h is of order Q , are assumed to be of order $1/\alpha_s$. With this definition the counting of powers of α_s and of the large logarithm L_\perp is shown in Table 1. The non-logarithmic terms that the resummation does not provide are easily accounted for by adding the matching corrections. The matching corrections are a finite contribution and add the effect of fixed-order corrections while removing the logarithmic overlap through a fixed-order expansion of the resummation.

2.0.1 Soft function

The jet veto soft function has been calculated using an exponential regulator [27] in Ref. [25]. The calculation is divided into the sum of the soft function for a reference observable and a correction factor,

$$S(p_T^{\text{veto}}, R, \mu, \nu) = S_\perp(p_T^{\text{veto}}, \mu, \nu) + \Delta S(p_T^{\text{veto}}, R, \mu, \nu). \quad (2.4)$$

In Ref. [25] the reference observable is the transverse momentum of the color singlet system denoted by S_\perp . S_\perp can be derived from the expression given in Refs. [28, 29] after performing the Fourier transform to momentum space (see, for instance, the rules given in Table 1 of Ref. [30]). ΔS depends on the jet algorithm and contributes for two or more emissions. It thus depends only on double real emission diagrams.

2.0.2 Refactorization and reduced beam functions

For consistency with the transverse momentum resummation framework in CuTe-MCFM [31] we cast the factorization theorem in terms of the collinear anomaly framework. In this framework the rapidity logarithms are exponentiated directly instead of resummed by solving rapidity RG equations [32, 33]. For this we rewrite the square bracket in Eq. (2.2) as follows,

$$\begin{aligned} & \mathcal{B}_q(\xi_1, Q, p_T^{\text{veto}}, R, \mu, \nu) \mathcal{B}_{\bar{q}}(\xi_2, Q, p_T^{\text{veto}}, R, \mu, \nu) \mathcal{S}(p_T^{\text{veto}}, R, \mu, \nu) \\ &= \left(\frac{Q}{p_T^{\text{veto}}} \right)^{-2F_{qq}(p_T^{\text{veto}}, R, \mu)} e^{2h^F(p_T^{\text{veto}}, \mu)} \bar{B}_q(\xi_1, p_T^{\text{veto}}, R, \mu) \bar{B}_{\bar{q}}(\xi_2, p_T^{\text{veto}}, R, \mu). \end{aligned} \quad (2.5)$$

The ν dependence vanishes in this combination of beam and soft functions.

We have factored out $e^{h^{F/A}(p_T^{\text{veto}}, \mu)}$ from each beam function, resulting in the reduced beam functions \bar{B} . By construction $h^{F/A}$ are solutions of the RGE equation,

$$\frac{d}{d \ln \mu} h^{F/A}(p_T^{\text{veto}}, \mu) = 2\Gamma_{\text{cusp}}^{F/A}(\mu) \ln \frac{\mu}{p_T^{\text{veto}}} - 2\gamma^{q/g}(\mu), \quad (2.6)$$

with boundary condition $h^{F/A}(\mu, \mu) = 0$. The superscripts F or A signify whether the color is treated in the fundamental (F) or adjoint (A) representation, corresponding to a quark initiated process or a gluon initiated process, respectively. The exact form of $h^{F/A}(p_T^{\text{veto}}, \mu)$, determined by solving Eq. (2.6), is given in Appendix C.1. In terms of the reduced beam functions the jet-vetoed cross-section is now given by,

$$\frac{d^2 \sigma(p_T^{\text{veto}})}{dQ^2 dy} = \frac{d\sigma_0}{dQ^2} \bar{H}(Q, \mu, p_T^{\text{veto}}) \bar{B}_q(\xi_1, p_T^{\text{veto}}, R, \mu) \bar{B}_{\bar{q}}(\xi_2, p_T^{\text{veto}}, R, \mu) + \mathcal{O}(p_T^{\text{veto}}/Q), \quad (2.7)$$

The choice of $h^{F/A}$ in Eq. (2.6) divides Eq. (2.2) into two separately RG invariant pieces, the product of the two reduced beam functions ($\bar{B}_q \bar{B}_{\bar{q}}$), and the hard function, (\bar{H})

$$\bar{H}(Q, \mu, p_T^{\text{veto}}) = |C^V(-Q^2, \mu)|^2 \left(\frac{Q}{p_T^{\text{veto}}} \right)^{-2F_{qq}(p_T^{\text{veto}}, R, \mu)} e^{2h^F(p_T^{\text{veto}}, \mu)}. \quad (2.8)$$

For quark-initiated processes the functions C^V and F_{qq} obey the following RG equations.

$$\frac{d}{d \ln \mu} C^V(-Q^2, \mu) = \left[\Gamma_{\text{cusp}}^F(\mu) \ln \frac{-Q^2}{\mu^2} + 2\gamma^q(\mu) \right] C^V(-Q^2, \mu), \quad (2.9)$$

$$\frac{d}{d \ln \mu} F_{qq}(p_T^{\text{veto}}, R, \mu) = 2\Gamma_{\text{cusp}}^F(\mu). \quad (2.10)$$

Eqs. (2.9) and (2.10) are structurally the same for the gluon case with different anomalous dimensions.

The function \bar{H} is RG invariant due to the RGE's satisfied by C^V and F_{qq} and h_F :

$$\frac{d}{d\mu}\bar{H}(Q, \mu, p_T^{\text{veto}}) = \mathcal{O}(\alpha_s^3).$$

Consequently, the remaining product of reduced beam functions is also RG invariant, up to the order calculated. In our case,

$$\frac{d}{d\mu}\bar{B}_q(\xi_1, p_T^{\text{veto}}, R, \mu) \bar{B}_{\bar{q}}(\xi_2, p_T^{\text{veto}}, R, \mu) = \mathcal{O}(\alpha_s^3). \quad (2.11)$$

The confirmation of Eq. (2.11) and the confirmation of the R -dependence of the collinear anomaly given in the next section are two simple checks of the results of Refs. [24, 25]. Full details of the formulas needed to perform this check are given in Appendix C.

If the scale p_T^{veto} is in the perturbative domain, the reduced beam function can be written in terms of the matching kernels \bar{I} as

$$\bar{B}_i(\xi, p_T^{\text{veto}}, R, \mu) = \sum_{j=g,q,\bar{q}} \int_{\xi}^1 \frac{dz}{z} \bar{I}_{ij}(z, p_T^{\text{veto}}, R, \mu) \phi_{j/P}(\xi/z, \mu),$$

where ϕ denotes the usual collinear parton distribution of a parton of flavor j in a proton P . The matching coefficients \bar{I} are extracted from I , the two-loop beam and soft functions of Refs. [24, 25] as,

$$\bar{I}_{ij}(z, p_T^{\text{veto}}, R, \mu) = e^{-h^{F/A}(p_T^{\text{veto}}, \mu)} I_{ij}(z, p_T^{\text{veto}}, R, \mu). \quad (2.12)$$

The coefficients in Ref. [24] are presented as a Laurent expansion in the jet radius parameter R . Analytic expressions are presented for all flavor channels except for a set of R -independent non-logarithmic terms which are presented as numerical grids. For our purposes we have interpolated the numerical grids using a spline fit. We give further details on the reduced beam functions in Appendix A.

2.1 The collinear anomaly coefficient and its approximations

The missing ingredient for a complete N³LL resummation is the three-loop collinear anomaly coefficient and therefore warrants a longer discussion. This limitation has been discussed in the literature and approximated in various ways. Here we discuss the uncertainty associated with the approximations and how we take it into account in our phenomenological predictions.

As presented in Eq. (2.10) the collinear anomaly coefficients obey the RG equations,

$$\frac{d}{d\ln\mu} F_{qq}(p_T^{\text{veto}}, R, \mu) = 2\Gamma_{\text{cusp}}^F(\mu), \quad (2.13)$$

$$\frac{d}{d\ln\mu} F_{gg}(p_T^{\text{veto}}, R, \mu) = 2\Gamma_{\text{cusp}}^A(\mu), \quad (2.14)$$

where, for example, F_{qq} has the expansion,

$$\begin{aligned}
F_{qq}(p_T^{\text{veto}}, R, \mu) &= \frac{\alpha_s}{4\pi} F_{qq}^{(0)}(p_T^{\text{veto}}, R, \mu) + \left(\frac{\alpha_s}{4\pi}\right)^2 F_{qq}^{(1)}(p_T^{\text{veto}}, R, \mu) \\
&+ \left(\frac{\alpha_s}{4\pi}\right)^3 F_{qq}^{(2)}(p_T^{\text{veto}}, R, \mu) + \left(\frac{\alpha_s}{4\pi}\right)^4 F_{qq}^{(3)}(p_T^{\text{veto}}, R, \mu) + \dots
\end{aligned} \tag{2.15}$$

While the logarithmic structure is given by the RG equations, the constant boundary parts $d_k^{\text{veto}}(R, B)$ where $B = F$ or A need to be determined by separate calculations and are also referred to as the rapidity anomalous dimensions in the framework of Refs. [32, 33]:

$$\begin{aligned}
F_{qq}^{(0)}(p_T^{\text{veto}}, R, \mu_h) &= \Gamma_0^F L_\perp + d_1^{\text{veto}}(R, F), \\
F_{qq}^{(1)}(p_T^{\text{veto}}, R, \mu_h) &= \frac{1}{2} \Gamma_0^F \beta_0 L_\perp^2 + \Gamma_1^F L_\perp + d_2^{\text{veto}}(R, F), \\
F_{qq}^{(2)}(p_T^{\text{veto}}, R, \mu_h) &= \frac{1}{3} \Gamma_0^F \beta_0^2 L_\perp^3 + \frac{1}{2} (\Gamma_0^F \beta_1 + 2\Gamma_1^F \beta_0) L_\perp^2 \\
&+ (\Gamma_2^F + 2\beta_0 d_2^{\text{veto}}(R, F)) L_\perp + d_3^{\text{veto}}(R, F), \\
F_{qq}^{(3)}(p_T^{\text{veto}}, R, \mu_h) &= \frac{1}{4} \beta_0^3 \Gamma_0^F L_\perp^4 + (\Gamma_1^F \beta_0^2 + \frac{5}{6} \Gamma_0^F \beta_0 \beta_1) L_\perp^3 \\
&+ (\frac{1}{2} \Gamma_0^F \beta_2 + \Gamma_1^F \beta_1 + \frac{3}{2} \Gamma_2^F \beta_0 + 3d_2^{\text{veto}}(R, F) \beta_0^2) L_\perp^2 \\
&+ (\Gamma_3^F + 3d_3^{\text{veto}}(R, F) \beta_0 + 2d_2^{\text{veto}}(R, F) \beta_1) L_\perp + d_4^{\text{veto}}(R, F).
\end{aligned} \tag{2.16}$$

The analogous expression for gluons ($F \rightarrow A$) is given in Eq. (D.1). The coefficients in the expansion of the cusp anomalous dimension, Γ_k^F , are given in Appendix B.2.

For single gluon emission $d_1^{\text{veto}}(R, B) = 0$. The function d_2^{veto} is defined below in Eq. (2.17). There is only partial information on d_3^{veto} from Refs. [14, 34, 35], and we have to rely on an approximation. To estimate the validity of this approximation we first study similar approximations of d_2^{veto} .

The function d_2^{veto} is given by [12],

$$\begin{aligned}
d_2^{\text{veto}}(R, B) &= d_2^B - 32C_B f(R, B), \text{ where} \\
d_2^B &= C_B \left[\left(\frac{808}{27} - 28\zeta_3 \right) C_A - \frac{224}{27} T_F n_f \right].
\end{aligned} \tag{2.17}$$

The function $f(R, B)$, which gives the dependence on the jet radius R , is known as an expansion about $R = 0$ up to terms including R^4 ,

$$\begin{aligned}
f(R, B) &= C_B \left(-\frac{\pi^2 R^2}{12} + \frac{R^4}{16} \right) \\
&+ C_A \left(c_L^A \ln R + c_0^A + c_2^A R^2 + c_4^A R^4 + \dots \right) \\
&+ T_F n_f \left(c_L^f \ln R + c_0^f + c_2^f R^2 + c_4^f R^4 + \dots \right).
\end{aligned} \tag{2.18}$$

The terms on the first line are due to independent emission, whereas the terms on the second and third lines are due to correlated emission [4]. The expansion coefficients are given in Appendix D in analytic and numerical form.

2.1.1 Approximations for d_2^{veto}

Using Eqs. (2.17) and (D.4) we have for the gluon case in the limit $n_f \rightarrow 0$ and retaining only logarithmic and constant terms in R ,

$$\begin{aligned} d_2^{\text{veto}}(R, A) &= -32C_A^2 \left[-\frac{1}{32C_A^2} d_2^A + c_L^A \ln R + c_0^A \right] \\ &\simeq -32C_A^2 \left[-1.096259 \ln R + 0.7272641 \right] \\ &\sim 32C_A^2 \times \ln \left(\frac{R}{2} \right). \end{aligned} \quad (2.19)$$

This result was used as a basis for an approximation to d_3^{veto} in ref. [12]. However, the leading color ($n_f = 0$) approximation is rather poor. With full n_f dependence, but retaining only logarithmic and constant terms in R and setting $n_f = 5$ we have

$$\begin{aligned} d_2^{\text{veto}}(R, B) &= 32C_B C_A \left[(1.096 + 0.0295n_f) \ln R - (0.72726 + 0.12445n_f) \right] \\ &\sim 32C_B C_A \left[1.2435 \ln \left(\frac{R}{2.96} \right) \right]. \end{aligned} \quad (2.20)$$

In Fig. 1 we show $d_2^{\text{veto}}(R, A)$ and its approximations in units of d_2^A as a function of the jet radius R . As a reminder, d_2^A is the non- R dependent part of d_2 , see Eq. (2.17). We first compare the full result (red) with the inclusion of terms up order R^2 (green). This shows that the R expansion converges quickly and it is sufficient to consider only terms up to R^4 for practical applications. Including only the logarithm and the constant (blue) gives a reasonable approximation for sufficiently small R , with percent-level deviations around $R = 0.4$. The leading color approximation (magenta) works only crudely as a first guess and could be used in the absence of any better estimate.

2.1.2 The function d_3^{veto}

While the complete d_3^{veto} is unknown so far, we can extract the leading logarithmic term from results in the literature. Given that this approximation works reasonably well for d_2^{veto} for $R \sim 0.4$, it is reasonable to expect a similar behavior for d_3^{veto} . We further estimate the uncertainty associated with such an approximation.

From Eq. (2.15) the collinear anomaly coefficient at $\mu = p_T^{\text{veto}}$ is given by,

$$F_{gg}(p_T^{\text{veto}}, R, p_T^{\text{veto}}) = \left(\frac{\alpha_s}{4\pi} \right)^2 d_2^{\text{veto}}(R, A) + \left(\frac{\alpha_s}{4\pi} \right)^3 d_3^{\text{veto}}(R, A) + \dots \quad (2.21)$$

Therefore, expanding the collinear anomaly we have that

$$\begin{aligned} \left(\frac{Q}{p_T^{\text{veto}}} \right)^{-2F_{gg}(p_T^{\text{veto}}, p_T^{\text{veto}})} &= 1 - 2 \left(\frac{\alpha_s(p_T^{\text{veto}})}{4\pi} \right)^2 \ln \left(\frac{Q}{p_T^{\text{veto}}} \right) d_2^{\text{veto}}(R, A) \\ &\quad - 2 \ln \left(\frac{\alpha_s(p_T^{\text{veto}})}{4\pi} \right)^3 \ln \left(\frac{Q}{p_T^{\text{veto}}} \right) d_3^{\text{veto}}(R, A) + \mathcal{O}(\alpha_s^4). \end{aligned} \quad (2.22)$$

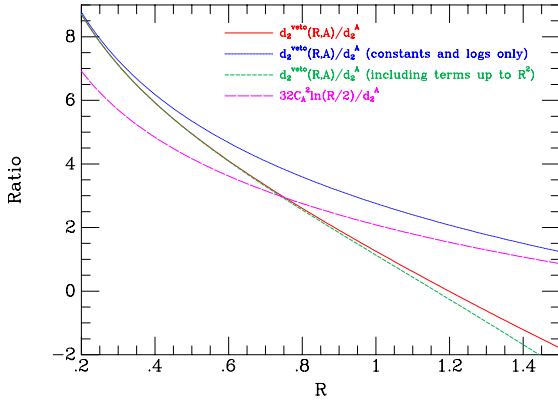


Figure 1: Approximations of $d_2^{\text{veto}}(R, A)$ scaled by the constant d_2^A . The full result, Eq. (2.17) is plotted in red. The approximation retaining only constant terms and logarithms of R is shown in blue. The approximation retaining constant terms and logarithms of R and R^2 terms is shown in green. The leading color ansatz, Eq. (2.19), derived setting $n_f = 0$, is $32C_A^2 \ln(R/2)$ and is shown in magenta. The red, blue and green curves are all plotted for $n_f = 5$.

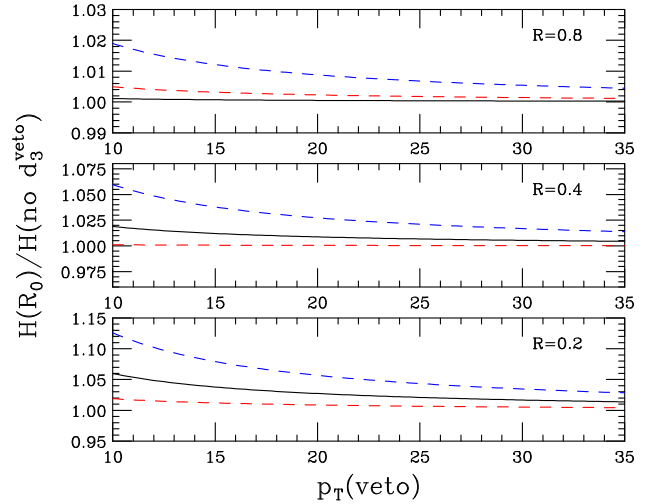


Figure 2: Effect of R_0 variation in d_3^{veto} as given by Eq. (2.24) with $Q = 125$ GeV and $n_f = 5$, compared to the case $d_3^{\text{veto}} = 0$: $R_0 = 1$ (black), $R_0 = 0.5$ (red, dashed), $R_0 = 2$ (blue, dashed).

At order α_s^3 the leading term in the limit $R \rightarrow 0$ can be extracted from Eq. (C.2) of Ref. [14] which reads,

$$\begin{aligned} \mathcal{F}_{\text{LLR},31}^{\text{correl}}(R) &= \left(\frac{\alpha_s}{4\pi}\right)^3 \ln\left(\frac{Q}{p_T^{\text{veto}}}\right) \cdot 128C_A \ln^2 \frac{R}{R_0} \\ &\times \left[1.803136C_A^2 - 0.589237n_f 2T_R C_A + 0.36982C_F n_f 2T_R - 0.05893n_f^2 4T_R^2\right]. \end{aligned} \quad (2.23)$$

Comparing the third-order coefficient in the two equations we thus have for a general color representation

$$\begin{aligned} d_3^{\text{veto}}(R, B) &= -64C_B \ln^2\left(\frac{R}{R_0}\right) (1.803136C_A^2 + 0.36982C_F n_f - 0.589237C_A n_f - 0.05893n_f^2) \\ &= -8.38188 \times 64C_B \ln^2\left(\frac{R}{R_0}\right) \text{ for } n_f = 5. \end{aligned} \quad (2.24)$$

Hence, the sign of the leading term in the small R limit is known. In this limit d_3^{veto} leads to an increase in the cross-section. This approximation only gives the leading R behavior, and it has been suggested that one may plausibly take $\frac{1}{2} < R_0 < 2$ as an uncertainty envelope [14].

Since d_3^{veto} enters through the collinear anomaly as an overall factor, we consider the impact of varying R_0 in Fig. 2. For typical values of $p_T^{\text{veto}} = 30$ GeV (as considered in this paper for the

Table 2: Input and derived parameters used for our numerical estimates.

M_W	80.385 GeV	Γ_W	2.0854 GeV
M_Z	91.1876 GeV	Γ_Z	2.4952 GeV
G_μ	$1.166390 \times 10^{-5} \text{ GeV}^{-2}$		
m_t	173.2 GeV	m_h	125 GeV
$m_W^2 = M_W^2 - iM_W\Gamma_W$	$(6461.748225 - 167.634879 i) \text{ GeV}^2$		
$m_Z^2 = M_Z^2 - iM_Z\Gamma_Z$	$(8315.17839376 - 227.53129952 i) \text{ GeV}^2$		
$\cos^2 \theta_W = m_W^2/m_Z^2$	$(0.7770725897054007 + 0.001103218322282256 i)$		
$\alpha = \frac{\sqrt{2}G_\mu}{\pi}M_W^2(1 - \frac{M_W^2}{M_Z^2})$	$7.56246890198475 \times 10^{-3}$ giving $1/\alpha \approx 132.23 \dots$		

comparison with experimental studies) there is an effect of less than two percent for $R = 0.4$. This is in agreement with the deviations we found for d_2^{veto} for this approximation.

We take into account this variation in our uncertainty estimates, see Section 3.3. A definitive statement on this issue will have to await an exact calculation of d_3^{veto} .

3 Setup for phenomenology

Before discussing phenomenological results, we list our input parameters, the method for matching to fixed order, and the approach for estimating uncertainties at fixed order and at the resummed level.

3.1 Input parameters

The input values used in our numerical studies are shown in Table 2. As indicated in the table we use the complex mass scheme for the W and Z boson masses. The number of light quarks, n_f , is set equal to five, except for the case of W^+W^- -production where $n_f = 4$. We use the PDF distribution NNPDF31_nnlo_as_0118 except for W^+W^- where we use NNPDF31_nnlo_as_0118_nf_4 [36]. Note that we use these NNLO parton distributions even in our lower order predictions.

In the cases of WW and ZZ production, at $\mathcal{O}(\alpha_s^2)$ the cross-section receives contributions from processes with two gluons in the initial state. When performing the resummed calculations we include such contributions at NLL relative to the leading order, which is of order α_s^2 . For the complete process the terms included are of order $\alpha_s^n L^k$ with $2n - 4 > k > \max(n - 2, 0)$ and hence they contribute at N³LL. Because of the large flux of gluons, one might worry that this formal counting is not appropriate. However, these contributions only represent about 3% of the cross-section for $p_T^{\text{veto}} = 10 \text{ GeV}$, rising to about 6–8% for $p_T^{\text{veto}} = 60 \text{ GeV}$. Therefore, neglecting higher order corrections to these contributions, which are not implemented in our code, is justified.

We match the resummation and fixed-order $N^k\text{LO}$ corrections using a naive additive scheme as follows,

$$\sigma^{\text{N}^{(k+1)}\text{LL}+\text{N}^{(k)}\text{LO}}(p_T^{\text{veto}}) = \sigma^{\text{N}^{(k+1)}\text{LL}}(p_T^{\text{veto}}) + \sigma^{\Delta,k}(p_T^{\text{veto}}), \text{ where} \quad (3.1)$$

$$\sigma^{\Delta}(p_T^{\text{veto}}) = \sigma^{\text{N}^k\text{LO}}(p_T^{\text{veto}}) - \left. \text{d}\sigma^{\text{N}^{(k+1)}\text{LL}}(p_T^{\text{veto}}) \right|_{\text{exp. to N}^k\text{LO}}. \quad (3.2)$$

The matching correction $\sigma^{\Delta}(p_T^{\text{veto}})$ is defined as a function of p_T^{veto} , using the difference between the fixed-order contribution and the resummed result expanded to the same fixed order. The limit $p_T^{\text{veto}} \rightarrow 0$ of $\sigma^{\Delta}(p_T^{\text{veto}})$ is finite, which also allows its use as a higher-order subtraction scheme.

The use of a naive matching without a transition mechanism that switches off the resummation at large p_T^{veto} is justified since the matching corrections for all considered cases in this paper are small; even in the most extreme case they are less than 20%. In other words, the resummation alone provides a good description of the cross-sections and does not need to be switched off. Any transition function to turn off the resummation at large p_T^{veto} would have a very small effect. This is in contrast to transverse-momentum resummation where a transition function is necessary [31].

3.2 Uncertainty estimates at fixed order

Ultimately the resummed predictions should offer a practical advantage compared to the fixed-order predictions. In many cases, the quantity $\log(Q/p_T^{\text{veto}})$ is not very large, and it may not seem worthwhile to use resummed results. However, as we will show, the resummation works remarkably well on its own and has matching corrections of only up to around 20%, often much less. The clear separation of scales and the resummation then allow for smaller and more reliable uncertainty estimates. To set the stage, we first examine perturbative convergence and uncertainties at fixed order for quark and gluon induced boson processes, as well as for WW and ZZ production.

Constructing jet-vetoed cross-sections at fixed order requires the combination of different cross-sections. However, if we naively subtract the jet cross-section from the inclusive result, it can result in underestimated uncertainties and narrowing uncertainty bands. To avoid this, different methods have been proposed in the literature, of which we compare the following two.

One strategy, which we term the "two-scale" approach, is to consider the different relevant scales Q and p_T^{veto} of the vetoed cross-section σ_0 , and include both of them in the uncertainty estimate through a multi-point variation around both scales [8]. To compute this uncertainty, we separately vary the renormalization scale μ_r and the factorization scale μ_f over the values $\{\mu_h, 2\mu_h, \mu_h/2, p_T^{\text{veto}}, 2p_T^{\text{veto}}, p_T^{\text{veto}}/2\}$, where μ_h depends on the process under consideration. An estimate of the uncertainty is then obtained by adding in quadrature the maximum deviations from $\mu_r = \mu_f = \mu_h$, from μ_r and μ_f variation separately.

Another approach, advocated by Refs. [14, 37], takes the jet-veto efficiency (JVE) as the central quantity, which is the ratio of jet-vetoed cross-section to total cross-section. By combining the uncertainties of these two quantities in quadrature, one obtains a more robust estimate of the uncertainty in the jet-vetoed cross-section. This is because the uncertainties are considered uncorrelated: the uncertainties in the jet-veto efficiency are typically due to non-cancellation of real and virtual contributions, while those in the total cross-section are connected with large corrections from higher orders [14].

For our JVE approach, we follow the simplest formulation (“scheme (a)” of Ref. [14]) to compute a JVE-based uncertainty. For this we consider variation over the scales $\{\mu_h, 2\mu_h, \mu_h/2\}$ of σ_{incl} and combine in quadrature the uncertainty from the calculation of the 0-jet efficiency ($\sigma_0/\sigma_{\text{incl}}$) and the uncertainty from the inclusive calculation. Our final fixed-order uncertainty band is the envelope of the two-scale and JVE approaches.

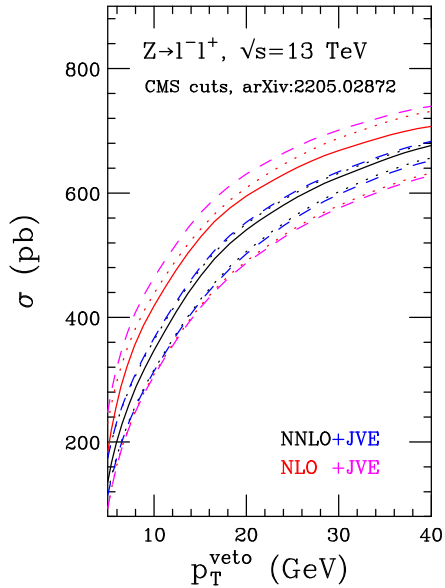
With these procedures, our fixed-order results for Z and H production are shown in Fig. 3. For Z production we use the canonical choice $\mu_h = Q$, where Q is the invariant mass in the final state. For Higgs production we use $\mu_h = Q/2$, guided by the calculation of the inclusive cross-section where such a choice results in markedly-improved perturbative convergence. We observe that for Z production the NNLO uncertainty band is wholly contained within the NLO one, while for the Higgs case the bands at least overlap somewhat throughout the range. For Higgs production following the combined two-scale and JVE approach results in a significantly larger uncertainty at both NLO and NNLO, especially at smaller values of p_T^{veto} . On the other hand, for Z production the additional uncertainty from the JVE approach is very small and negligible at NNLO.

Predictions for WW and ZZ production (with $\mu_h = Q$) are shown in Fig. 4. The limited overlap between the NLO and NNLO bands indicates that uncertainties are underestimated, even with the generous scale uncertainty procedure that we follow. The additional uncertainty resulting from the JVE procedure is small, especially at NNLO, because the scale uncertainty of the inclusive cross-sections is very small.

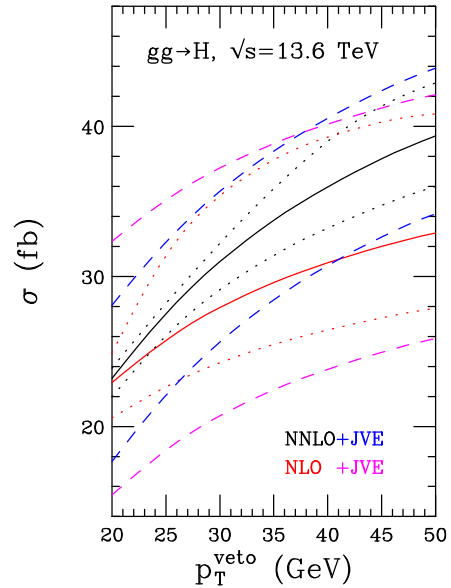
3.3 Uncertainty estimates at the resummed and matched level

For our central predictions, we set the resummation and factorization scales to $\mu = p_T^{\text{veto}}$ and the hard scale (corresponding to the renormalization scale) to $\mu_h = Q$, where Q is the invariant mass of the color-singlet final state. The exception is Higgs production, where we choose $\mu_h = Q/2$ as previously discussed. For the collinear anomaly coefficient d_3^{veto} , we use the form given in Eq. (2.24) [14] with $R_0 = 1$.

Complications arising at fixed order, described in Section 3.2, are not present in the resummed case and therefore we can follow a simpler approach where we vary all scales in our formalism and take the envelope, as detailed below. While the matching of resummed predictions to fixed-order could still introduce a complication, the matching corrections are not dominant. The bulk of the cross-section comes from the resummation and it allows us to follow the simple

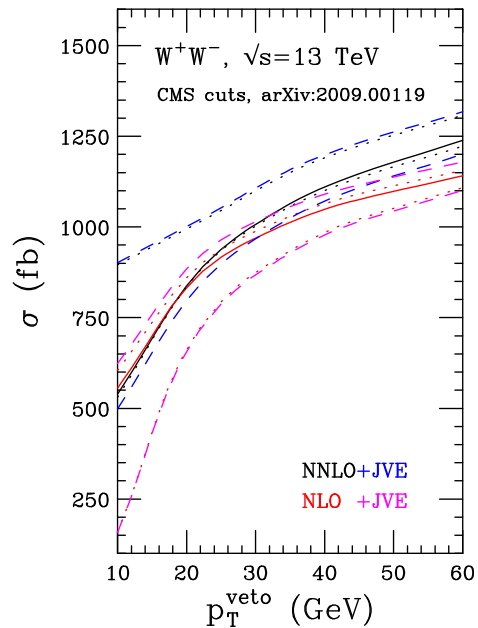


(a) Z production using the setup of ref. [38].

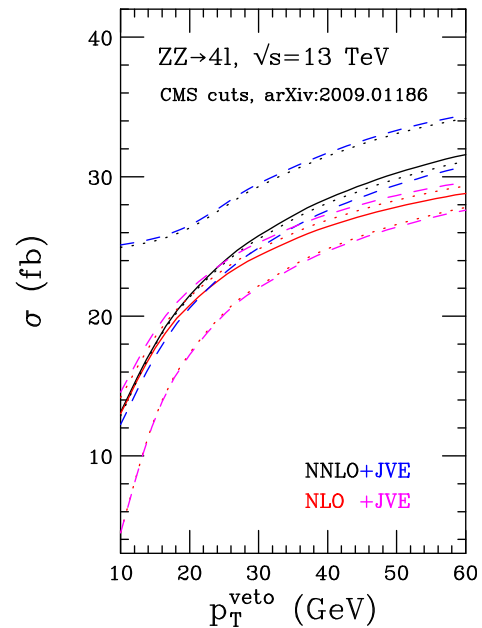


(b) H production.

Figure 3: Comparison of NLO and NNLO fixed order predictions as a function of the jet veto. Central predictions solid, uncertainty estimates using either the two-scale approach (dotted) or the envelope of that and the JVE approach (dashed).



(a) WW production using the setup of ref. [39].



(b) ZZ production using the setup of ref. [40].

Figure 4: Comparison of NLO and NNLO fixed order predictions as a function of the jet veto. Central predictions solid, uncertainty estimates using either the two-scale approach (dotted) or the envelope of that and the JVE approach (dashed).

procedure of varying all scales in the naively obtained (without JVE) jet-veto cross-section too.

The small and narrowing uncertainty bands at fixed order would typically appear in regions where the resummation is found to be dominant, i.e. where fixed-order contributes very little through the matching corrections. In practice we observe that the size of uncertainties are overall uniform in both the resummation and large p_T^{veto} fixed-order regions, as can be seen in all of our following predictions. This supports the conclusion that our procedure is sufficient.

Overall, our procedure for estimating uncertainties is as follows.

1. For the resummation (fixed-order) parts we vary both the resummation (factorization) and hard (renormalization) scales by a factor of two about their central values, adding the excursions in quadrature to obtain the total scale uncertainty.
2. For the resummation we re-introduce the rapidity scale in Eq. (2.5) by re-writing the collinear anomaly factor as follows [12, 41]:

$$\left(\frac{Q}{p_T^{\text{veto}}}\right)^{-2F_{ii}(p_T^{\text{veto}}, R, \mu)} = \left(\frac{Q}{\nu}\right)^{-2F_{ii}(p_T^{\text{veto}}, R, \mu)} \left(\frac{\nu}{p_T^{\text{veto}}}\right)^{-2F_{ii}(p_T^{\text{veto}}, R, \mu)}. \quad (3.3)$$

For $\nu \sim p_T^{\text{veto}}$ the second factor can be expanded since it does not contain a large logarithm. We vary the rapidity scale ν in the range $[p_T^{\text{veto}}/2, 2p_T^{\text{veto}}]$ for gluon-initiated processes and in the range $[p_T^{\text{veto}}/6, 6p_T^{\text{veto}}]$ for quark-initiated processes. The large variation for quark-initiated processes ensures overlapping uncertainty bands at NNLL and N³LL_p; this is achieved by the range given above, as demonstrated explicitly in Sections 4 and 5.

3. The parameter R_0 in d_3^{veto} is varied between 0.5 and 2.

We first combine the scale uncertainties (1 and 2) in quadrature and then, to obtain our total uncertainty, add the variation of R_0 (3) linearly.

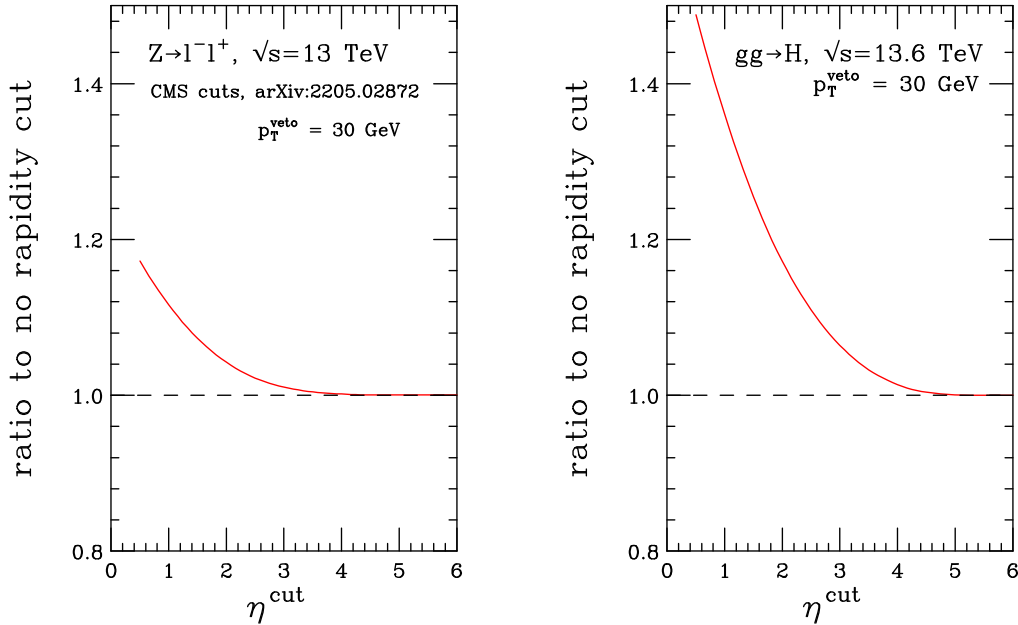
3.4 Effects of cuts on rapidity at fixed order

The usual jet veto resummation described so far imposes no cut on the jet rapidity. This is in contrast to experimental analyses, see Table 3, which impose such a cut because of limited detector acceptance and to diminish the effect of pileup. Ref. [42] identifies three different regimes, depending on p_t , Q and y_{cut} .

- For $p_T^{\text{veto}}/Q \gg \exp(-y_{\text{cut}})$ standard jet veto resummation should apply, effects due to the rapidity cut are corrections power suppressed by $Q \exp(-y_{\text{cut}})/p_T^{\text{veto}}$.
- For $p_T^{\text{veto}}/Q \sim \exp(-y_{\text{cut}})$ the effects of a rapidity cut must be treated as a leading power correction.
- For $p_T^{\text{veto}}/Q \ll \exp(-y_{\text{cut}})$ the logarithmic structure is changed already at leading log level, and non-global logarithms appear.

Table 3: Jet rapidity cuts applied in the experimental studies examined later in this paper.

Process	Ref.	y_{cut}
Higgs	–	no study
Z (CMS)	[38]	2.4
W (ATLAS)	[43]	4.4
WW (CMS)	[39]	4.5
WZ (ATLAS)	[44]	4.5
WZ (CMS)	[45]	2.5
ZZ (CMS)	–	no study



(a) Z production following the setup of ref. [38].

(b) H production.

Figure 5: Effect of the jet rapidity cut at NNLO with $p_T^{\text{veto}} = 30$ GeV.

We estimate the practical impact of experimentally used jet rapidity cuts at fixed order. Including the rapidity cut in the resummation requires large changes and ingredients, which are also only available a low order so far [42].

The effect of the jet rapidity cut for the Z and Higgs production cases is illustrated in Fig. 5. These calculations are performed at NNLO for $p_T^{\text{veto}} = 30$ GeV. The rapidity cut plays a bigger role for Higgs production: for example for $y_{\text{cut}} = 2.5$ the cross-section is 11% larger than the result with no rapidity cut, compared to only 2% for Z production. This is due to the larger logarithm ($\log(m_H/p_T^{\text{veto}})/\log(m_Z/p_T^{\text{veto}}) \approx 1.28$) and the larger color prefactor ($C_A/C_F = 2.25$) in Higgs production. However, for $y_{\text{cut}} = 4.5$ the effect of the rapidity cut is negligible in both cases.

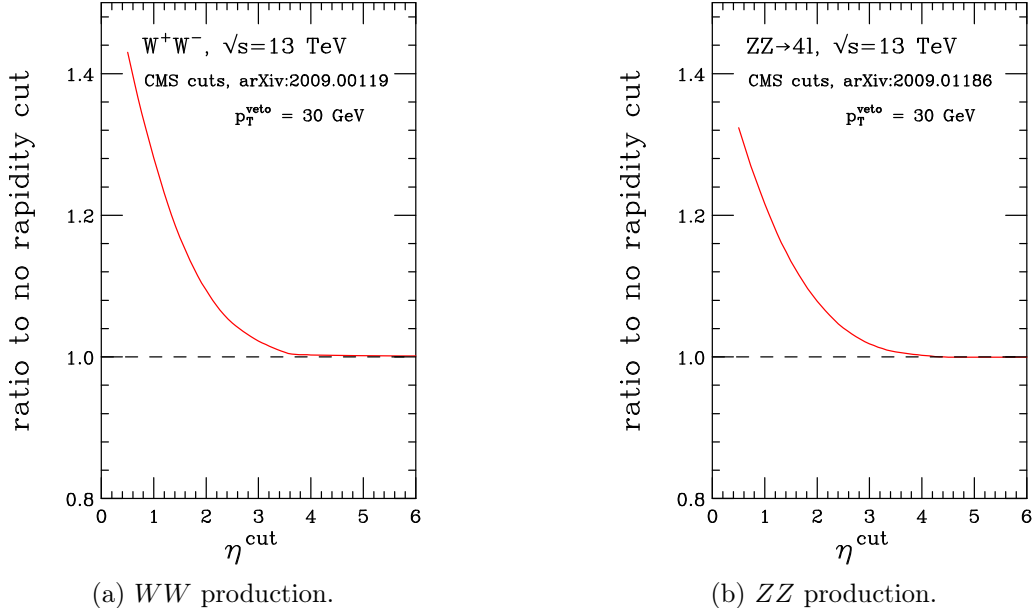


Figure 6: Effect of the jet rapidity cut at NNLO with $p_T^{\text{veto}} = 30$ GeV.

The corresponding results for diboson processes are shown in Fig. 6. In this case, the disparity between Q and p_T^{veto} is much larger, so the rapidity cut can play a crucial role, although the effect is still not as important as for Higgs production. For $y_{\text{cut}} = 2.5$ the WW and ZZ cross-sections 4% larger than the results with no rapidity cut, and the effect of $y_{\text{cut}} = 4.5$ is negligible.

4 Comparison with JetVHeto

While jet-veto resummed phenomenology has been extensively studied in the literature, the only public codes that permit detailed predictions use JetVHeto or RadISH. For jet-veto resummation RadISH implements the analytic JetVHeto resummation formula [5]. The codes rely on the formalism of the CAESAR approach [4, 46] extended to NNLL [5]. An extension of the RadISH code has been used to perform joint jet-veto and boson transverse momentum resummation [47].

For our comparisons we use RadISH version 3.0.0 [48, 49] and JetVHeto version 3.0.0 [5, 14, 37] including small- R resummation [4, 35] as part of MCFM-RE [16]. Both codes operate at the level of NNLL and we have checked that they give indeed the same results.

In our comparison, we would like focus on the differences in the resummation part, since the fixed-order part is identical in each calculation. We explore how central values and uncertainties compare at NNLL to our results and in how far $N^3\text{LL}_p$ results improve the perturbative convergence. However, the matching to fixed-order is handled differently in each formalism. Different matching schemes (e.g. additive or multiplicative schemes of various

types) probe higher-order effects. It has also been advocated to match at the level of jet-veto efficiencies [14]. Fortunately, matching corrections are generally small for jet-veto scales of 30 to 40 GeV for all considered boson and di-boson processes. We therefore focus on the resummation in our comparison.

The JetVHeto formalism considers three scales μ_R , μ_F and Q that are all similar in magnitude to the hard scale. To ensure that the resummation switches off for $p_T^{\text{veto}} \gtrsim Q$, the resummed logarithms are modified through the prescription $\log(Q/p_T^{\text{veto}}) \rightarrow 1/p \log((Q/p_T^{\text{veto}})^p + 1)$. For JetVHeto p has a default value of 5 [14], while for RadISH the default choice is 4. For comparison purposes we use $p = 5$ in both cases. It is evident that for sufficiently small p_T^{veto} the precise value of p does not matter. Changing this parameter has a similar effect to turning off the resummation with a transition function. In principle this demands a fully matched calculation, but the matching corrections of our considered cases are small and we have checked that the effect of changing p to 3 or 4 is subleading compared to the scale uncertainties. Here we focus on those scale uncertainties.

In ref. [14] it has been argued that the Q should be varied by a factor of $\frac{3}{2}$ around its central value, based on new insights from convergence at N³LO for Higgs production. For simplicity, we use a more conservative variation by a factor of two. We independently vary μ_R, μ_F and Q by a factor of two around a central scale of $m_{\ell\ell}$ for Z -boson production and around $m_H/2$ for Higgs production. Our uncertainty bands for this comparison are obtained by taking the envelope of these results.

Z -boson production

For the comparison of Z production we choose a central hard scale of $m_{\ell\ell}$ with results shown in Fig. 7. We find that the uncertainty bands of our MCFM NNLL predictions mostly contain those obtained by JetVHeto (as estimated according to our procedure just described). Furthermore, the uncertainty bands of both NNLL predictions overlap with our N³LL_p results, indicating robust uncertainties.

At N³LL_p uncertainties decrease dramatically compared to NNLL, but they are quite asymmetric, which suggests that a symmetrization of uncertainties may be necessary in this case. We also observe that without the large uncertainties at NNLL, there would be no overlap between the N³LL_p results and NNLL. This highlights the importance of carefully estimating and comparing uncertainties to accurately assess the compatibility of different methods and results.

H -boson production

In our study of Higgs production, we choose a central hard scale of $m_H/2$ and show results in Fig. 8. All results are computed in the $m_t \rightarrow \infty$ theory and rescaled by a factor of 1.0653 to account for finite top-quark mass effects, see Eq. (G.5).

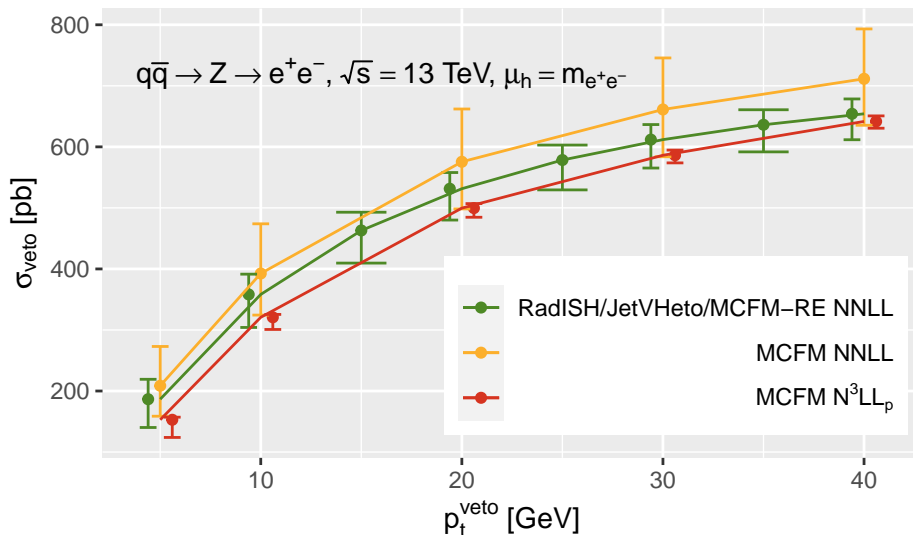


Figure 7: Comparison of JetVHeto NNLL resummation with our NNLL and N³LL_p results for Z production with cuts as in Table 4.

The Higgs case is distinct from Z production since it is gluon-gluon initiated instead of quark-initiated. In this case, our predictions agree well with the JetVHeto results, but our uncertainties at NNLL are again much larger.

Note that we vary the JetVHeto scale Q by a factor of two, while the JetVHeto authors vary by a factor of 3/2 in the Higgs case. This difference in the amount of variation may require some tuning in our formalism, at least at the NNLL level. However, the perturbative convergence is again excellent with small uncertainties at N³LL_p and central predictions that agree well with NNLL.

5 Phenomenological results

In this section, we present the results of our phenomenological studies, which are based on the uncertainty procedure, matching to fixed-order, and input parameters described in Section 3. We compare our findings with experimental results from the literature and discuss their implications.

5.1 Z and W production

The process of Z production has already been extensively studied in the literature, thus enabling a variety of cross-checks of our calculation. The implementation of the hard function and its evolution has been verified by comparison with the explicit results given in Table 1 of ref. [50]. The full machinery of the resummation and matching procedure can also be compared with the results of ref. [5], with which we find excellent agreement within uncertainties, see also Section 4.

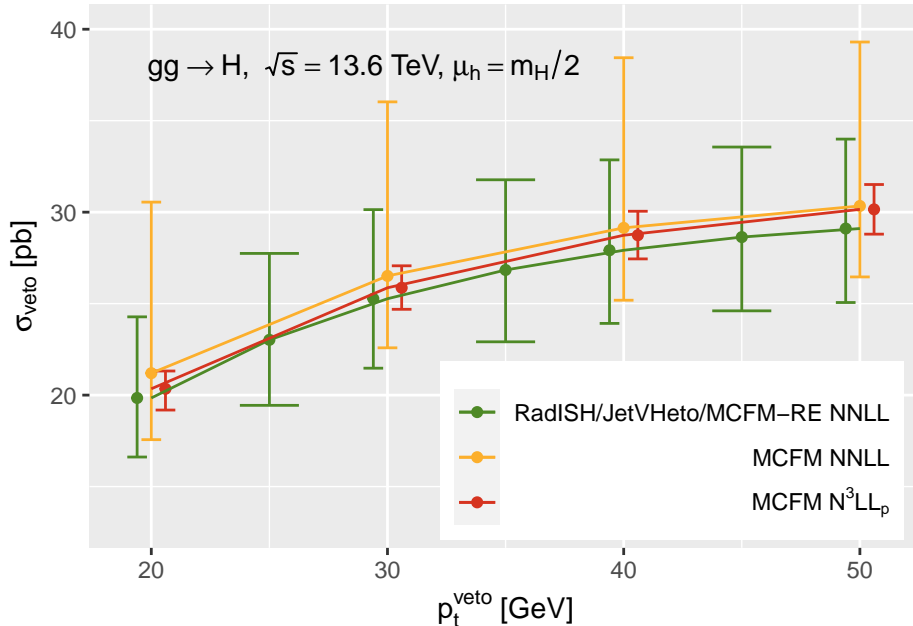


Figure 8: Comparison of JetVHeto NNLL resummation with our NNLL and $N^3\text{LL}_p$ results for non-decaying H production.

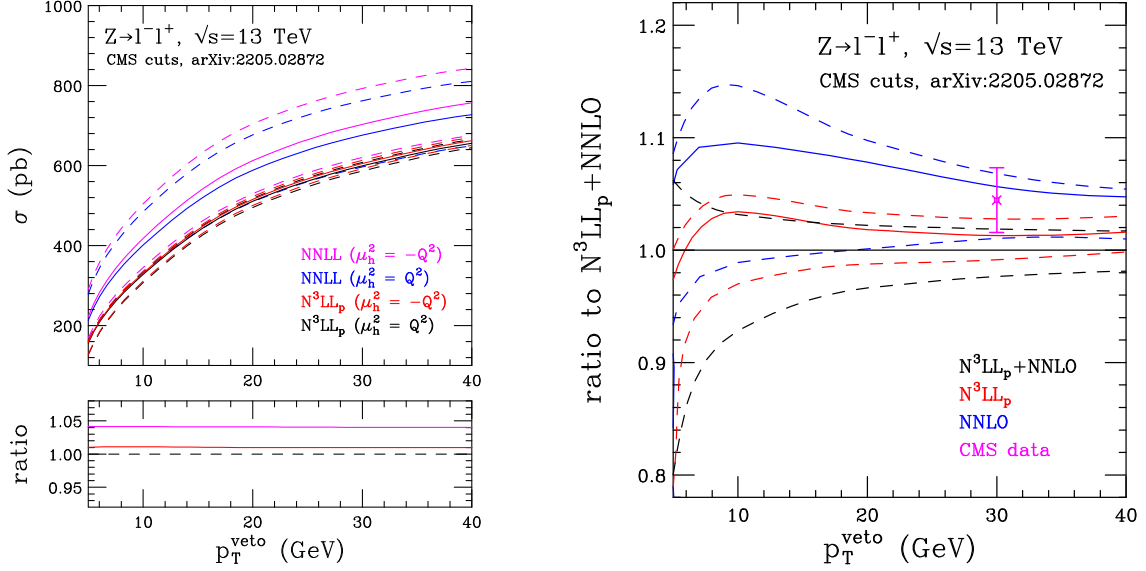
Table 4: Cuts used in the analysis of Z production, adapted from ref. [38].

lepton cuts	$q_T^{l_1} > 30 \text{ GeV}, q_T^{l_2} > 20 \text{ GeV}, \eta^l < 2.4$
lepton pair mass	$71 \text{ GeV} < m_{l^-l^+} < 111 \text{ GeV}$
jet veto	anti- $k_T, R = 0.4, 0\text{-jet events only}$

We first investigate the impact of choosing a time-like hard scale in the resummed result for Z production. Previous work has shown that choosing a space-like hard scale ($\mu_h^2 = Q^2$) can lead to significant corrections in the perturbative expansion of some processes, while a time-like hard scale ($\mu_h^2 = -Q^2$) can resum certain π^2 contributions [51] using a complex strong coupling.

For this comparison we consider purely resummed results at NNLL and $N^3\text{LL}_p$, only considering uncertainties originating from scale variation (items 1 and 2 of our uncertainty procedure in Section 3.3). We consider the process $pp \rightarrow Z/\gamma^* \rightarrow \ell^- \ell^+$, i.e. a final state of definite lepton flavor. We use the same set of cuts and vetoes as in the $\sqrt{s} = 13 \text{ TeV}$ CMS analysis [38], but extend the veto to jets of all rapidities, rather than only those with $|y| < 2.4$. This difference, and the effect of matching to NNLO, is discussed in detail in Section 5.1.1.

Our results are shown in Fig. 9a as a function of the value of the jet veto. We observe that the results do not depend strongly on the choice of hard scale, with a difference of about 4% at NNLL and only 1% at $N^3\text{LL}_p$. This indicates that resumming the π^2 terms results in only



(a) Predictions are computed using a central choice for the hard scale given by either $\mu_h^2 = Q^2$ or $\mu_h^2 = -Q^2$. The lower panel shows the ratio of the result for $\mu_h^2 = -Q^2$ to the one for $\mu_h^2 = Q^2$.

(b) Predictions and CMS measurement as ratio to matched result.

Figure 9: Comparison of NNLL and $N^3\text{LL}_p$ predictions for Z production as a function of the jet veto, using the setup of ref. [38] (central predictions solid, uncertainty estimate according to the text, dashed).

a small enhancement of the cross-section for W and Z production. Based on these findings, we use the space-like hard scale ($\mu_h^2 = Q^2$) in our subsequent studies of Z and W boson production, as it is the more commonly used choice in the literature.

5.1.1 CMS Z production

As previously mentioned, the CMS measurement we are comparing to includes a jet rapidity cut of $|y| < 2.4$. To assess the importance of this restriction, we first compare the NNLO predictions with and without the rapidity cut, as a function of the jet veto value. This comparison, shown in Table 5, helps us better understand the limitations of our analysis.

We use the quantity $\epsilon(p_T^{\text{veto}})$ to quantify the increase in the cross-section when the rapidity cut is applied, defined as

$$\epsilon(p_T^{\text{veto}}) = \frac{\sigma_{0\text{-jet}}(y_{\text{cut}} = 2.4)}{\sigma_{0\text{-jet}}(\text{no } y_{\text{cut}})} - 1. \quad (5.1)$$

The experimental measurement we are comparing to uses a jet veto of $p_T^{\text{veto}} = 30$ GeV, for which the rapidity cut has only a 3% effect on the cross-section. This suggests that our calculation with an all-rapidity jet veto is appropriate for comparing to the experimental measurement. However, as p_T^{veto} decreases, the impact of the rapidity cut becomes more significant, until at

Table 5: The $Z + 0$ -jet cross-section prediction at NNLO ($\mu = Q$), with and without a jet rapidity cut.

p_T^{veto} [GeV]	5	10	20	30	40
$\sigma_{0\text{-jet}}(\text{no } y_{\text{cut}})$ [pb]	140	347	539	627	675
$\sigma_{0\text{-jet}}(y_{\text{cut}} = 2.4)$ [pb]	242	411	569	643	685
ϵ	0.73	0.18	0.06	0.03	0.01

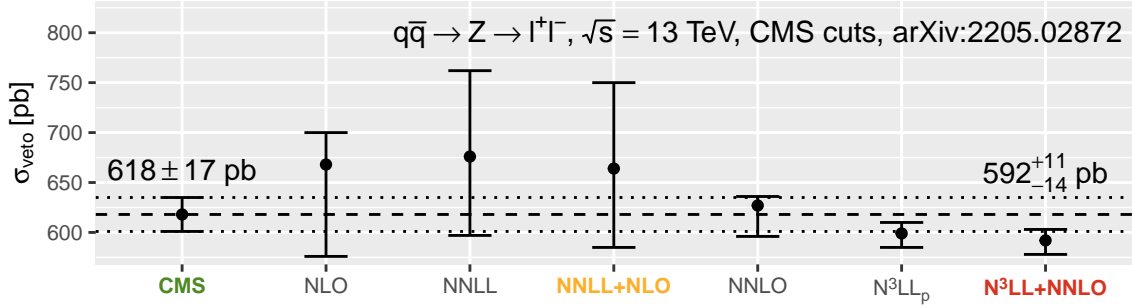


Figure 10: Comparison of Z -boson jet-vetoed predictions with the CMS [38] 13 TeV measurement. Shown are results at fixed-order, purely resummed and matched.

$p_T^{\text{veto}} = 5$ GeV it is no longer appropriate to neglect the rapidity cut. This is consistent with the arguments of Ref. [42], which suggest that the standard jet veto resummation formalism should suffice as long as $\ln(Q/p_T^{\text{veto}}) \ll y_{\text{cut}}$. In our case, $\ln(Q/p_T^{\text{veto}})$ ranges from 0.8 to 2.9 for p_T^{veto} from 40 down to 5 GeV, so the standard jet veto resummation should be appropriate, albeit with sizeable power corrections, for $y_{\text{cut}} = 2.4$ except for the smallest values of p_T^{veto} .

We now turn to a comparison with the CMS result [38], which uses a jet threshold of 30 GeV. Our comparison with fixed-order, purely resummed and matched predictions is shown in Fig. 10. We find that the fixed-order and resummed results differ by only a few percent, indicating that resummation is not necessary for this value of the jet veto. This is because the quantity $\ln(M_Z/p_T^{\text{veto}}) = 1.1$ is not large enough to require resummation. The CMS measurement yields a cross-section of 618 ± 17 pb, while our best prediction is 592^{+11}_{-14} pb.

We study the production of Z bosons as a function of the jet veto in Fig. 9b. We observe that the difference between the resummed and central fixed-order results is small, even for the smallest values of p_T^{veto} considered. However, the uncertainties in the fixed-order prediction are larger across the whole range, particularly for small p_T^{veto} . For values of p_T^{veto} in the range of 20 to 40 GeV, which are of practical interest, the $N^3\text{LL}_p$ uncertainty is smaller than the NNLO uncertainty by about a factor of 1.5.

5.1.2 ATLAS W production

We now perform a comparison with $\sqrt{s} = 8$ TeV ATLAS data on W production [43]. For this study, jets were identified using the anti- k_T algorithm with $R = 0.4$ and must satisfy

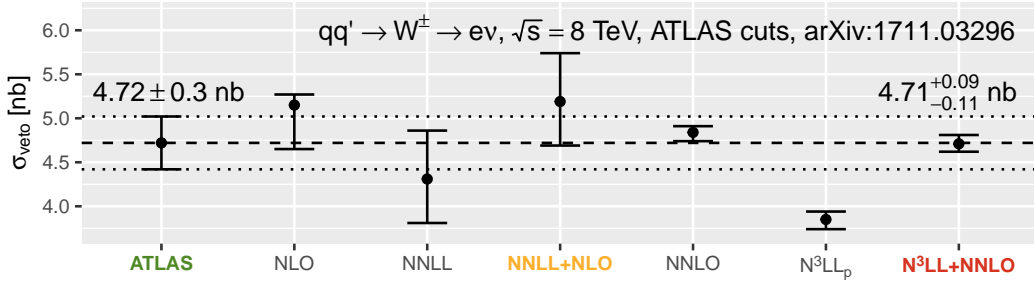


Figure 11: Comparison of W -boson jet-vetoed predictions with the ATLAS [43] 8 TeV measurement. Shown are results at fixed-order, purely resummed and matched.

$p_T > 30$ GeV and $|y| < 4.4$. We have checked at fixed order that this large rapidity cut has a negligible impact of a few per mille, i.e. results are unchanged within the numerical precision to which we work.

Summing over both W charges and including only the decay into electrons we compare our predictions in Fig. 11. We show results at fixed order, at the resummed level, and at the matched level. The effect of matching is large and we thus conclude that this value for the jet veto is outside the sensible range for a purely resummed result, unlike for the Z study in the previous subsection.

We observe excellent agreement with the theoretical prediction, albeit with a larger experimental uncertainty. The experimentally measured cross-section is 4.72 ± 0.30 nb while our best prediction is $4.71^{+0.09}_{-0.11}$ nb. Since this measurement corresponds to an integrated luminosity of only 20 fb^{-1} it is clear that the high-luminosity LHC will eventually be able to provide a much keener test of perturbative QCD in this process.

5.2 W^+W^- production

Experimental studies of WW production were performed by both ATLAS [52, 53] and CMS [39, 54]. Here we focus on the CMS analysis of ref. [39] since it provides a measurement of the 0-jet cross-section as a function of the jet p_T veto. This cross-section measurement corresponds to a sum over both electron and muon decays of the W bosons, which we denote by the label $pp \rightarrow W^-W^+ \rightarrow 2\ell 2\nu$. In order to account for this in our calculation, we compute the result for $pp \rightarrow e^- \mu^+ \bar{\nu}_e \nu_\mu$ at NNLO and multiply it by the factor that accounts exactly for all lepton combinations through NLO. The impact of ZZ contributions in the same-flavor case results in a slight enhancement over the naïve factor of four. We find that, independent of the value of the jet veto in the range that we consider, this factor is equal to 4.15.

The CMS analysis only imposes a jet rapidity cut of $y_{\text{cut}} = 4.5$, so our expectation is that the standard jet veto resummation formalism should be appropriate for p_T^{veto} values between 60 and 10 GeV, since in this case the logarithm of the ratio of Q to p_T^{veto} are in the range of 1.3 to 3.1. This expectation is supported by the NNLO analysis in Table 6, which shows only a

small 2% effect from the rapidity cut for $p_T^{\text{veto}} = 10$ GeV (and none for values above that). Unlike the processes considered so far, Q is no longer set by a resonance mass but is instead a distribution with a peak slightly above the $2M_W$ threshold. For illustration, we have used an average value of $Q \sim 220$ GeV.

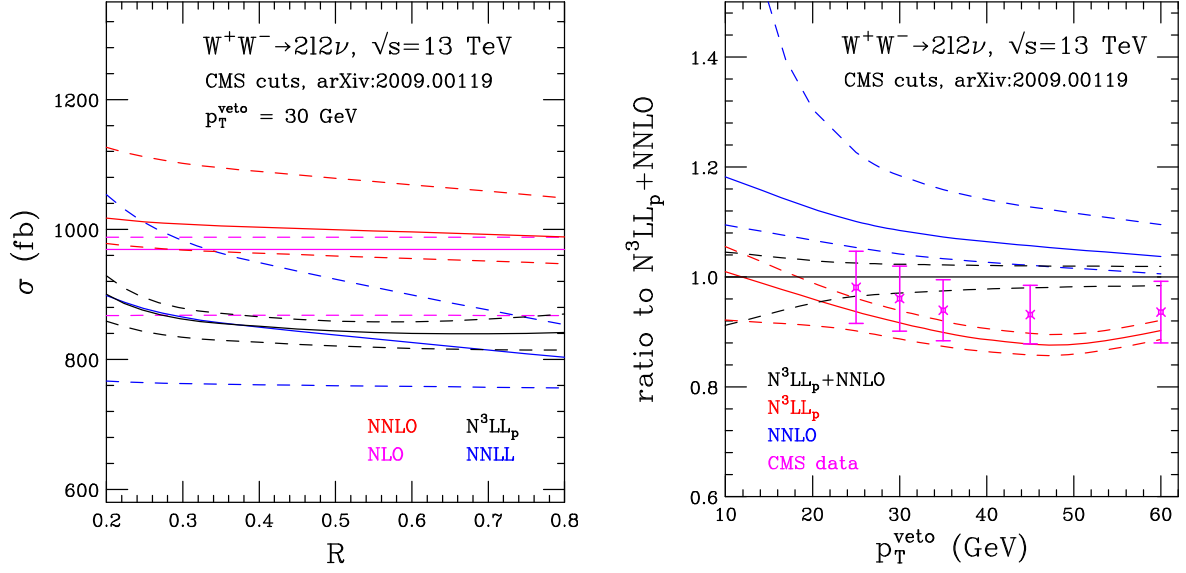
We first fix the value of $p_T^{\text{veto}} = 30$ GeV and study the sensitivity of the pure fixed-order and resummed calculations to the jet-clustering parameter R . The results are shown in Fig. 12a. At NLO, there is at most one additional parton, so the NLO result does not depend on the value of R . However, the NNLL result exhibits a mild dependence on R , which is most noticeable in the size of the uncertainties. These uncertainties are much larger for smaller values of R , as was previously observed and discussed in the context of Higgs production in Ref. [12]. At NNLO, the fixed-order calculation becomes sensitive to the value of R , although the dependence is very small. At N^3LL_p , the dependence is reduced compared to NNLL, especially at small R . Overall, these results suggest that the jet-clustering parameter has a mild effect on the predictions of the fixed-order and resummed calculations for WW production. We have not investigated the effect of small R resummation [14] on these results.

In Fig. 12b, we extend our previous analysis of the jet-veto dependence of WW production, which was presented in Ref. [55]. The effect of matching is substantial for values of p_T^{veto} greater than 20 GeV, so for typical jet vetoes in the range of 20 to 40 GeV, matched predictions are important. We find that the fixed-order description is only capable of providing an adequate result for the highest value of p_T^{veto} studied here. A comparison with the CMS measurement shows better agreement with the matched resummed calculation, although the experimental uncertainties are still substantial, corresponding to an integrated luminosity of 36 fb^{-1} . A breakdown of the estimated uncertainty on the matched $\text{N}^3\text{LL}_p + \text{NNLO}$ prediction, into the categories described in Section 3.3, is shown in Fig. 13. The uncertainty from the variation of the hard (renormalization) and resummation (factorization) scales dominates, except for the very lowest values of p_T^{veto} where the uncertainty on d_3^{veto} becomes significant.

We eagerly anticipate a measurement with more statistics in order to hone this comparison. Future measurements with higher precision and larger data samples will provide a more stringent test of the theoretical predictions and help to refine our understanding of WW production at the LHC.

Table 6: The $pp \rightarrow W^-W^+ \rightarrow 2\ell 2\nu + 0\text{-jet}$ cross-section at NNLO, with and without a jet rapidity cut.

p_T^{veto} [GeV]	10	25	30	35	45	60
$\sigma_{0\text{-jet}}(\text{no } y_{\text{cut}})$ [fb]	535	963	1004	1054	1145	1237
$\sigma_{0\text{-jet}}(y_{\text{cut}} = 4.5)$ [fb]	548	963	1004	1054	1145	1237
ϵ	0.02	0.00	0.00	0.00	0.00	0.00



(a) Jet radius R dependence of fixed-order and purely resummed results.

(b) Predictions and CMS measurement as a ratio to the matched result.

Figure 12: Comparison of NNLO, $N^3\text{LL}_p$ and matched $N^3\text{LL}_p + \text{NNLO}$ results for W^+W^- production.

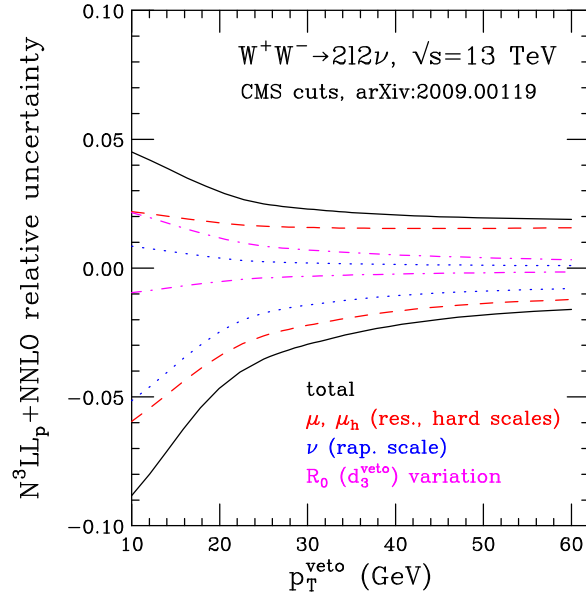


Figure 13: Uncertainty breakdown of the $N^3\text{LL}_p + \text{NNLO}$ results for W^+W^- production.

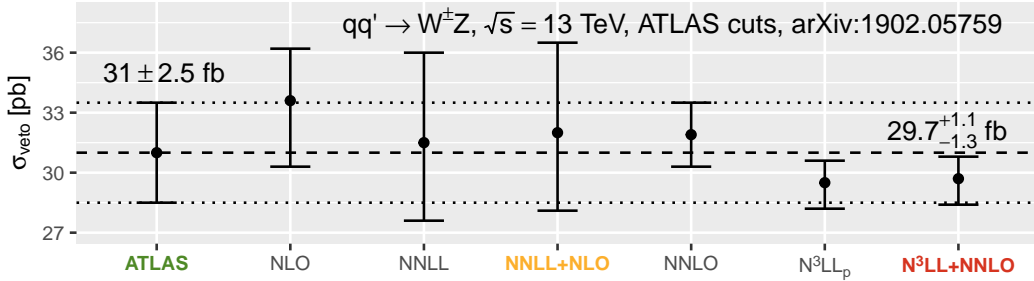


Figure 14: Comparison of $W^\pm Z$ jet-vetoed predictions with the ATLAS 13 TeV measurement [44]. Shown are results at fixed order, purely resummed and matched.

5.3 $W^\pm Z$ production

5.3.1 ATLAS

For $W^\pm Z$ production, we first compare our results with an analysis from the ATLAS collaboration at $\sqrt{s} = 13$ TeV [44]. The 0-jet cross-section is measured with jets defined by the anti- k_T algorithm with $p_T > 25$ GeV, $|y| < 4.5$, and $R = 0.4$.

Since $\ln(Q/p_T^{\text{veto}}) = 2.3$ (for $p_T^{\text{veto}} = 25$ GeV, using an average Q of about 240 GeV), we expect that standard jet veto resummation should be applicable in this case, since $y_{\text{cut}} = 4.5$. We have checked that the effect of the rapidity cut is at the per mille level, which is less than our numerical precision.

The ATLAS result is presented for a single leptonic channel and summed over both W charges. The corresponding theoretical predictions at fixed order, at the resummed level, and at the matched level are shown in Fig. 14.

Overall, the measurement is in good agreement with both the $N^3\text{LL}_p + \text{NNLO}$ and NNLO predictions, within the mutual uncertainties. Only a more precise measurement would be able to definitively support the need for resummation in this case. Since the ATLAS analysis includes only 36 fb^{-1} of data, it is likely that a more precise measurement will be possible in the near future.

5.3.2 CMS

We now contrast the ATLAS study of the $W^\pm Z$ process with one from CMS [45]. In the CMS study, jets are defined by the anti- k_T algorithm with $p_T > 25$ GeV, $|y| < 2.5$, and $R = 0.4$.

To assess the applicability of the jet-rapidity inclusive resummation framework, we must compare $\ln(Q/p_T^{\text{veto}}) = 2.3$ with $y_{\text{cut}} = 2.5$. This suggests that the standard jet veto resummation formalism may not be appropriate in this case, and that the use of y_{cut} -dependent beam functions [42] may be necessary to provide a reliable theoretical prediction. Despite this, we

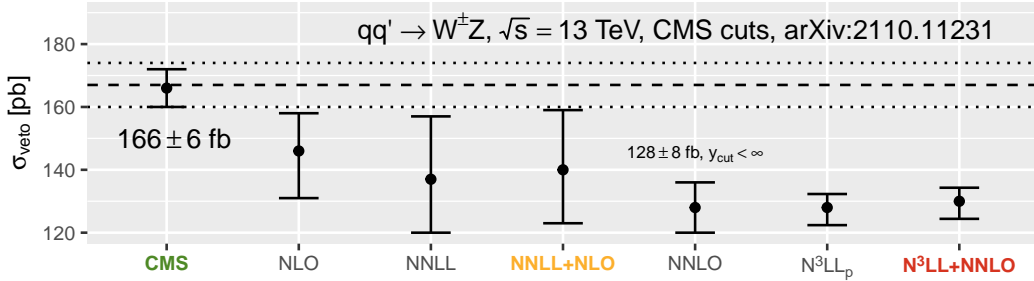


Figure 15: Comparison of $W^\pm Z$ jet-vetoed predictions with the CMS [45] 13 TeV measurement. Shown are results at fixed-order, purely resummed and matched, all without a rapidity cut.

$$\begin{array}{l|l}
 \text{lepton cuts} & \begin{array}{l} q_T^{l_1} > 20 \text{ GeV}, q_T^{l_2} > 10 \text{ GeV}, \\ q_T^{l_{3,4}} > 5 \text{ GeV}, |\eta^l| < 2.5 \end{array} \\
 \text{lepton pair mass} & 60 \text{ GeV} < m_{l-l^+} < 120 \text{ GeV} \\
 \text{jet veto} & \text{anti-}k_T, R = 0.5
 \end{array}$$

Table 7: Fiducial cuts used for the ZZ analysis, taken from the CMS study in Ref. [40].

still pursue the comparison here, without using y_{cut} -dependent beam functions, to examine the limitations of our approach.

The CMS result for $W^\pm Z$ production is presented after summing over all lepton flavors and both W charges. On the theoretical side, we perform a similar analysis, but ignore same-flavor effects that only enter at the 2% level. To construct the jet-vetoed cross-section for the CMS measurement, we combine the differential results in Figure 14(c) of Ref. [45] with the inclusive cross-sections reported in Table 6 of the same reference. Our results are shown in Fig. 15.

We find that neither the resummed prediction nor the NNLO one are in good agreement with the CMS data, even when the NNLO calculation takes the jet rapidity cut into account (increasing the NNLO result from 128 fb to 137 fb). This suggests that resummation is required in this case, and that the use of y_{cut} -dependent beam functions is necessary to provide a reliable theoretical prediction. Overall, these results highlight the importance of using appropriate resummation techniques to accurately predict $W^\pm Z$ production at the LHC with a small jet rapidity cut.

5.4 ZZ production

In the absence of jet-vetoed cross-sections for comparison, we use the cuts from a recent CMS study [40] to investigate our theoretical predictions for ZZ production as a function of p_T^{veto} . In the results that follow we consider a sum over Z decays into both electrons and muons, which we denote by $pp \rightarrow ZZ \rightarrow 4$ leptons, and apply the cuts shown in Table 7.

We expect that standard jet veto resummation should provide good predictions for $y_{\text{cut}} = 4.5$, since $\ln(Q/p_T^{\text{veto}})$ is in the range of 1.4 to 3.2 for p_T^{veto} values between 60 and 10 GeV, using an

Table 8: The $ZZ + 0$ -jet cross-section at NNLO ($\mu = Q$), with and without a jet rapidity cut.

p_T^{veto} [GeV]	10	20	30	40	50	60
$\sigma_{0\text{-jet}}(\text{no } y_{\text{cut}})$ [fb]	13.3	21.5	25.8	28.4	30.3	31.6
$\sigma_{0\text{-jet}}(y_{\text{cut}} = 4.5)$ [fb]	13.4	21.5	25.8	28.4	30.3	31.6
$\sigma_{0\text{-jet}}(y_{\text{cut}} = 2.5)$ [fb]	14.9	22.4	26.3	28.8	30.6	31.8
$\epsilon(y_{\text{cut}} = 4.5)$	0.01	0.00	0.00	0.00	0.00	0.00
$\epsilon(y_{\text{cut}} = 2.5)$	0.12	0.04	0.02	0.01	0.01	0.01

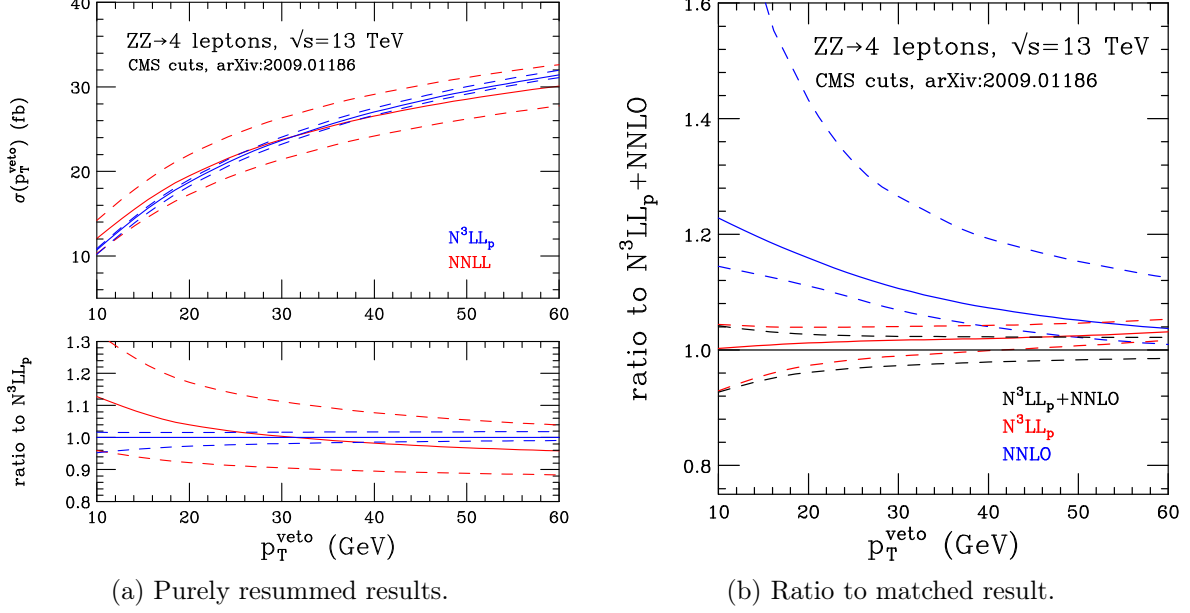


Figure 16: Comparison of NNLO, N^3LL_p and matched N^3LL_p+NNLO results for ZZ production as a function of the jet veto.

average Q of about 240 GeV. For $y_{\text{cut}} = 2.5$, we expect larger rapidity effects for the smallest values of p_T^{veto} . This is supported by our analysis in Table 8, which shows only a very small (1%) effect from a rapidity cut of $y_{\text{cut}} = 4.5$ for $p_T^{\text{veto}} = 10$ GeV (and no effect for higher values). Even for $y_{\text{cut}} = 2.5$, the rapidity cut has a relevant effect only for p_T^{veto} values below 30 GeV, and is mostly insignificant beyond that.

Fig. 16a shows a comparison of the dependence on p_T^{veto} for purely-resummed results at two different logarithmic orders. The central predictions are very similar at NNLO and N^3LL_p and are consistent within uncertainties for all values of p_T^{veto} . Fig. 16b compares the matched N^3LL_p+NNLO and NNLO results. The NNLO prediction has large uncertainties over the whole range of p_T^{veto} and only overlaps with N^3LL_p+NNLO around 40 GeV and higher. The difference between the central resummed and fixed-order results is significant (around 10%) for typical values of p_T^{veto} around 30 GeV. For most relevant values of p_T^{veto} at the LHC, resummation is clearly important for providing a precision prediction for this process.

5.5 Higgs production

For gluon fusion Higgs production an important topic is the inclusion of finite top-quark mass effects. Although at NNLO these could be included exactly [56, 57], the mass effects are not relevant in the jet-vetoed case [58] at the current level of precision. A simple overall one-loop rescaling factor that takes into account the full mass dependence is sufficient to introduce mass effects into $m_t \rightarrow \infty$ EFT predictions. In the resummation formalism, the coefficient for the matching of Higgs production in QCD onto SCET can be calculated in two ways, referred to as one-step and two-step procedures.

5.5.1 One-step and two-step schemes

The one-step procedure is based on the observation that the ratio m_H/m_t is not large in a logarithmic sense (c.f. $\rho = m_H^2/m_t^2 \approx 1/2$ and $\alpha_s \log 1/\rho \approx 0.07$). This procedure matches the full QCD result, typically obtained at higher orders as an expansion in the parameter r , onto SCET at the scale $\mu_h \sim m_H$. In this way, terms of order ρ are retained, but logs of m_t/m_H are neglected.

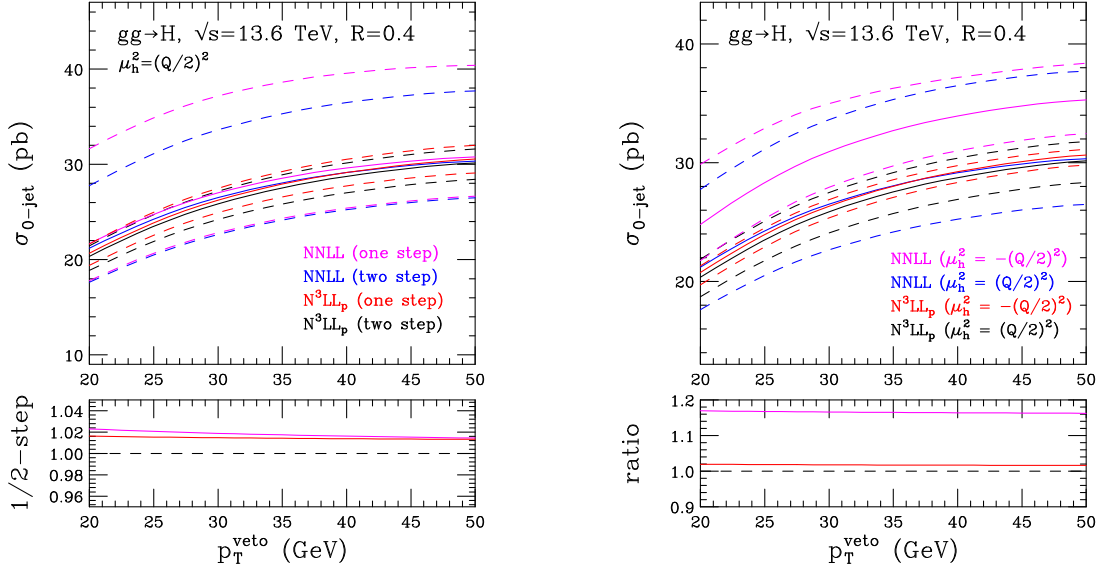
In the two-step procedure outlined in Refs. [59–62], the top quark is first integrated out at a scale $\mu_t \cong m_t$, and then the QCD effective Lagrangian is matched onto the SCET at a scale $\mu_h \cong m_H$. Running between μ_t and μ_h allows one to sum logarithms of m_t/m_H , and finite top-mass effects are included by scaling the result by a correction factor obtained at leading order (an increase with respect to the EFT result by a factor of 1.0653, see Eq. (G.5)). Terms enhanced by powers of m_H/m_t are thus only included in an approximate fashion at NLO and beyond. The one-step procedure is described in detail in Appendix G.1 and the two-step procedure is described in Appendix G.2.

We compare the numerical difference between the one- and two-step schemes, computed at $\sqrt{s} = 13.6$ TeV and for $R = 0.4$ in Fig. 17a. Guided by fixed-order results, and in accord with previous studies of this process [14], we set the hard (renormalization) scale using $\mu_h = Q/2$. We observe that the one-step scheme results in a cross-section that is about 1.7–2.3% larger at NNLL and only 1.6% larger at N³LL_p. This small difference occurs if one works rigorously at a fixed order of α_s . Working at a fixed order in α_s in the component parts of the two-step scheme can lead to larger differences, as described in more detail in Appendix G.3.

5.5.2 Time-like vs. space-like μ_h^2

We now study the impact of choosing a time-like hard scale for the calculation of the Higgs cross-section. To do this, we compare $\mu_h^2 = (Q/2)^2$ (the space-like scale) with $\mu_h^2 = -(Q/2)^2$ (the time-like scale). The use of a time-like hard scale allows us to resum certain π^2 terms, by employing a complex strong coupling [51]. For this comparison, we consider purely resummed results at NNLL and N³LL_p accuracy.

Results are shown in Fig. 17b, for the two-step scheme computed at $\sqrt{s} = 13.6$ TeV with $R = 0.4$. We observe that at NNLL, the resummation of the π^2 terms significantly enhances



(a) Results in the one- or two-step scheme. The lower panel shows the ratio of the one-step to the two-step result.

(b) Results using a central scale of either $\mu_h^2 = Q^2$ or $\mu_h^2 = -Q^2$. The lower panel shows the ratio of the result for $\mu_h^2 = -Q^2$ to the one for $\mu_h^2 = Q^2$.

Figure 17: Comparison of NNLL and N^3LL_p predictions for Higgs production at $\sqrt{s} = 13.6$ TeV as a function of the jet veto.

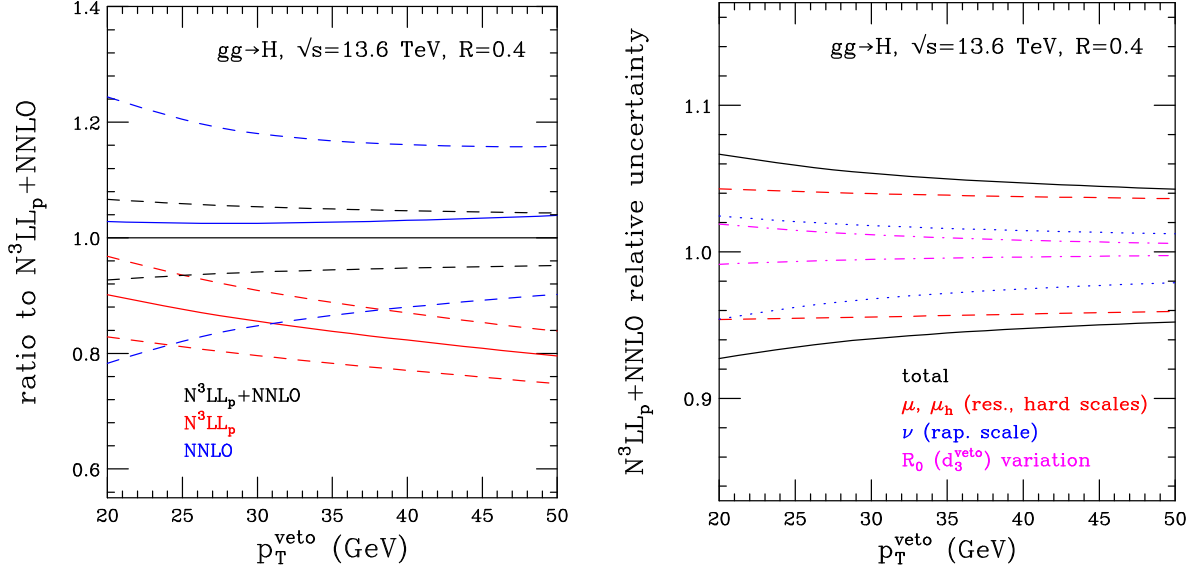
the cross-section by 17%. However, at N^3LL_p accuracy, this resummation only leads to a small increase of 2% in the cross-section.

Results for the matched vetoed cross-section are shown in Fig. 18a. After matching, we observe substantial agreement between the NNLO and N^3LL_p +NNLO calculations within uncertainties. The central predictions differ by about 5% across the range, but the uncertainties are substantially smaller in the resummed calculation.

The estimated uncertainty on the matched N^3LL_p +NNLO prediction, broken down into the various sources that we consider, is shown in Fig. 18b. Although the uncertainty from the variation of d_3^{veto} reaches 2% for $p_T^{\text{veto}} = 20$ GeV, the uncertainty from the variation of the hard (renormalization) and resummation (factorization) scales dominates across the entire range.

6 Conclusions

We have presented a comprehensive study of jet-veto resummation in the production of color singlet final states using the most up-to-date theoretical ingredients and achieving N^3LL_p accuracy. Our implementation in MCFM improves upon previous public NNLL calculations by reducing theoretical uncertainties, as demonstrated by comparisons with ATLAS and CMS



(a) Comparison of NNLL, $N^3\text{LL}_p$ and $N^3\text{LL}_p + \text{NNLO}$ predictions.

(b) Uncertainty breakdown of the $N^3\text{LL}_p + \text{NNLO}$ prediction.

Figure 18: Results for Higgs production at $\sqrt{s} = 13.6$ TeV as a function of the jet veto.

results. Once the one remaining theoretical element, d_3^{veto} , becomes available, it will be simple to upgrade our predictions to full $N^3\text{LL}$ accuracy.

The primary motivation for this work comes from the need for reliable and accurate predictions of jet-veto cross-sections in processes such as Higgs boson and W^+W^- production, which are commonly used to study new physics at the LHC. In these processes, the imposition of a jet veto is often necessary to suppress backgrounds and enhance sensitivity to new physics signals. Experimental results going beyond these two processes are much less frequent. We encourage the experimental collaborations to consider measurements of more Standard Model processes with a jet veto, as larger data samples become available, to better understand the dependence of these processes on the jet veto parameters p_T^{veto} and R .

In addition to providing improved predictions for jet-veto cross-sections, our work also serves as a valuable tool for testing and validation of general purpose shower Monte Carlo programs. Our code allows for a detailed investigation of the dependence on the jet parameters p_T^{veto} and R , providing a benchmark for assessing the logarithmic accuracy and reliability of Monte Carlo simulations in this important class of processes.

Our analysis shows that at the currently experimentally used values of p_T^{veto} in W and Z production, the logarithms are not large enough to justify the use of jet-veto resummation. In these cases, fixed-order perturbation theory, which can be used to give the results with a jet veto over a limited range of rapidities, is simpler and sufficient. We have also found that attempts to resum π^2 terms using a timelike renormalization point have little numerical

importance at N^3LL_p if the p_T^{veto} scale is around 20 to 30 GeV.

The production of a Higgs boson is an exception among single-boson processes. In this case, the combination of larger corrections from color factors and slightly larger values of the scale (m_H) appearing in the jet veto logarithms make resummation an important tool for improving the accuracy of predictions. In the appendix we have investigated the differences between the one-step and two-step procedures for calculating the hard function at the scale of p_T^{veto} . We find agreement within 2% of these two approaches.

The W^+W^- production process, where the jet veto has experimental importance, requires both resummation and matching to NNLO. For the ZZ process resummation is mandatory but the matching to fixed order is less important. Although this reflects the expectation that the resummed prediction is more accurate for systems of higher invariant mass, these findings depend on the exact nature of the cuts for each process. Our work provides a comprehensive theoretical framework for studying jet vetoes in vector boson pair processes, and as data becomes available, a comparative experimental study would be of great interest and could help to validate our theoretical predictions.

Acknowledgments

RKE would like to thank Simone Alioli, Thomas Becher, Andrew Gilbert, Pier Monni and Philip Sommer for useful discussions. In addition, RKE would like to thank TTP in Karlsruhe for hospitality during the drafting of this paper. TN would like to thank Robert Szafron for useful discussions. SS is supported in part by the SERB-MATRICES under Grant No. MTR/2022/000135. This manuscript has been authored by Fermi Research Alliance, LLC under Contract No. DE-AC02-07CH11359 with the U.S. Department of Energy, Office of Science, Office of High Energy Physics. This research used resources of the Wilson High-Performance Computing Facility at Fermilab. This research also used resources of the National Energy Research Scientific Computing Center (NERSC), a U.S. Department of Energy Office of Science User Facility located at Lawrence Berkeley National Laboratory, operated under Contract No. DE-AC02-05CH11231 using NERSC award HEP-ERCAP0021890.

A Reduced beam functions

We have used the two loop beam function in the presence of a jet veto calculated in Ref. [24]. Their calculation, together with the corresponding soft function [25] has been performed in SCET using the exponential rapidity regulator [27]. The beam function for quark initiated processes in the presence of a jet veto has also been presented in Mellin space in Ref. [63].

The calculation in Ref. [24] has a perturbative expansion,

$$I_{ij} = \sum_{k=0}^{\infty} \left(\frac{\alpha_s}{4\pi}\right)^k I_{ij}^{(k)}. \quad (\text{A.1})$$

The beam functions with a jet veto are decomposed into a reference observable, the beam function for the transverse momentum of a color singlet observable and a remainder term accounting for the effects of jet clustering,

$$I_{ij}(x, Q, p_T^{\text{veto}}, R; \mu, \nu) = I_{ij}^\perp(x, Q, p_T^{\text{veto}}; \mu, \nu) + \Delta I_{ij}(x, Q, p_T^{\text{veto}}, R; \mu, \nu). \quad (\text{A.2})$$

Since the divergence structure of the reference observable is the same as the beam function with a jet veto, ΔI_{ij} can be calculated in four dimensions. Results for the reference observable are available in Refs. [64, 65].

The reduced beam function kernels \bar{I} as used in our setup are extracted from the coefficient I as

$$\bar{I}_{ij}(z, p_T^{\text{veto}}, R, \mu) = e^{-h^A(p_T^{\text{veto}}, \mu)} I_{ij}(z, p_T^{\text{veto}}, R, \mu). \quad (\text{A.3})$$

They similarly follow a perturbative expansion

$$\bar{I}_{ik}(z, p_T^{\text{veto}}, R, \mu) = \delta_{ik} \delta(1-z) + \frac{\alpha_s}{4\pi} \bar{I}_{ik}^{(1)}(z, p_T^{\text{veto}}, \mu) + \left(\frac{\alpha_s}{4\pi}\right)^2 \bar{I}_{ik}^{(2)}(z, p_T^{\text{veto}}, R, \mu) + \mathcal{O}(\alpha_s^3). \quad (\text{A.4})$$

Contributions at order α_s

The α_s contributions to \bar{I} were first obtained in Refs. [3, 50] and read,

$$\bar{I}_{ij}(z, p_T^{\text{veto}}, R, \mu) = \delta(1-z) \delta_{ij} + \frac{\alpha_s}{4\pi} \left[-2P_{ij}^{(1)}(z) L_\perp + R_{ij}^{(1)}(z) \right] + \mathcal{O}(\alpha_s^2), \quad (\text{A.5})$$

where $L_\perp = 2 \ln(\mu/p_T^{\text{veto}})$. R is the jet measure used in Eq. (2.1) and $R^{(1)}(z)$ is a remainder function given below. At this order there is no dependence on the jet radius, R .

Throughout this paper we expand in powers of $\alpha_s/(4\pi)$. The one exception to this rule are the perturbative DGLAP splitting functions,

$$P_{ij}(z) = \frac{\alpha_s}{2\pi} P^{(1)}(z) + \left(\frac{\alpha_s}{2\pi}\right)^2 P^{(2)}(z) + \dots \quad (\text{A.6})$$

Explicit expressions for $P^{(1)}$ and $P^{(2)}$ are given in Appendices C.2 and C.3. The remainder functions at order α_s are [66]

$$\begin{aligned} R_{qq}^{(1)}(z) &= C_F \left[2(1-z) - \frac{\pi^2}{6} \delta(1-z) \right], & R_{qg}^{(1)}(z) &= 4T_F z(1-z), \\ R_{gg}^{(1)}(z) &= -C_A \frac{\pi^2}{6} \delta(1-z), & R_{gq}^{(1)}(z) &= 2C_F z. \end{aligned} \quad (\text{A.7})$$

where $C_A = 3, C_F = \frac{4}{3}, T_F = \frac{1}{2}$.

Contributions at order α_s^2

At order α_s^2 we have

$$\begin{aligned} \bar{I}_{ik}^{(2)}(z, p_T^{\text{veto}}, R, \mu) &= [2P_{ij}^{(1)}(x) \otimes P_{jk}^{(1)}(y) - \beta_0 P_{ik}^{(1)}(z)] L_\perp^2 \\ &+ [-4P_{ik}^{(2)}(z) + \beta_0 R_{ik}^{(1)}(z) - 2R_{ij}^{(1)}(x) \otimes P_{jk}^{(1)}(y)] L_\perp + R_{ik}^{(2)}(z, R). \end{aligned} \quad (\text{A.8})$$

In this equation \otimes represents a convolution,

$$f(x) \otimes g(y) = \int_0^1 dx \int_0^1 dy f(x) g(y) \delta(z - xy) = \int_z^1 \frac{dy}{y} f(z/y) g(y). \quad (\text{A.9})$$

Explicit expressions for $P^{(1)}$ and $P^{(2)}$ are given in Appendices C.2 and C.3. The expressions for $P^{(1)} \otimes P^{(1)}$, $R^{(1)} \otimes P^{(1)}$ are given in appendix C.4.

The results from Refs. [24, 25] recast in the language of reduced beam functions allow us to extract $R_{ik}^{(2)}(z, R)$. We have checked that the reduced beam functions have the form predicted by Eqs. (A.5) and (A.8). In addition, we have confirmed the known results for the α_s^2 R -dependent contribution to the collinear anomaly exponent. The result for the collinear anomaly exponent is given in Section 2.1.

A.1 Structure of the two-loop reduced beam function

While a numerical evaluation of the analytical formulas for the reduced beam functions is possible, we choose to perform a spline interpolation for improved numerical efficiency.

The reduced beam functions contain distributions of the following structure,

$$\begin{aligned} \bar{I}_{ij}^{(2)}(z, p_T^{\text{veto}}, R, \mu) &= \bar{I}_{ij,-1}^{(2)}(p_T^{\text{veto}}, R, \mu) \delta(1-z) + \bar{I}_{ij,0}^{(2)}(p_T^{\text{veto}}, R, \mu) D_0(1-z) \\ &+ \bar{I}_{ij,1}^{(2)}(p_T^{\text{veto}}, R, \mu) D_1(1-z) + \bar{I}_{ij,2}^{(2)}(z, p_T^{\text{veto}}, R, \mu), \end{aligned} \quad (\text{A.10})$$

where,

$$D_0(1-z) = \frac{1}{[1-z]_+}, \quad D_1(1-z) = \left[\frac{\ln(1-z)}{(1-z)} \right]_+. \quad (\text{A.11})$$

$\bar{I}_{ij,2}^{(2)}(z, p_T^{\text{veto}}, R, \mu)$ contains terms which are regular at $z = 1$.

The analytic results for the beam function of Ref. [24] are presented as a power series in R up to powers of R^8 . The functions themselves contain powers of $1/(1-z)^n$, in certain cases up to $n = 7$ or 8 . However, these singularities at $z = 1$ are fictitious as can be seen by explicit expansion. The beam functions require special treatment in this region for numerical stability.

The dominant region in the convolution of the function \bar{I} with the parton distributions is precisely the region $z \sim 1$. If we assume a parton distribution $f(x) \sim 1/x$ we have,

$$\bar{I} \otimes f = \int_x^1 \frac{dz}{z} \bar{I}(z) f(x/z) \sim \frac{1}{x} \int_x^1 dz \bar{I}(z), \quad (\text{A.12})$$

showing that all regions of z contribute equally to the integral. However if, as expected, the parton distribution function falls off more rapidly as $x \rightarrow 1$, say $f(x) \sim (1-x)^n/x$,

$$\bar{I} \otimes f = \int_x^1 \frac{dz}{z} \bar{I}(z) f(x/z) \sim \frac{1}{x} \int_x^1 dz \bar{I}(z) (1-x/z)^n. \quad (\text{A.13})$$

Thus, it is precisely the large values of z which are crucial for the integral. In other words, the parton shower process is dominated by cascade from nearby values of x . Larger cascades from more distant points are suppressed by the fall-off of the parton distributions. In view of the importance of the region $z = 1$, for numerical stability we perform an expansion about $z = 1$.

The absolute value of $R^{(2)}$ for the various parton transitions is shown in Fig. 19. Individual R -dependent terms contain expressions of the form $R^{2n}/(1-z)^k$ where k can be a high power. However, the singularity at $z = 1$ is only apparent. The resultant limiting forms obtained by series expansion about $z = 1$ are shown by the dashed lines in the figures. In practice, we switch to the expanded form at $z = 0.9$, although the figures demonstrate that the expanded forms are accurate down to much smaller values of z .

B Definition of the beta function and anomalous dimensions

The coefficients β_n , Γ_n^A and γ_n^g have perturbative expansions in powers of the renormalized coupling. Details are presented below.

B.1 Expansion of β -function

The beta function is defined as,

$$\begin{aligned} \frac{d\alpha_s(\mu)}{d \ln \mu} &= \beta(\mu) = -2\alpha_s(\mu) \sum_{n=0}^{\infty} \beta_n \left(\frac{\alpha_s}{4\pi} \right)^{n+1} \\ &= -2\alpha_s(\mu) \frac{\alpha_s(\mu)}{4\pi} \left[\beta_0 + \beta_1 \frac{\alpha_s(\mu)}{4\pi} + \beta_2 \left(\frac{\alpha_s(\mu)}{4\pi} \right)^2 + \beta_3 \left(\frac{\alpha_s(\mu)}{4\pi} \right)^3 + \dots \right]. \end{aligned} \quad (\text{B.1})$$

The coefficients of the $\overline{\text{MS}}$ β function to four loops are [67–69],

$$\begin{aligned} \beta_0 &= \frac{11}{3} C_A - \frac{4}{3} T_F n_f, \\ \beta_1 &= \frac{34}{3} C_A^2 - \left(\frac{20}{3} C_A + 4C_F \right) T_F n_f, \\ \beta_2 &= \frac{2857}{54} C_A^3 + \left(C_F^2 - \frac{205}{18} C_F C_A - \frac{1415}{54} C_A^2 \right) 2T_F n_f + \left(\frac{11}{9} C_F + \frac{79}{54} C_A \right) 4T_F^2 n_f^2, \\ \beta_3 &= C_A^4 \left(\frac{150653}{486} - \frac{44}{9} \zeta_3 \right) + C_A^3 T_F n_f \left(-\frac{39143}{81} + \frac{136}{3} \zeta_3 \right) \\ &\quad + C_A^2 C_F T_F n_f \left(\frac{7073}{243} - \frac{656}{9} \zeta_3 \right) + C_A C_F^2 T_F n_f \left(-\frac{4204}{27} + \frac{352}{9} \zeta_3 \right) \end{aligned}$$

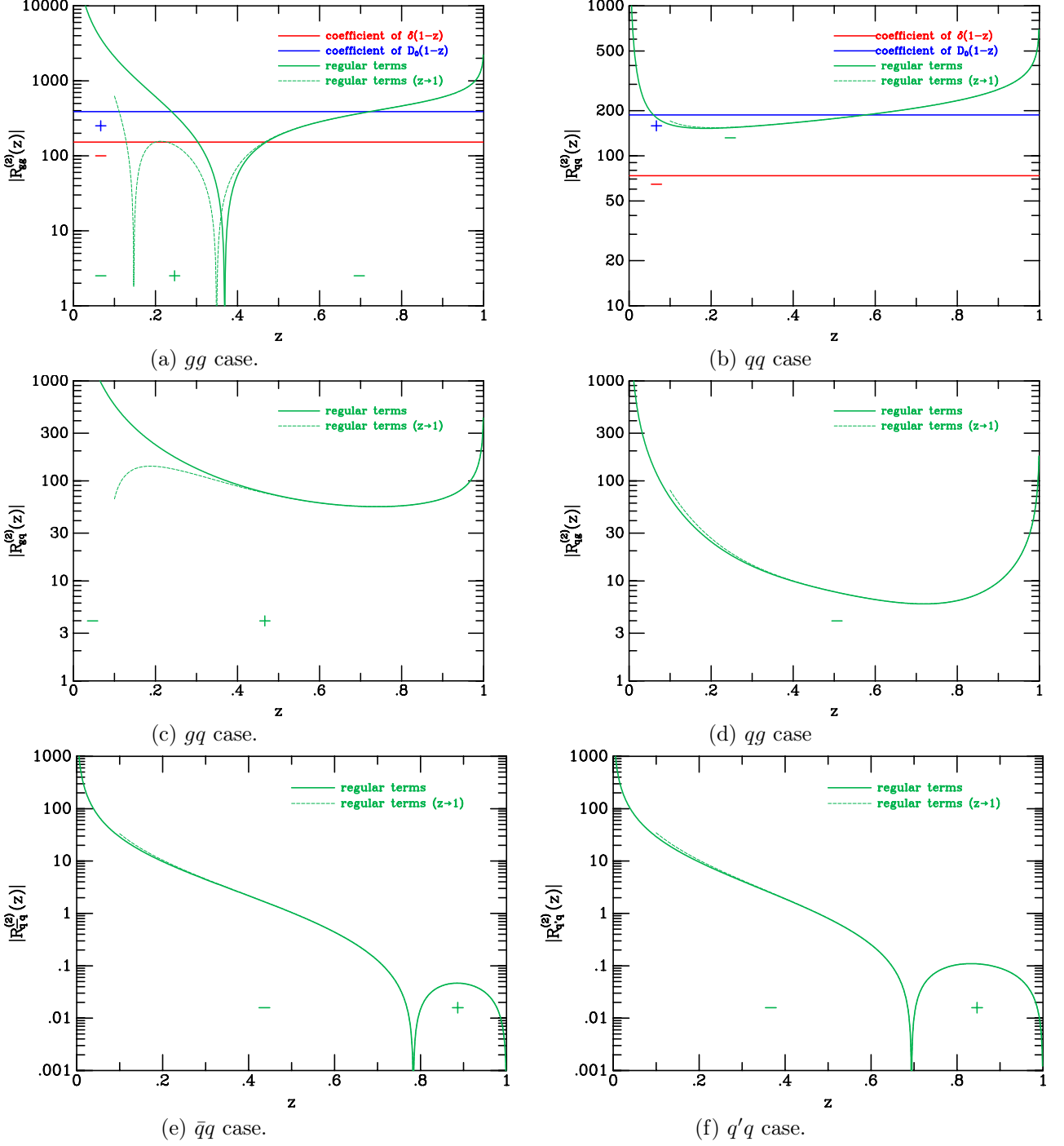


Figure 19: Absolute value of $R^{(2)}$ for jet measure $R = 0.5$. The $\bar{q}'q$ case is the same as the $q'q$ case. The sign of the contribution in the various regions is indicated.

$$+46C_F^3 T_F n_f + C_A^2 T_F^2 n_f^2 \left(\frac{7930}{81} + \frac{224}{9} \zeta_3 \right) + C_F^2 T_F^2 n_f^2 \left(\frac{1352}{27} - \frac{704}{9} \zeta_3 \right)$$

$$\begin{aligned}
& +C_A C_F T_F^2 n_f^2 \left(\frac{17152}{243} + \frac{448}{9} \zeta_3 \right) + \frac{424}{243} C_A T_F^3 n_f^3 + \frac{1232}{243} C_F T_F^3 n_f^3 \\
& + \frac{d_A^{abcd} d_A^{abcd}}{N_A} \left(-\frac{80}{9} + \frac{704}{3} \zeta_3 \right) + n_f \frac{d_F^{abcd} d_A^{abcd}}{N_A} \left(\frac{512}{9} - \frac{1664}{3} \zeta_3 \right) \\
& + n_f^2 \frac{d_F^{abcd} d_F^{abcd}}{N_A} \left(-\frac{704}{9} + \frac{512}{3} \zeta_3 \right). \tag{B.2}
\end{aligned}$$

For the normalization of the $SU(N)$ generators, the conventions of Refs. [69, 70] are,

$$\begin{aligned}
\frac{d_A^{abcd} d_A^{abcd}}{N_A} &= \frac{N^2(N^2 + 36)}{24}, & \frac{d_F^{abcd} d_A^{abcd}}{N_A} &= \frac{N(N^2 + 6)}{48}, & \frac{d_F^{abcd} d_F^{abcd}}{N_A} &= \frac{N^4 - 6N^2 + 18}{96N^2}, \\
N_A &= N^2 - 1, & N_F &= N. \tag{B.3}
\end{aligned}$$

Numerical values for the β -function coefficients are,

$$\begin{aligned}
\beta_0 &= 11 - \frac{2}{3} n_f, \\
\beta_1 &= 102 - \frac{38}{3} n_f, \\
\beta_2 &= \frac{2857}{2} - \frac{5033}{18} n_f + \frac{325}{54} n_f^2, \\
\beta_3 &= \frac{149753}{6} + 3564 \zeta_3 - \left(\frac{1078361}{162} + \frac{6508}{27} \zeta_3 \right) n_f + \left(\frac{50065}{162} + \frac{6472}{81} \zeta_3 \right) n_f^2 \\
&+ \frac{1093}{729} n_f^3. \tag{B.4}
\end{aligned}$$

B.2 Cusp Anomalous Dimension

The cusp anomalous dimension depends on the label B which takes the two values, $B = A, F$ for gluons and quarks, respectively. Its perturbative expansion is,

$$\Gamma_{\text{cusp}}^B(\mu) = \sum_{n=0}^{\infty} \Gamma_n^B \left(\frac{\alpha_s}{4\pi} \right)^{n+1}. \tag{B.5}$$

The coefficients up to four loops are [71, 72],

$$\Gamma_0^B = 4C_B, \quad (\text{B.6})$$

$$\Gamma_1^B = 16C_B \left\{ C_A \left(\frac{67}{36} - \frac{\pi^2}{12} \right) - \frac{5}{9} n_f T_F \right\}, \quad (\text{B.7})$$

$$\Gamma_2^B = 64C_B \left\{ C_A^2 \left(\frac{11\zeta_3}{24} + \frac{245}{96} - \frac{67\pi^2}{216} + \frac{11\pi^4}{720} \right) + n_f T_F C_F \left(\zeta_3 - \frac{55}{48} \right) \right. \\ \left. + n_f T_F C_A \left(-\frac{7\zeta_3}{6} - \frac{209}{216} + \frac{5\pi^2}{54} \right) - \frac{1}{27} (n_f T_F)^2 \right\}, \quad (\text{B.8})$$

$$\Gamma_3^B = 256C_B \left\{ C_A^3 \left(\frac{1309\zeta_3}{432} - \frac{11\pi^2\zeta_3}{144} - \frac{\zeta_3^2}{16} - \frac{451\zeta_5}{288} + \frac{42139}{10368} - \frac{5525\pi^2}{7776} + \frac{451\pi^4}{5760} - \frac{313\pi^6}{90720} \right) \right. \\ \left. + n_f T_F C_A^2 \left(-\frac{361\zeta_3}{54} + \frac{7\pi^2\zeta_3}{36} + \frac{131\zeta_5}{72} - \frac{24137}{10368} + \frac{635\pi^2}{1944} - \frac{11\pi^4}{2160} \right) \right. \\ \left. + n_f T_F C_F C_A \left(\frac{29\zeta_3}{9} - \frac{\pi^2\zeta_3}{6} + \frac{5\zeta_5}{4} - \frac{17033}{5184} + \frac{55\pi^2}{288} - \frac{11\pi^4}{720} \right) \right. \\ \left. + n_f T_F C_F^2 \left(\frac{37\zeta_3}{24} - \frac{5\zeta_5}{2} + \frac{143}{288} \right) + (n_f T_F)^2 C_A \left(\frac{35\zeta_3}{27} - \frac{7\pi^4}{1080} - \frac{19\pi^2}{972} + \frac{923}{5184} \right) \right. \\ \left. + (n_f T_F)^2 C_F \left(-\frac{10\zeta_3}{9} + \frac{\pi^4}{180} + \frac{299}{648} \right) + (n_f T_F)^3 \left(-\frac{1}{81} + \frac{2\zeta_3}{27} \right) \right\} \\ + 256 \frac{d_B^{abcd} d_A^{abcd}}{N_B} \left(\frac{\zeta_3}{6} - \frac{3\zeta_3^2}{2} + \frac{55\zeta_5}{12} - \frac{\pi^2}{12} - \frac{31\pi^6}{7560} \right) \\ + 256 n_f \frac{d_B^{abcd} d_F^{abcd}}{N_B} \left(\frac{\pi^2}{6} - \frac{\zeta_3}{3} - \frac{5\zeta_5}{3} \right). \quad (\text{B.9})$$

In addition to the relations in Eq. (B.3) we need the related quantities,

$$\frac{d_F^{abcd} d_A^{abcd}}{N_F} = \frac{(N^2 - 1)(N^2 + 6)}{48}, \quad \frac{d_F^{abcd} d_F^{abcd}}{N_F} = \frac{(N^2 - 1)(N^4 - 6N^2 + 18)}{96N^3}. \quad (\text{B.10})$$

B.3 Non-cusp anomalous dimension

The non-cusp anomalous dimension has the expansion,

$$\gamma^{q,g}(\mu) = \sum_{n=0}^{\infty} \gamma_n^{q,g} \left(\frac{\alpha_s}{4\pi} \right)^{n+1}. \quad (\text{B.11})$$

We take the coefficients up to three loops from ref. [73] Eq. I.4,

$$\gamma_0^q = -3C_F, \quad (\text{B.12})$$

$$\begin{aligned} \gamma_1^q &= C_F^2 \left(2\pi^2 - \frac{3}{2} - 24\zeta_3 \right) + C_F C_A \left(26\zeta_3 - \frac{961}{54} - \frac{11\pi^2}{6} \right) \\ &\quad + C_F T_F n_f \left(\frac{130}{27} + \frac{2\pi^2}{3} \right), \end{aligned} \quad (\text{B.13})$$

$$\begin{aligned} \gamma_2^q &= C_F^3 \left(-\frac{29}{2} - 3\pi^2 - \frac{8\pi^4}{5} - 68\zeta_3 + \frac{16\pi^2}{3}\zeta_3 + 240\zeta_5 \right) \\ &\quad + C_F^2 C_A \left(-\frac{151}{4} + \frac{205\pi^2}{9} + \frac{247\pi^4}{135} - \frac{844}{3}\zeta_3 - \frac{8\pi^2}{3}\zeta_3 - 120\zeta_5 \right) \\ &\quad + C_F C_A^2 \left(-\frac{139345}{2916} - \frac{7163\pi^2}{486} - \frac{83\pi^4}{90} + \frac{3526}{9}\zeta_3 - \frac{44\pi^2}{9}\zeta_3 - 136\zeta_5 \right) \\ &\quad + C_F^2 T_F n_f \left(\frac{2953}{27} - \frac{26\pi^2}{9} - \frac{28\pi^4}{27} + \frac{512}{9}\zeta_3 \right) \\ &\quad + C_F C_A T_F n_f \left(-\frac{17318}{729} + \frac{2594\pi^2}{243} + \frac{22\pi^4}{45} - \frac{1928}{27}\zeta_3 \right) \\ &\quad + C_F T_F^2 n_f^2 \left(\frac{9668}{729} - \frac{40\pi^2}{27} - \frac{32}{27}\zeta_3 \right). \end{aligned} \quad (\text{B.14})$$

From ref. [74], Eq A5 we take,

$$\gamma_0^g = -\beta_0, \quad (\text{B.15})$$

$$\begin{aligned} \gamma_1^g &= C_A^2 \left(\frac{11\pi^2}{18} - \frac{692}{27} + 2\zeta_3 \right) + C_A T_F n_f \left(\frac{256}{27} - \frac{2\pi^2}{9} \right) + 4C_F T_F n_f \\ &= C_A^2 \left(2\zeta_3 - \frac{59}{9} \right) + C_A \beta_0 \left(\frac{\pi^2}{6} - \frac{19}{9} \right) - \beta_1, \end{aligned} \quad (\text{B.16})$$

$$\begin{aligned} \gamma_2^g &= C_A^3 \left(-\frac{97186}{729} + \frac{6109\pi^2}{486} - \frac{319\pi^4}{270} + \frac{122}{3}\zeta_3 - \frac{20\pi^2}{9}\zeta_3 - 16\zeta_5 \right) \\ &\quad + C_A^2 T_F n_f \left(\frac{30715}{729} - \frac{1198\pi^2}{243} + \frac{82\pi^4}{135} + \frac{712}{27}\zeta_3 \right) \\ &\quad + C_A C_F T_F n_f \left(\frac{2434}{27} - \frac{2\pi^2}{3} - \frac{8\pi^4}{45} - \frac{304}{9}\zeta_3 \right) \\ &\quad - 2C_F^2 T_F n_f + C_A T_F^2 n_f^2 \left(-\frac{538}{729} + \frac{40\pi^2}{81} - \frac{224}{27}\zeta_3 \right) - \frac{44}{9} C_F T_F^2 n_f^2. \end{aligned} \quad (\text{B.17})$$

Primary references for the calculation of these coefficients can be found in Ref. [73].

We now present results for γ^S and γ^t which are needed for the implementation of the two-step calculation of the hard function for Higgs boson production. Following Ref. [61] we have, for the first three expansion coefficients of the anomalous dimension γ^S that enters the evolution

equation of the hard matching coefficient C^S (see also [59, 60]),

$$\gamma_0^S = 0, \quad (\text{B.18})$$

$$\gamma_1^S = C_A^2 \left(-\frac{160}{27} + \frac{11\pi^2}{9} + 4\zeta_3 \right) + C_A T_F n_f \left(-\frac{208}{27} - \frac{4\pi^2}{9} \right) - 8C_F T_F n_f, \quad (\text{B.19})$$

$$\begin{aligned} \gamma_2^S = & C_A^3 \left[\frac{37045}{729} + \frac{6109\pi^2}{243} - \frac{319\pi^4}{135} + \left(\frac{244}{3} - \frac{40\pi^2}{9} \right) \zeta_3 - 32\zeta_5 \right] \\ & + C_A^2 T_F n_f \left(-\frac{167800}{729} - \frac{2396\pi^2}{243} + \frac{164\pi^4}{135} + \frac{1424}{27} \zeta_3 \right) \\ & + C_A C_F T_F n_f \left(\frac{1178}{27} - \frac{4\pi^2}{3} - \frac{16\pi^4}{45} - \frac{608}{9} \zeta_3 \right) + 8C_F^2 T_F n_f \\ & + C_A T_F^2 n_f^2 \left(\frac{24520}{729} + \frac{80\pi^2}{81} - \frac{448}{27} \zeta_3 \right) + \frac{176}{9} C_F T_F^2 n_f^2. \end{aligned} \quad (\text{B.20})$$

The function γ^t is given by,

$$\gamma^t(\alpha_s) = \alpha_s^2 \frac{d}{d\alpha_s} \left(\frac{\beta(\alpha_s)}{\alpha_s^2} \right) = -2\beta_1 \left(\frac{\alpha_s}{4\pi} \right)^2 - 4\beta_2 \left(\frac{\alpha_s}{4\pi} \right)^3 - 6\beta_3 \left(\frac{\alpha_s}{4\pi} \right)^4 + \mathcal{O}(\alpha_s^5). \quad (\text{B.21})$$

As shown in Eq. (G.22) μ independence provides the constraint,

$$2\gamma^g(\alpha_s) = \gamma^t(\alpha_s) + \gamma^S(\alpha_s) + \beta(\alpha_s)/\alpha_s, \quad (\text{B.22})$$

leading to the simple relationship between the coefficients in γ^g and γ^S ,

$$\gamma_0^S = 2\gamma_0^g + 2\beta_0, \gamma_1^S = 2\gamma_1^g + 4\beta_1, \gamma_2^S = 2\gamma_2^g + 6\beta_2, \gamma_3^S = 2\gamma_3^g + 8\beta_3. \quad (\text{B.23})$$

C Definitions for beam function ingredients

C.1 Exponent h

We define the auxiliary functions h^B for $B = F, A$ which, when combined with the hard function and the collinear anomaly factor, will yield a renormalization group invariant hard function. $h^{F/A}$ is defined to satisfy the RGE equation,

$$\frac{d}{d \ln \mu} h^{F/A}(p_T^{\text{veto}}, \mu) = 2\Gamma_{\text{cusp}}^{F/A}(\mu) \ln \frac{\mu}{p_T^{\text{veto}}} - 2\gamma^{q/g}(\mu), \quad (\text{C.1})$$

The factor h removes logarithms from the beam function and has a perturbative expansion in terms of the renormalized coupling,

$$h^B(p_T^{\text{veto}}, \mu) = \frac{\alpha_s}{4\pi} h_0^B + \left(\frac{\alpha_s}{4\pi} \right)^2 h_1^B + \left(\frac{\alpha_s}{4\pi} \right)^3 h_2^B + \left(\frac{\alpha_s}{4\pi} \right)^4 h_3^B + \dots \quad (\text{C.2})$$

Thus for the particular case $B = F$ we have that,

$$\begin{aligned}
h_0^F(p_T^{\text{veto}}, \mu) &= \frac{1}{4}\Gamma_0^F L_\perp^2 - \gamma_0^q L_\perp, \\
h_1^F(p_T^{\text{veto}}, \mu) &= \frac{1}{12}\Gamma_0^F \beta_0 L_\perp^3 + \frac{1}{4}(\Gamma_1^F - 2\gamma_0^q \beta_0)L_\perp^2 - \gamma_1^q L_\perp, \\
h_2^F(p_T^{\text{veto}}, \mu) &= \frac{1}{24}\Gamma_0^F \beta_0^2 L_\perp^4 + \left(\frac{1}{12}\Gamma_0^F \beta_1 + \frac{1}{6}\Gamma_1^F \beta_0 - \frac{1}{3}\gamma_0^q \beta_0^2\right)L_\perp^3 \\
&\quad + \left(\frac{1}{4}\Gamma_2^F - \frac{1}{2}\gamma_0^q \beta_1 - \gamma_1^q \beta_0\right)L_\perp^2 - \gamma_2^q L_\perp, \\
h_3^F(p_T^{\text{veto}}, \mu) &= +\frac{1}{40}\Gamma_0^F \beta_0^3 L_\perp^5 + \left(\frac{5}{48}\Gamma_0^F \beta_0 \beta_1 + \frac{1}{8}\Gamma_1^F \beta_0^2 - \frac{1}{4}\gamma_0^q \beta_0^3\right)L_\perp^4 \\
&\quad + \left(\frac{1}{12}\Gamma_0^F \beta_2 + \frac{1}{6}\Gamma_1^F \beta_1 + \frac{1}{4}\Gamma_2^F \beta_0 - \frac{5}{6}\gamma_0^q \beta_0 \beta_1 - \gamma_1^q \beta_0^2\right)L_\perp^3 \\
&\quad + \left(\frac{1}{4}\Gamma_3^F - \frac{1}{2}\gamma_0^q \beta_2 - \gamma_1^q \beta_1 - \frac{3}{2}\gamma_2^q \beta_0\right)L_\perp^2 - \gamma_3^q L_\perp, \tag{C.3}
\end{aligned}$$

where $L_\perp = 2 \ln(\mu/p_T^{\text{veto}})$. The corresponding result for $B = A, q = g$, (i.e. for incoming gluons) is given by a similar expression *mutatis mutandis*. The expansion coefficients of the β -function, $\Gamma_{\text{cusp}}^{F/A}$ and $\gamma^{q/g}$, used in Eq. (C.3), are as given in Appendices B.1, B.2 and B.3.

C.2 One loop splitting functions

The one-loop DGLAP splitting functions as defined in [75] are

$$P_{qq}^{(1)}(z) = C_F \left(\frac{1+z^2}{1-z} \right)_+, \tag{C.4}$$

$$P_{qg}^{(1)}(z) = T_F [z^2 + (1-z)^2], \tag{C.5}$$

$$P_{gg}^{(1)}(z) = 2C_A \left[\frac{z}{(1-z)_+} + \frac{1-z}{z} + z(1-z) \right] + \frac{\beta_0}{2} \delta(1-z), \tag{C.6}$$

$$P_{gq}^{(1)}(z) = C_F \frac{1+(1-z)^2}{z}, \tag{C.7}$$

C.3 Two loop splitting functions

Now we turn to the two-loop anomalous dimensions that contribute at sub-leading log level to the transitions between parton types. In the quark sector there are four independent transitions that we must produce values for (viz. $q' \leftarrow q, \bar{q}' \leftarrow q, q \leftarrow q$ and $\bar{q} \leftarrow q$). They are expressed in terms of four functions,

$$P_{q'q}^{(2)} = P_{qq}^{S(2)}, P_{\bar{q}'q}^{(2)} = P_{\bar{q}q}^{S(2)}, P_{qq}^{(2)} = P_{qq}^{V(2)} + P_{qq}^{S(2)}, P_{\bar{q}q}^{(2)} = P_{\bar{q}q}^{V(2)} + P_{\bar{q}q}^{S(2)}. \tag{C.8}$$

At next-to-leading order, the functions P_{qq}^S and $P_{\bar{q}q}^S$ are non-zero, but we have the additional relation, $P_{qq}^S = P_{\bar{q}q}^S$. To facilitate the presentation we define the auxiliary functions,

$$p_{qq}(z) = \frac{2}{1-z} - 1 - z, \quad p_{qq}^{(r)}(z) = -1 - z, \quad (\text{C.9})$$

$$p_{qg}(z) = z^2 + (1-z)^2, \quad (\text{C.10})$$

$$p_{gq}(z) = \frac{1 + (1-z)^2}{z}, \quad (\text{C.11})$$

$$p_{gg}(z) = \frac{1}{1-z} + \frac{1}{z} - 2 + z(1-z), \quad p_{gg}^{(r)}(z) = \frac{1}{z} - 2 + z(1-z). \quad (\text{C.12})$$

The two valence functions needed for the quark sector are, [76–78],

$$\begin{aligned} P_{qq}^{V(2)}(z) &= C_F^2 \left\{ - \left[2 \ln z \ln(1-z) + \frac{3}{2} \ln z \right] p_{qq}(z) \right. \\ &\quad \left. - \left(\frac{3}{2} + \frac{7}{2} z \right) \ln z - \frac{1}{2} (1+z) \ln^2 z - 5(1-z) \right\} \\ &\quad + C_F C_A \left\{ (1+z) \ln z + \frac{20}{3} (1-z) + \left[\frac{1}{2} \ln^2 z + \frac{11}{6} \ln z \right] p_{qq}(z) \right. \\ &\quad \left. + \left[\frac{67}{18} - \frac{\pi^2}{6} \right] \left(\frac{1}{(1-z)_+} + p_{qq}^{(r)}(z) \right) \right\} \\ &\quad - C_F T_F n_f \left\{ \frac{4}{3} (1-z) + \frac{2}{3} p_{qq}(z) \ln z + \frac{10}{9} \left(\frac{1}{(1-z)_+} + p_{qq}^{(r)}(z) \right) \right\} \\ &\quad + \left\{ C_F^2 \left[\frac{3}{8} - \frac{\pi^2}{2} + 6\zeta_3 \right] + C_F C_A \left[\frac{17}{24} + \frac{11\pi^2}{18} - 3\zeta_3 \right] \right. \\ &\quad \left. - C_F T_F n_f \left[\frac{1}{6} + \frac{2\pi^2}{9} \right] \right\} \delta(1-z), \quad (\text{C.13}) \end{aligned}$$

$$P_{\bar{q}q}^{V(2)}(z) = C_F \left(C_F - \frac{C_A}{2} \right) \left\{ 2p_{qq}(-z) S_2(z) + 2(1+z) \ln z + 4(1-z) \right\}, \quad (\text{C.14})$$

and for the singlet function we have,

$$P_{qq}^{S(2)} = C_F T_F \left\{ \frac{20}{9z} - 2 + 6z - \frac{56}{9} z^2 + (1 + 5z + \frac{8}{3} z^2) \ln z - (1+z) \ln^2 z \right\}. \quad (\text{C.15})$$

The other three transitions are simply given by,

$$P_{qg}^{(2)} = C_F T_F \left\{ 2 - \frac{9}{2} z - \left(\frac{1}{2} - 2z \right) \ln z - \left(\frac{1}{2} - z \right) \ln^2 z + 2 \ln(1-z) \right\}$$

$$\begin{aligned}
& + \left[\ln^2 \left(\frac{1-z}{z} \right) - 2 \ln \left(\frac{1-z}{z} \right) - \frac{\pi^2}{3} + 5 \right] p_{qg}(z) \Big\} \\
& + C_A T_F \left\{ \frac{91}{9} + \frac{7}{9} z + \frac{20}{9z} + \left(\frac{68}{3} z - \frac{19}{3} \right) \ln z \right. \\
& - 2 \ln(1-z) - (1+4z) \ln^2 z + p_{qg}(-z) S_2(z) \\
& \left. + \left[-\frac{1}{2} \ln^2 z + \frac{22}{3} \ln z - \ln^2(1-z) + 2 \ln(1-z) + \frac{\pi^2}{6} - \frac{109}{9} \right] p_{qg}(z) \right\}, \quad (C.16)
\end{aligned}$$

$$\begin{aligned}
P_{gq}^{(2)}(z) & = C_F^2 \left\{ -\frac{5}{2} - \frac{7z}{2} + \left(2 + \frac{7}{2} z \right) \ln z - \left(1 - \frac{1}{2} z \right) \ln^2 z \right. \\
& - 2z \ln(1-z) - \left[3 \ln(1-z) + \ln^2(1-z) \right] p_{gq}(z) \Big\} \\
& + C_F C_A \left\{ \frac{28}{9} + \frac{65}{18} z + \frac{44}{9} z^2 - \left(12 + 5z + \frac{8}{3} z^2 \right) \ln z \right. \\
& + (4+z) \ln^2 z + 2z \ln(1-z) + S_2(z) p_{gq}(-z) \\
& \left. + \left[\frac{1}{2} - 2 \ln z \ln(1-z) + \frac{1}{2} \ln^2 z + \frac{11}{3} \ln(1-z) + \ln^2(1-z) - \frac{\pi^2}{6} \right] p_{gq}(z) \right\} \\
& + C_F T_F n_f \left\{ -\frac{4}{3} z - \left[\frac{20}{9} + \frac{4}{3} \ln(1-z) \right] p_{gq}(z) \right\}, \quad (C.17)
\end{aligned}$$

$$\begin{aligned}
P_{gg}^{(2)}(z) & = C_F T_F n_f \left\{ -16 + 8z + \frac{20}{3} z^2 + \frac{4}{3z} - (6+10z) \ln z - (2+2z) \ln^2 z \right\} \\
& + C_A T_F n_f \left\{ 2 - 2z + \frac{26}{9} \left(z^2 - \frac{1}{z} \right) - \frac{4}{3} (1+z) \ln z \right. \\
& \left. - \frac{20}{9} \left(\frac{1}{(1-z)_+} + p_{gg}^{(r)}(z) \right) \right\} \\
& + C_A^2 \left\{ \frac{27}{2} (1-z) + \frac{67}{9} \left(z^2 - \frac{1}{z} \right) - \left(\frac{25}{3} - \frac{11}{3} z + \frac{44}{3} z^2 \right) \ln z \right. \\
& + 4(1+z) \ln^2 z + 2p_{gg}(-z) S_2(z) \\
& \left. + \left[\ln^2 z - 4 \ln z \ln(1-z) \right] p_{gg}(z) + \left[\frac{67}{9} - \frac{\pi^2}{3} \right] \left(\frac{1}{(1-z)_+} + p_{gg}^{(r)}(z) \right) \right\} \\
& + \left\{ C_A^2 \left[\frac{8}{3} + 3\zeta_3 \right] - C_F T_F n_f - \frac{4}{3} C_A T_F n_f \right\} \delta(1-z). \quad (C.18)
\end{aligned}$$

The function $S_2(z)$ is defined by

$$S_2(z) = \int_{\frac{z}{1+z}}^{\frac{1}{1+z}} \frac{dy}{y} \ln \left(\frac{1-y}{y} \right). \quad (\text{C.19})$$

In terms of the dilogarithm function

$$\text{Li}_2(z) = - \int_0^z \frac{dy}{y} \ln(1-y), \quad (\text{C.20})$$

we have

$$S_2(z) = -2 \text{Li}_2(-z) + \frac{1}{2} \ln^2 z - 2 \ln z \ln(1+z) - \frac{\pi^2}{6}. \quad (\text{C.21})$$

C.4 $P^{(1)} \otimes P^{(1)}$ and $R^{(1)} \otimes P^{(1)}$

We give here expressions for the convolutions of functions appearing in the beam functions. The convolutions are defined as in Eq. (A.9). Similar expressions have been given in [1, 12] The convolutions of the one-loop DGLAP kernels from Eqs. (C.4) are,

$$P_{qq}^{(1)} \otimes P_{qq}^{(1)} = C_F T_F \left(2z - \frac{1}{2} + (2z - 4z^2 - 1) \ln z + (2 - 4z(1-z)) \ln(1-z) \right), \quad (\text{C.22})$$

$$\begin{aligned} P_{gg}^{(1)} \otimes P_{gg}^{(1)} &= C_A T_F \left(2(1+4z) \ln z + \frac{4}{3z} + 1 + 8z - \frac{31}{3} z^2 \right) \\ &+ (2C_A \ln(1-z) + \frac{\beta_0}{2}) P_{gg}^{(1)}(z), \end{aligned} \quad (\text{C.23})$$

$$P_{qq}^{(1)} \otimes P_{qq}^{(1)} = C_F^2 \left(2 - \frac{1}{2} z + (2-z) \ln z \right) + 2C_F P_{qq}^{(1)}(z) \ln(1-z), \quad (\text{C.24})$$

$$\begin{aligned} P_{gg}^{(1)} \otimes P_{gg}^{(1)} &= C_A C_F \left(8 + z + \frac{(4z^3 - 31)}{3z} - \frac{4(1+z+z^2)}{z} \ln z \right) \\ &+ (2C_A \ln(1-z) + \frac{\beta_0}{2}) P_{gg}^{(1)}(z), \end{aligned} \quad (\text{C.25})$$

$$P_{gq}^{(1)} \otimes P_{gq}^{(1)} = C_F T_F \left(2(1+z) \ln z + 1 - z + \frac{4(1-z^3)}{3z} \right), \quad (\text{C.26})$$

$$\begin{aligned} P_{qq}^{(1)} \otimes P_{qq}^{(1)} &= C_F^2 \left(8 \left[\frac{\ln(1-z)}{(1-z)} \right]_+ - 4(1+z) \ln(1-z) - 2(1-z) \right. \\ &\left. + \left(3 + 3z - \frac{4}{(1-z)} \right) \ln z \right) + 3C_F P_{qq}^{(1)}(z) - C_F^2 \left(\frac{9}{4} + 4\zeta_2 \right) \delta(1-z), \end{aligned} \quad (\text{C.27})$$

$$\begin{aligned} P_{gg}^{(1)} \otimes P_{gg}^{(1)} &= 4C_A^2 \left(2 \left[\frac{\ln(1-z)}{(1-z)} \right]_+ + 2 \left(\frac{1-z}{z} + z(1-z) - 1 \right) \ln(1-z) + 3(1-z) \right. \\ &\left. - \left(\frac{1}{1-z} + \frac{1}{z} - z^2 + 3z \right) \ln z - \frac{11(1-z^3)}{3z} \right) \\ &+ \beta_0 P_{gg}^{(1)}(z) - \left(\frac{\beta_0^2}{4} + 4C_A^2 \zeta_2 \right) \delta(1-z). \end{aligned} \quad (\text{C.28})$$

The convolutions of lowest order DGLAP kernels, Eq. (C.4) with the one-loop finite terms in the beam functions, Eq. (A.7) are,

$$R_{gg}^{(1)} \otimes P_{gg}^{(1)} = -C_A \zeta_2 P_{gg}^{(1)}(z), \quad (\text{C.29})$$

$$R_{qq}^{(1)} \otimes P_{qq}^{(1)} = 2C_F T_F \left((1-z)(1+2z) + 2z \ln z \right), \quad (\text{C.30})$$

$$R_{qq}^{(1)} \otimes P_{qq}^{(1)} = C_F \left(C_F (1-z) (4 \ln(1-z) - 2 \ln z - 1) - \zeta_2 P_{qq}^{(1)}(z) \right), \quad (\text{C.31})$$

$$R_{qq}^{(1)} \otimes P_{qq}^{(1)} = -4C_F T_F \left(1 + z \ln z - \frac{(1+2z^3)}{3z} \right), \quad (\text{C.32})$$

$$R_{qq}^{(1)} \otimes P_{gg}^{(1)} = -C_A T_F \left(16z \ln z - \frac{68}{3} z^2 + 20z + 4 - \frac{4}{3z} \right) \\ + \left(2C_A \ln(1-z) + \frac{\beta_0}{2} \right) R_{qq}^{(1)}(z), \quad (\text{C.33})$$

$$R_{qq}^{(1)} \otimes P_{qq}^{(1)} = C_F T_F (2z^2 + 2z - 4 - (2+4z) \ln z) - C_F \zeta_2 P_{qq}^{(1)}(z), \quad (\text{C.34})$$

$$R_{qq}^{(1)} \otimes P_{qq}^{(1)} = -C_F^2 (2z \ln z - 4z \ln(1-z) - z - 2), \quad (\text{C.35})$$

$$R_{gg}^{(1)} \otimes P_{qq}^{(1)} = -C_A \zeta_2 P_{qq}^{(1)}(z). \quad (\text{C.36})$$

D Rapidity anomalous dimension

Solving the collinear anomaly RG equation (Eq. (2.13)) as an expansion in α_s (Eq. (2.15)) we have that,

$$F_{gg}^{(0)}(p_T^{\text{veto}}, \mu_h) = \Gamma_0^A L_\perp + d_1^{\text{veto}}(R, A), \\ F_{gg}^{(1)}(p_T^{\text{veto}}, \mu_h) = \frac{1}{2} \Gamma_0^A \beta_0 L_\perp^2 + \Gamma_1^A L_\perp + d_2^{\text{veto}}(R, A), \\ F_{gg}^{(2)}(p_T^{\text{veto}}, \mu_h) = \frac{1}{3} \Gamma_0^A \beta_0^2 L_\perp^3 + \frac{1}{2} (\Gamma_0^A \beta_1 + 2\Gamma_1^A \beta_0) L_\perp^2 \\ + (\Gamma_2^A + 2\beta_0 d_2^{\text{veto}}(R, A)) L_\perp + d_3^{\text{veto}}(R, A), \\ F_{gg}^{(3)}(p_T^{\text{veto}}, \mu_h) = \frac{1}{4} \beta_0^3 \Gamma_0^A L_\perp^4 + (\Gamma_1^A \beta_0^2 + \frac{5}{6} \Gamma_0^A \beta_0 \beta_1) L_\perp^3 \\ + \left(\frac{1}{2} \Gamma_0^A \beta_2 + \Gamma_1^A \beta_1 + \frac{3}{2} \Gamma_2^A \beta_0 + 3d_2^{\text{veto}}(R, A) \beta_0^2 \right) L_\perp^2 \\ + (\Gamma_3^A + 3d_3^{\text{veto}}(R, A) \beta_0 + 2d_2^{\text{veto}}(R, A) \beta_1) L_\perp + d_4^{\text{veto}}(R, A). \quad (\text{D.1})$$

where $L_\perp = 2 \ln(\mu_h/p_T^{\text{veto}})$. The corresponding result for F_{qq} is given in Eq. (2.16). Because F_{gg} appears in the exponent, we see that d_1^{veto} contributes in NLL, d_2^{veto} in NNLL, and d_3^{veto} in N³LL.

D.1 d_2^{veto} expansion

The expansion coefficients for d_2^{veto} , which is defined in Eq. (2.18), are given by [4, 5, 12],

$$\begin{aligned}
c_L^A &= \frac{131}{72} - \frac{\pi^2}{6} - \frac{11}{6} \ln 2 = -1.096259, \\
c_0^A &= -\frac{805}{216} + \frac{11\pi^2}{72} + \frac{35}{18} \ln 2 + \frac{11}{6} \ln^2 2 + \frac{\zeta_3}{2} = 0.6106495, \\
c_2^A &= \frac{1429}{172800} + \frac{\pi^2}{48} + \frac{13}{180} \ln 2 = 0.263947, \\
c_4^A &= -\frac{9383279}{406425600} - \frac{\pi^2}{3456} + \frac{587}{120960} \ln 2 = -0.0225794, \\
c_6^A &= \frac{74801417}{97542144000} - \frac{23}{67200} \ln 2 = 5.29625 \cdot 10^{-4}, \\
c_8^A &= -\frac{50937246539}{2266099089408000} - \frac{\pi^2}{24883200} + \frac{28529}{1916006400} \ln 2 = -1.25537 \cdot 10^{-5}, \\
c_{10}^A &= \frac{348989849431}{243708656615424000} - \frac{3509}{3962649600} \ln 2 = 8.18201 \cdot 10^{-7}.
\end{aligned} \tag{D.2}$$

and

$$\begin{aligned}
c_L^f &= -\frac{23}{36} + \frac{2}{3} \ln 2 = -0.1767908, \\
c_0^f &= \frac{157}{108} - \frac{\pi^2}{18} - \frac{8}{9} \ln 2 - \frac{2}{3} \ln^2 2 = -0.03104049, \\
c_2^f &= \frac{3071}{86400} - \frac{7}{360} \ln 2 = 0.0220661, \\
c_4^f &= -\frac{168401}{101606400} + \frac{53}{30240} \ln 2 = -4.42544 \cdot 10^{-4}, \\
c_6^f &= \frac{7001023}{48771072000} - \frac{11}{100800} \ln 2 = 6.79076 \cdot 10^{-5}, \\
c_8^f &= -\frac{5664846191}{566524772352000} + \frac{4001}{479001600} \ln 2 = -4.20958 \cdot 10^{-6}, \\
c_{10}^f &= \frac{68089272001}{83774850711552000} - \frac{13817}{21794572800} \ln 2 = 3.73334 \cdot 10^{-7},
\end{aligned} \tag{D.3}$$

We see that for values of the jet radius $R < 1$ the terms c_6, c_8 and c_{10} can be dropped.

For the gluon case the expansion of the function in numerical form is,

$$\begin{aligned}
f(R, A) &= -(1.0963 C_A + 0.1768 T_{Fnf}) \ln R + (0.6106 C_A - 0.0310 T_{Fnf}) \\
&\quad + (-0.5585 C_A + 0.0221 T_{Fnf}) R^2 \\
&\quad + (0.0399 C_A - 0.0004 T_{Fnf}) R^4 + \dots,
\end{aligned} \tag{D.4}$$

whereas for the quark case we have

$$\begin{aligned}
f(R, F) &= -(1.0963 C_A + 0.1768 T_{Fnf}) \ln R + (0.6106 C_A - 0.0310 T_{Fnf}) \\
&\quad + (-0.8225 C_F + 0.2639 C_A + 0.0221 T_{Fnf}) R^2 \\
&\quad + (0.0625 C_F - 0.02258 C_A - 0.0004 T_{Fnf}) R^4 + \dots.
\end{aligned} \tag{D.5}$$

E Renormalization Group Evolution

The evolution equation matching for a generic hard matching coefficient C has the form,

$$\frac{d}{d \ln \mu} \ln C(Q^2, \mu) = \left[\Gamma_{\text{cusp}}(\alpha_s(\mu)) \ln \frac{Q^2}{\mu^2} + \gamma(\alpha_s(\mu)) \right]. \quad (\text{E.1})$$

Following ref. [26] the solution to the evolution equation Eq. (E.1) is,

$$C(Q^2, \mu) = \exp [2S(\mu_h, \mu) - a^\gamma(\mu_h, \mu)] \left(\frac{Q^2}{\mu_h^2} \right)^{-a^\Gamma(\mu_h, \mu)} C(Q^2, \mu_h), \quad (\text{E.2})$$

$$\ln C(Q^2, \mu) = 2S(\mu_h, \mu) - a^\gamma(\mu_h, \mu) - a^\Gamma(\mu_h, \mu) \ln \left(\frac{Q^2}{\mu_h^2} \right) + \ln C(Q^2, \mu_h), \quad (\text{E.3})$$

where $\mu_h \sim Q$ is a hard matching scale at which the Wilson coefficient C is calculated using fixed-order perturbation theory. The Sudakov exponent S and the exponents a^γ, a^Γ are the solutions to the auxiliary differential equations,

$$\frac{d}{d \ln \mu} S(\nu, \mu) = -\Gamma_{\text{cusp}}(\alpha_s(\mu)) \ln \frac{\mu}{\nu}, \quad (\text{E.4})$$

$$\frac{d}{d \ln \mu} a^\Gamma(\nu, \mu) = -\Gamma_{\text{cusp}}(\alpha_s(\mu)), \quad (\text{E.5})$$

$$\frac{d}{d \ln \mu} a^\gamma(\nu, \mu) = -\gamma(\alpha_s(\mu)). \quad (\text{E.6})$$

with the boundary conditions $S(\nu, \nu) = a^\Gamma(\nu, \nu) = a^\gamma(\nu, \nu) = 0$ at $\mu = \nu$. Differentiating Eq. (E.3) we recover Eq. (E.1).

The solutions to the evolution equation are conveniently expressed in terms of the running coupling,

$$a^\Gamma(\nu, \mu) = - \int_{\alpha_s(\nu)}^{\alpha_s(\mu)} d\alpha \frac{\Gamma_{\text{cusp}}(\alpha)}{\beta(\alpha)}, \quad (\text{E.7})$$

$$S(\nu, \mu) = - \int_{\alpha_s(\nu)}^{\alpha_s(\mu)} d\alpha \frac{\Gamma_{\text{cusp}}(\alpha)}{\beta(\alpha)} \int_{\alpha_s(\nu)}^{\alpha} \frac{d\alpha'}{\beta(\alpha')}. \quad (\text{E.8})$$

Substituting the values for the beta function coefficients in the $\overline{\text{MS}}$ scheme given in Appendix B.1 and the values for cusp anomalous dimension given in Appendix B.2 into Eq. (E.7) we obtain,

$$a^\Gamma(\mu_h, \mu) = a_0^\Gamma + a_1^\Gamma + a_2^\Gamma + a_3^\Gamma, \quad (\text{E.9})$$

where the coefficients in the expansion are,

$$a_0^\Gamma = \frac{\Gamma_0 \ln(r)}{2\beta_0}, \quad r = \alpha_s(\mu)/\alpha_s(\mu_h), \quad (\text{E.10})$$

$$a_1^\Gamma = \frac{\alpha_s(\mu_h)(r-1)(\beta_0\Gamma_1 - \beta_1\Gamma_0)}{8\pi\beta_0^2}, \quad (\text{E.11})$$

$$a_2^\Gamma = \frac{\alpha_s^2(\mu_h)(r^2-1)(-\beta_0\beta_1\Gamma_1 + \beta_0(\beta_0\Gamma_2 - \beta_2\Gamma_0) + \beta_1^2\Gamma_0)}{64\pi^2\beta_0^3}, \quad (\text{E.12})$$

$$a_3^\Gamma = -\alpha_s^3(\mu_h)(r^3-1) \times \frac{(\beta_0^2(-\beta_0\Gamma_3 + \beta_2\Gamma_1 + \beta_3\Gamma_0) - \beta_0\beta_1^2\Gamma_1 + \beta_0\beta_1(\beta_0\Gamma_2 - 2\beta_2\Gamma_0) + \beta_1^3\Gamma_0)}{384\pi^3\beta_0^4}. \quad (\text{E.13})$$

The solution for a^γ follows from the one for a^Γ by making the replacement $\Gamma_k \rightarrow \gamma_k$. The non-cusp anomalous dimensions γ are given in Appendix B.3.

Evaluating Eq. (E.8) to obtain the evolution for S we get,

$$S(\mu_h, \mu) = S^0 + S^1 + S^2. \quad (\text{E.14})$$

with,

$$S^0 = \frac{1}{8\beta_0^3} \left(\frac{8\pi\beta_0\Gamma_0(r + r(-\ln(r)) - 1)}{\alpha_s(\mu_h)r} + 2(r-1)(\beta_1\Gamma_0 - \beta_0\Gamma_1) + \ln(r)(2\beta_0\Gamma_1 + \beta_1\Gamma_0 \ln(r) - 2\beta_1\Gamma_0) \right), \quad (\text{E.15})$$

$$S^1 = -\frac{\alpha_s(\mu_h)}{32\pi\beta_0^4} \left(2\ln(r)(-\beta_0\beta_1\Gamma_1r + \beta_0\beta_2\Gamma_0 + \beta_1^2\Gamma_0(r-1)) + (r-1)(-\beta_0\beta_1\Gamma_1(r-3) + \beta_0(\beta_0(r-1)\Gamma_2 - \beta_2\Gamma_0(r+1)) + \beta_1^2\Gamma_0(r-1)) \right), \quad (\text{E.16})$$

$$S^2 = \frac{\alpha_s^2(\mu_h)}{256\pi^2\beta_0^5} \left(2\ln(r)(\beta_1r^2(-\beta_0\beta_1\Gamma_1 + \beta_0(\beta_0\Gamma_2 - \beta_2\Gamma_0) + \beta_1^2\Gamma_0) - \Gamma_0(\beta_0^2\beta_3 - 2\beta_0\beta_1\beta_2 + \beta_1^3)) + (r-1)(\beta_0^2(2(\beta_0(r+1)\Gamma_3 - 2\beta_2\Gamma_1) - \beta_3\Gamma_0(r+1)) + \beta_0\beta_1^2\Gamma_1(r+5) + \beta_0\beta_1(\beta_2\Gamma_0(r+5) - 3\beta_0(r+1)\Gamma_2) - 4\beta_1^3\Gamma_0) \right). \quad (\text{E.17})$$

E.1 Recovery of the double log formula

As we have seen S satisfies a RGE given by Eq. (E.4) with a solution given by Eq. (E.8). The leading term in S_0 , Eq. (E.15) is

$$S_0 \approx \frac{\pi\Gamma_0}{\beta_0^2\alpha_s(\mu_h)} \left(1 + \ln\left(\frac{1}{r}\right) - \frac{1}{r} \right), \quad (\text{E.18})$$

where $r = \alpha_s(\mu)/\alpha_s(\mu_h)$. In this form the presence of a double log is obscured. We can easily recover the double log by retaining only the leading terms. The leading expression for r is given by solving the equation for the beta function,

$$\frac{1}{r} = 1 - \frac{\alpha_s(\mu_h)}{2\pi} \beta_0 \ln\left(\frac{\mu_h}{\mu}\right), \quad (\text{E.19})$$

$$S_0 \approx \frac{\pi\Gamma_0}{\beta_0^2\alpha_s(\mu_h)} \left[\frac{\alpha_s(\mu_h)}{2\pi} \beta_0 \ln\left(\frac{\mu_h}{\mu}\right) + \ln\left(1 - \frac{\alpha_s(\mu_h)}{2\pi} \beta_0 \ln\left(\frac{\mu_h}{\mu}\right)\right) \right]. \quad (\text{E.20})$$

Expanding for small $\alpha_s(\mu_h) \ln(\mu_h/\mu)$ we get,

$$S(\mu_h, \mu) \approx -\frac{\Gamma_0}{2} \frac{\alpha_s(\mu_h)}{4\pi} \ln^2\left(\frac{\mu_h}{\mu}\right). \quad (\text{E.21})$$

This gives the expected log squared with a negative sign.

F The hard function for the Drell-Yan process

The form factors of the vector current have been presented several places in the literature [79–84]. The bare form factor is given as,

$$F^{q,\text{bare}}(q^2, \mu^2) = 1 + \left(\frac{\alpha_s^{\text{bare}}}{4\pi}\right) (\Delta)^\epsilon \mathcal{F}_1^q + \left(\frac{\alpha_s^{\text{bare}}}{4\pi}\right)^2 (\Delta)^{2\epsilon} \mathcal{F}_2^q + \mathcal{O}(\alpha_s^3), \quad (\text{F.1})$$

where,

$$\Delta = 4\pi e^{-\gamma_E} \left(\frac{\mu^2}{-q^2 - i0} \right). \quad (\text{F.2})$$

In the following we will drop $4\pi e^{-\gamma_E}$, so that all poles should be understood in the $\overline{\text{MS}}$ sense. The values found for the bare coefficients are,

$$\begin{aligned} \mathcal{F}_1^q = C_F & \left[-\frac{2}{\epsilon^2} - \frac{3}{\epsilon} + \zeta_2 - 8 + \epsilon \left(\frac{3\zeta_2}{2} + \frac{14\zeta_3}{3} - 16 \right) \right. \\ & \left. + \epsilon^2 \left(\frac{47\zeta_2^2}{20} + 4\zeta_2 + 7\zeta_3 - 32 \right) \right] + \mathcal{O}(\epsilon^3), \end{aligned} \quad (\text{F.3})$$

$$\begin{aligned} \mathcal{F}_2^q = C_F^2 & \left[\frac{2}{\epsilon^4} + \frac{6}{\epsilon^3} - \frac{1}{\epsilon^2} \left(2\zeta_2 - \frac{41}{2} \right) - \frac{1}{\epsilon} \left(\frac{64\zeta_3}{3} - \frac{221}{4} \right) \right. \\ & \left. - \left(13\zeta_2^2 - \frac{17\zeta_2}{2} + 58\zeta_3 - \frac{1151}{8} \right) \right] \\ & + C_F C_A \left[-\frac{11}{6\epsilon^3} + \frac{1}{\epsilon^2} \left(\zeta_2 - \frac{83}{9} \right) - \frac{1}{\epsilon} \left(\frac{11\zeta_2}{6} - 13\zeta_3 + \frac{4129}{108} \right) \right. \\ & \left. + \left(\frac{44\zeta_2^2}{5} - \frac{119\zeta_2}{9} + \frac{467\zeta_3}{9} - \frac{89173}{648} \right) \right] \\ & + C_F n_f \left[\frac{1}{3\epsilon^3} + \frac{14}{9\epsilon^2} + \frac{1}{\epsilon} \left(\frac{\zeta_2}{3} + \frac{353}{54} \right) + \left(\frac{14\zeta_2}{9} - \frac{26\zeta_3}{9} + \frac{7541}{324} \right) \right] + \mathcal{O}(\epsilon). \end{aligned} \quad (\text{F.4})$$

The renormalized form factor can then be written as,

$$F^q(\mu^2, q^2, \epsilon) = 1 + \left(\frac{\alpha_s(\mu)}{4\pi}\right) F_1^q(\mu^2, q^2, \epsilon) + \left(\frac{\alpha_s(\mu)}{4\pi}\right)^2 F_2^q(\mu^2, q^2, \epsilon) + \mathcal{O}(\alpha_s^3). \quad (\text{F.5})$$

where,

$$\begin{aligned} F_1^q(\mu^2, q^2, \epsilon) &= \Delta^\epsilon \mathcal{F}_1^q, \\ F_2^q(\mu^2, q^2, \epsilon) &= \Delta^{2\epsilon} \mathcal{F}_2^q - \frac{\beta_0}{\epsilon} \Delta^\epsilon \mathcal{F}_1^q. \end{aligned} \quad (\text{F.6})$$

In the full theory the matrix element between on-shell massless quark and gluon states, after charge renormalization is given by $F^q(\mu^2, q^2, \epsilon)$. Charge renormalization has removed the UV poles, but the renormalized form factor still contains IR poles.

The matrix element in the effective theory involves only scaleless, dimensionally regulated integrals and hence is equal to zero. This vanishing can be interpreted as a cancellation between ultra-violet and infrared poles:

$$\frac{1}{\epsilon_{\text{IR}}} - \frac{1}{\epsilon_{\text{UV}}}. \quad (\text{F.7})$$

After matching, the IR poles in the on-shell matrix element are effectively transformed into UV poles and need to be renormalized as follows,

$$\begin{aligned} C^V(\alpha_s(\mu^2), \mu^2, q^2) &= \lim_{\epsilon \rightarrow 0} (Z^V(\epsilon, \mu^2 q^2))^{-1} F^q(\mu^2, q^2, \epsilon), \\ \ln [C^V(\alpha_s(\mu^2), \mu^2, q^2)] &= \ln [F_q(\mu^2, q^2, \epsilon)] - \ln [Z^V(\epsilon, \mu^2, q^2)]. \end{aligned} \quad (\text{F.8})$$

The renormalization constant, Z^V contains only pure pole terms,

$$\begin{aligned} \ln Z^V(\epsilon, \mu^2, q^2) &= \left(\frac{\alpha_s}{4\pi}\right) \left[-\frac{\Gamma_0^F}{2\epsilon^2} + \frac{1}{2\epsilon} \left(\Gamma_0^F L + 2\gamma_0^q \right) \right] \\ &+ \left(\frac{\alpha_s}{4\pi}\right)^2 \left[\frac{3\Gamma_0^F \beta_0}{8\epsilon^3} - \frac{1}{\epsilon^2} \left[\frac{\Gamma_0^F \beta_0}{4} L - C_F (C_A \left(\frac{16}{9} + \zeta_2\right) + \frac{4}{9} n_f) \right] + \frac{1}{4\epsilon} \left(\Gamma_1^F L + 2\gamma_1^q \right) \right], \end{aligned} \quad (\text{F.9})$$

where $L = \ln((-q^2 - i0)/\mu^2)$.

The matching coefficients have a perturbative expansion in terms of the renormalized coupling,

$$C^V(\alpha_s(\mu^2), \mu^2, q^2) = 1 + \sum_{n=1}^{\infty} \left(\frac{\alpha_s(\mu^2)}{4\pi}\right)^n C_n^V(\mu^2, q^2). \quad (\text{F.10})$$

The matching coefficients, which are known to two loop order [85, 86] (and beyond [84]) for Drell-Yan production, can be obtained from Eq. (F.8):

$$C_1^V = C_F \left(-L^2 + 3L - 8 + \zeta_2 \right), \quad (\text{F.11})$$

$$\begin{aligned}
C_2^V &= C_F^2 \left(\frac{1}{2} L^4 - 3L^3 + \left(\frac{25}{2} - \zeta_2 \right) L^2 + \left(-\frac{45}{2} + 24\zeta_3 - 9\zeta_2 \right) L \right. \\
&\quad \left. + \frac{255}{8} - 30\zeta_3 + 21\zeta_2 - \frac{83}{10} \zeta_2^2 \right) \\
&\quad + C_F C_A \left(\frac{11}{9} L^3 + \left(-\frac{233}{18} + 2\zeta_2 \right) L^2 + \left(\frac{2545}{54} - 26\zeta_3 + \frac{22}{3} \zeta_2 \right) L \right. \\
&\quad \left. - \frac{51157}{648} + \frac{313}{9} \zeta_3 - \frac{337}{18} \zeta_2 + \frac{44}{5} \zeta_2^2 \right) \\
&\quad + C_F n_f \left(-\frac{2}{9} L^3 + \frac{19}{9} L^2 + \left(-\frac{209}{27} - \frac{4}{3} \zeta_2 \right) L + \frac{4085}{324} + \frac{2}{9} \zeta_3 + \frac{23}{9} \zeta_2 \right), \quad (\text{F.12})
\end{aligned}$$

where $L = \ln((-q^2 - i0)/\mu^2)$. C^V satisfies the renormalization group equation,

$$\frac{d}{d \ln \mu} \ln[C^V(\alpha_s(\mu^2), \mu^2, q^2)] = \Gamma_{\text{cusp}}^F(\mu) \ln\left(\frac{-q^2 - i0}{\mu^2}\right) + 2\gamma^q(\mu), \quad (\text{F.13})$$

with the anomalous dimensions as given in Appendix B.2 and Appendix B.3.

The derivation of the hard function for boson pair processes has been described in Ref. [87].

G The hard function for Higgs production

G.1 Implementation of one-step procedure

The one-step procedure [1, 13] is based on the observation that the ratio m_t/m_H is not large. For an on-shell Higgs boson the parameter, $m_H^2/m_t^2 \approx \frac{1}{2}$ whereas $\alpha_s \ln(m_t^2/m_H^2) \approx 0.65\alpha_s$, indicating that power corrections should be more important than resumming logarithms. The matching is performed at a scale μ_h by integrating out the top quark and all gluons and light quarks with off-shellness above μ_h .

The hard Wilson coefficient so defined satisfies the RGE,

$$\mu \frac{d}{d\mu} \ln C^H(m_t^2, q^2, \mu^2) = \Gamma_{\text{cusp}}^A(\alpha_s(\mu)) \ln\left(\frac{-q^2 - i0}{\mu^2}\right) + 2\gamma^g[\alpha_s(\mu)], \quad (\text{G.1})$$

where Γ_{cusp} and γ^g are given in Eqs. (B.5) and (B.11). As a consequence of Eq. (G.1) the Wilson coefficient has the following structure,

$$\begin{aligned}
C^H(m_t^2, q^2, \mu_h^2) &= \alpha_s(\mu_h) F_0^H\left(\frac{q^2}{4m_t^2}\right) \left\{ 1 + \frac{\alpha_s(\mu_h)}{4\pi} \left[C_1^H\left(\frac{-q^2 - i0}{\mu_h^2}\right) + F_1^H\left(\frac{q^2}{4m_t^2}\right) \right] \right. \\
&\quad \left. + \left(\frac{\alpha_s(\mu_h)}{4\pi} \right)^2 \left[C_2^H\left(\frac{-q^2 - i0}{\mu_h^2}, \frac{q^2}{4m_t^2}\right) + F_2^H\left(\frac{q^2}{4m_t^2}\right) \right] \right\}, \quad (\text{G.2})
\end{aligned}$$

The finite terms can be derived from Ref. [88],

$$F_0^H(z) = \frac{3}{2z} - \frac{3}{2z} \Big|_1 - \frac{1}{z} \Big| \begin{cases} \arcsin^2(\sqrt{z}), & 0 < z \leq 1, \\ \ln^2[-i(\sqrt{z} + \sqrt{z-1})], & z > 1, \end{cases} \quad (\text{G.3})$$

$$\approx 1 + \frac{7z}{30} + \frac{2z^2}{21} + \frac{26z^3}{525} + \frac{512z^4}{17325} + O(z^5), \quad z < 1. \quad (\text{G.4})$$

For the values of m_t and m_H in Table 2,

$$|F_0^H(z_0)|^2 = 1.0653, \quad z_0 = \frac{m_H^2}{4m_t^2}. \quad (\text{G.5})$$

The coefficients C_1^H and C_2^H are fixed by the Eq. (G.1).

$$C_1^H(L) = C_A \left(-L^2 + \frac{\pi^2}{6} \right), \quad (\text{G.6})$$

$$\begin{aligned} C_2^H(L, z) &= \frac{1}{2} C_A^2 L^4 + \frac{1}{3} C_A \beta_0 L^3 + C_A \left[\left(-\frac{4}{3} + \frac{\pi^2}{6} \right) C_A - \frac{5}{3} \beta_0 - F_1(z) \right] L^2 \\ &+ \left[\left(\frac{59}{9} - 2\zeta_3 \right) C_A^2 + \left(\frac{19}{9} - \frac{\pi^2}{3} \right) C_A \beta_0 - F_1(z) \beta_0 \right] L. \end{aligned} \quad (\text{G.7})$$

where $z = q^2/4/m_t^2$ and $L = \ln[(-q^2 - i0)/\mu_h^2]$.

The full analytic m_t dependence of the virtual two-loop corrections to $gg \rightarrow H$ in terms of harmonic polylogarithms were obtained in Refs. [89–91]. For our purposes the results expanded in m_H^2/m_t^2 from Refs. [88, 92, 93] will be sufficient. The functions $F_1^H(z), F_2^H(z)$ which, together with $F_0^H(z)$ in Eq. (G.4) encode the m_t dependence of the hard Wilson coefficient in Eq. (G.2). Following the procedure described in Appendix F they are easily extracted from Ref. [88],

$$\begin{aligned} F_1^H(z) &= \left(5 - \frac{38}{45} z - \frac{1289}{4725} z^2 - \frac{155}{1134} z^3 - \frac{5385047}{65488500} z^4 \right) C_A \\ &+ \left(-3 + \frac{307}{90} z + \frac{25813}{18900} z^2 + \frac{3055907}{3969000} z^3 + \frac{659504801}{1309770000} z^4 \right) C_F + \mathcal{O}(z^5) \quad (\text{G.8}) \\ F_2^H(z) &= (7C_A^2 + 11C_A C_F - 6C_F \beta_0) \ln(-4z - i0) + \left(-\frac{419}{27} + \frac{7\pi^2}{6} + \frac{\pi^4}{72} - 44\zeta_3 \right) C_A^2 \\ &+ \left(-\frac{217}{2} - \frac{\pi^2}{2} + 44\zeta_3 \right) C_A C_F + \left(\frac{2255}{108} + \frac{5\pi^2}{12} + \frac{23\zeta_3}{3} \right) C_A \beta_0 - \frac{5}{6} C_A T_F \\ &+ \frac{27}{2} C_F^2 + \left(\frac{41}{2} - 12\zeta_3 \right) C_F \beta_0 - \frac{4}{3} C_F T_F \\ &+ z \left[C_A^2 \left(\frac{11723}{384} \zeta_3 - \frac{404063}{14400} - \frac{223}{108} \ln(-4z - i0) - \frac{19}{135} \pi^2 \right) \right. \\ &+ C_F C_A \left(\frac{2297}{16} \zeta_3 - \frac{1099453}{8100} - \frac{242}{135} \ln(-4z - i0) - \frac{953}{540} \pi^2 + \frac{28}{15} \pi^2 \ln 2 \right) \\ &+ C_F^2 \left(\frac{13321}{96} \zeta_3 - \frac{36803}{240} + \frac{7}{3} \pi^2 - \frac{56}{15} \pi^2 \ln 2 \right) \\ &+ C_F \left(\frac{77}{12} \zeta_3 - \frac{4393}{405} - \frac{7337}{2700} \beta_0 + \frac{39}{10} \ln(-4z - i0) \beta_0 + \frac{28}{45} \pi^2 + \frac{7}{15} \pi^2 \beta_0 \right) \\ &+ C_A \left. \left(\frac{77}{384} \zeta_3 - \frac{64097}{129600} - \frac{269}{75} \beta_0 + \frac{2}{15} \ln(-4z - i0) - \frac{31}{180} \ln(-4z - i0) \beta_0 \right) \right] \\ &+ z^2 \left[C_A^2 \left(\frac{110251}{9216} \zeta_3 - \frac{3084463261}{254016000} - \frac{2869}{4536} \ln(-4z - i0) - \frac{1289}{28350} \pi^2 \right) \right. \end{aligned}$$

$$\begin{aligned}
& + C_F C_A \left(\frac{2997917}{23040} \zeta_3 - \frac{55535378557}{381024000} - \frac{18337}{28350} \ln(-4z - i0) - \frac{128447}{113400} \pi^2 + \frac{1714}{1575} \pi^2 \ln 2 \right) \\
& + C_F^2 \left(\frac{36173}{192} \zeta_3 - \frac{95081911}{453600} + \frac{857}{630} \pi^2 - \frac{3428}{1575} \pi^2 \ln 2 \right) \\
& + C_A \left(\frac{265053121}{1524096000} - \frac{16177}{92160} \zeta_3 - \frac{45617}{47250} \beta_0 + \frac{16}{315} \ln(-4z - i0) - \frac{623}{5400} \ln(-4z - i0) \beta_0 \right) \\
& + C_F \left(\frac{21973}{7680} \zeta_3 - \frac{8108339}{1555200} - \frac{509813}{3969000} \beta_0 - \frac{8}{15} \ln(-4z - i0) + \frac{29147}{18900} \ln(-4z - i0) \beta_0 \right. \\
& \left. + \frac{1714}{4725} \pi^2 + \frac{857}{3150} \pi^2 \beta_0 \right) \Big] + \mathcal{O}(z^3). \tag{G.9}
\end{aligned}$$

We can assess the quality of the expansion in z by numerical evaluation,

$$\begin{aligned}
C^H(m_t^2, q^2, q^2) & = \alpha_s(q) F_0(z) \left[1 + 15.9348 \frac{\alpha_s}{4\pi} (1 + 0.0158(8z) + .00098312(8z)^2) \right. \\
& + 97.0371 \left(\frac{\alpha_s}{4\pi} \right)^2 (1 + 0.1883(8z) + 0.0120(8z)^2) \\
& \left. + 143.466 \left(\frac{\alpha_s}{4\pi} \right)^2 \frac{\ln(-8z - i0)}{\pi} (1 + 0.0288(8z) + 0.001462(8z)^2) \right]. \tag{G.10}
\end{aligned}$$

In the vicinity of the Higgs boson pole ($8z \approx 1$) subsequent terms in the z expansion are expected to contribute below the percent level.

G.2 Implementation of the two-step procedure

In the two-step procedure of Refs. [59–62] one first integrates out the top quark at a scale $\mu_t \cong m_t$ and subsequently matches from the QCD effective Lagrangian onto SCET at $\mu_h \cong m_H$. Running between μ_h and μ_t allows one to sum logarithms of m_t/m_H , but one neglects power of m_H/m_t .

G.2.1 $C^t(m_t^2, \mu_t^2)$

For a heavy top quark the effective Lagrangian for the production of a top quark is given by,

$$\mathcal{L}_{\text{eff}} = C^t(m_t^2, \mu_t^2) \frac{H}{v} \frac{\alpha_s(\mu_t^2)}{12\pi} G_{\mu\nu a} G_a^{\mu\nu}, \tag{G.11}$$

where $v \approx 246$ GeV is the Higgs boson vacuum expectation value. The hard matching scale μ_t at which the Wilson coefficient can be computed perturbatively is of order m_t . The short distance coefficient $C^t(m_t^2, \mu^2)$ obeys the RGE,

$$\frac{d}{d \ln \mu} C^t(m_t^2, \mu^2) = \gamma^t(\alpha_s) C^t(m_t^2, \mu^2), \quad \gamma^t(\alpha_s) = \alpha_s^2 \frac{d}{d\alpha_s} \left(\frac{\beta(\alpha_s)}{\alpha_s^2} \right). \tag{G.12}$$

The expressions for the short-distance coefficient $C^t(m_t^2, \mu_t^2)$ at NNLO is,

$$C^t(m_t^2, \mu_t^2) = 1 + \frac{\alpha_s(\mu_t)}{4\pi} C_1^t + \left(\frac{\alpha_s(\mu_t)}{4\pi} \right)^2 C_2^t(m_t^2, \mu_t^2) + \dots, \tag{G.13}$$

where (c.f. Eq. (12) of Ref. [61]),

$$C_1^t = 5C_A - 3C_F$$

$$\begin{aligned}
C_2^t(m_t^2, \mu_t^2) &= \frac{27}{2}C_F^2 + \left(11 \ln \frac{m_t^2}{\mu_t^2} - \frac{100}{3}\right) C_F C_A - \left(7 \ln \frac{m_t^2}{\mu_t^2} - \frac{1063}{36}\right) C_A^2 \\
&\quad - \frac{4}{3}C_F T_F - \frac{5}{6}C_A T_F - \left(8 \ln \frac{m_t^2}{\mu_t^2} + 5\right) C_F T_F n_f - \frac{47}{9}C_A T_F n_f. \quad (\text{G.14})
\end{aligned}$$

The evolution of these coefficients to the resummation scale μ is described in Appendix A of Ref. [3]. The solution to the evolution equation Eq. (G.12) for C^t at scale μ is,

$$C^t(m_t^2, \mu^2) = \frac{\beta(\alpha_s(\mu))}{\alpha_s^2(\mu)} \frac{\alpha_s^2(\mu_t)}{\beta(\alpha_s(\mu_t))} C^t(m_t^2, \mu_t^2). \quad (\text{G.15})$$

The result at NNLO for the square of the coefficient function is,

$$\begin{aligned}
[C^t(m_t^2, \mu^2)]^2 &= 1 + \left(\frac{\alpha_s}{4\pi}\right) \left[2C_1^t + 2(r_t - 1)\frac{\beta_1}{\beta_0}\right] \\
&\quad + \left(\frac{\alpha_s}{4\pi}\right)^2 \left[(C_1^t)^2 + 2C_2^t(m_t^2, \mu_t^2) + \frac{(2\beta_2\beta_0 + \beta_1^2)}{\beta_0^2}(r_t - 1)^2\right. \\
&\quad \left.+ 2\frac{(2\beta_2\beta_0 + 2\beta_1\beta_0 C_1^t - \beta_1^2)}{\beta_0^2}(r_t - 1)\right], \quad (\text{G.16})
\end{aligned}$$

where $r_t = \alpha_s(\mu)/\alpha_s(\mu_t)$. This extends the NLO result in Eq. (2) of Ref. [3].

G.2.2 $C^S(-q^2, \mu_h)$

C^S is the Wilson coefficient matching the two gluon operator in Eq. (G.11) to an operator in SCET in which all the hard modes have been integrated out. The result for the matching coefficient C^S from Eqs.(16) and (17) of Ref. [61]. It is given by,

$$C^S(-q^2, \mu_h^2) = 1 + \sum_{n=1}^{\infty} C_n^S(L) \left(\frac{\alpha_s(\mu_h^2)}{4\pi}\right)^n. \quad (\text{G.17})$$

The coefficient C^S obeys the renormalization equation,

$$\frac{d}{d \ln \mu} C^S(-q^2 - i\epsilon, \mu^2) = \left[\Gamma_{\text{cusp}}^A(\alpha_s) \ln \frac{-q^2 - i\epsilon}{\mu^2} + \gamma^S(\alpha_s) \right] C^S(-q^2 - i\epsilon, \mu^2), \quad (\text{G.18})$$

with $L = \ln(-q^2 - i0)/\mu_h^2$ and γ^S is given in Eq (B.20).

The logarithmic terms are determined by Eq. (G.18). The full results for the one- and two-loop coefficients are,

$$\begin{aligned}
C_1^S &= C_A \left(-L^2 + \frac{\pi^2}{6} \right), \quad (\text{G.19}) \\
C_2^S &= C_A^2 \left[\frac{L^4}{2} + \frac{11}{9} L^3 + \left(-\frac{67}{9} + \frac{\pi^2}{6} \right) L^2 + \left(\frac{80}{27} - \frac{11\pi^2}{9} - 2\zeta_3 \right) L \right. \\
&\quad \left. + \frac{5105}{162} + \frac{67\pi^2}{36} + \frac{\pi^4}{72} - \frac{143}{9} \zeta_3 \right] + C_F T_F n_f \left(4L - \frac{67}{3} + 16\zeta_3 \right)
\end{aligned}$$

$$+ C_{AT_F n_f} \left[-\frac{4}{9} L^3 + \frac{20}{9} L^2 + \left(\frac{104}{27} + \frac{4\pi^2}{9} \right) L - \frac{1832}{81} - \frac{5\pi^2}{9} - \frac{92}{9} \zeta_3 \right]. \quad (\text{G.20})$$

The full result for the renormalization group invariant hard function in the two-step scheme is,

$$\begin{aligned} \bar{H}(m_t, m_H, p_T^{\text{veto}}) &= \left(\frac{\alpha_s(\mu)}{\alpha_s(p_T^{\text{veto}})} \right)^2 (C^t(m_t^2, \mu))^2 |C^S(-m_H^2, \mu)|^2 \\ &\times \left(\frac{m_H}{p_T^{\text{veto}}} \right)^{-2F_{gg}(p_T^{\text{veto}}, \mu)} e^{2h^A(p_T^{\text{veto}}, \mu)}. \end{aligned} \quad (\text{G.21})$$

The μ -independence of this hard function can be used to constrain γ^S ,

$$\frac{d}{d \ln \mu} \bar{H}(m_t, m_H, p_T^{\text{veto}}) = 0. \quad (\text{G.22})$$

Using Eqs. (B.1, G.12, G.18, 2.13, C.1) we can derive the relation between the collinear anomalous dimensions,

$$2\gamma^g(\alpha_s) = \gamma^t(\alpha_s) + \gamma^S(\alpha_s) + \beta(\alpha_s)/\alpha_s. \quad (\text{G.23})$$

This relation could be cast in a more transparent form by noting that the quantity $(\alpha_s C^S)$ obeys a similar evolution equation to Eq. (G.18),

$$\begin{aligned} &\frac{d}{d \ln \mu} [\alpha_s(\mu) C^S(-m_H^2 - i\epsilon, \mu^2)] = \\ &\alpha_s(\mu) \left[\Gamma_{\text{cusp}}^A(\alpha_s) \ln \frac{-m_H^2 - i\epsilon}{\mu^2} + \gamma^S(\alpha_s) \right] C^S(-m_H^2 - i\epsilon, \mu^2) + \beta(\alpha_s) C^S(-m_H^2 - i\epsilon, \mu^2) \\ &= \left[\Gamma_{\text{cusp}}^A(\alpha_s) \ln \frac{-m_H^2 - i\epsilon}{\mu^2} + \gamma^{S'}(\alpha_s) \right] [\alpha_s(\mu) C^S(-m_H^2 - i\epsilon, \mu^2)], \end{aligned} \quad (\text{G.24})$$

but with anomalous dimension $\gamma^{S'}(\alpha_s) = \gamma^S(\alpha_s) + \beta(\alpha_s)/\alpha_s$. We then have the relation $2\gamma^g(\alpha_s) = \gamma^t(\alpha_s) + \gamma^{S'}(\alpha_s)$. This indicates that after the second matching, the evolution down to a lower scale satisfies the same renormalization equation in both the one-step and the two-step schemes.

G.3 Assessment of the two schemes for the Higgs hard function

The two schemes for the calculation of the hard function have application in jet veto resummation but also in the resummation of the Higgs boson transverse momentum. A complete discussion of the error budget for Higgs boson production including scale dependence, parton distribution dependence, the influence of loops of b -quarks and electroweak corrections is beyond the scope of this paper. Here we shall simply compare and contrast the one-step and the two-step scheme, in the Higgs on shell region where $m_H^2 \approx m_t^2/2$.

It is easy to check the internal consistency of the two schemes in the limit where we drop terms of order $q^2/(4m_t^2)$. Setting $z = 0$ in Eq. (G.2) and evaluating all coefficient functions at

a common scale μ , we have that,

$$\alpha_s(\mu) C^t(m_t^2, \mu^2) C^S(-q^2, \mu^2) = C^H(m_t^2, q^2, \mu^2)_{z=0} + O(\alpha_s^4). \quad (\text{G.25})$$

We can test this equivalence numerically. We start by fixing $\mu^2 = q^2$ and consider the quantities that enter the calculation of the cross-section, i.e. the square of the absolute values. In the two-step scheme we have,

$$\begin{aligned} |C^t(m_t^2, q^2)|^2 &= 1 + 0.1957 + 0.0204, \\ |C^S(-q^2, q^2)|^2 &= 1 + 0.6146 + 0.2155, \end{aligned} \quad (\text{G.26})$$

where the second and third terms represent the $\mathcal{O}(\alpha_s)$ and $\mathcal{O}(\alpha_s^2)$ terms respectively, evaluated using $\alpha_s(q^2) = 0.1118$. In the one-step case we get,

$$|C^H_{z=0}(m_t^2, q^2, q^2)/\alpha_s(q)|^2 = 1 + 0.8104 + 0.3563. \quad (\text{G.27})$$

Performing a strict fixed-order truncation of the product of the two-step result we have,

$$[|C^t(m_t^2, q^2)|^2 |C^S(-q^2, q^2)|^2]_{\text{expanded}} = 1 + 0.8104 + 0.3563, \quad (\text{G.28})$$

which is in perfect agreement with the one-step case. This indicates that the numerical implementation of the two procedures is correct. If we instead evaluate the product after the individual expansions have been performed, a choice of equal formal accuracy, we have,

$$|C^t(m_t^2, q^2)|^2_{\text{expanded}} |C^S(-q^2, q^2)|^2_{\text{expanded}} = 1 + 0.9306 + 0.2953. \quad (\text{G.29})$$

This results in a significant difference. We therefore work with with the strict fixed-order truncation throughout this paper.

We now restore the z -dependence in F_1^H and F_2^H in Eq. (G.2), but still keep $z = 0$ in the overall factor $F_0^H(z)$. We then find that the ratio of the one-step to the two-step becomes 1.0028 at NLO and 1.0053 at NNLO, i.e. these corrections are very small. Now we allow the matching scale for the top quark, μ_t to take its natural value, $\mu_t = m_t$ and find one/two-step ratios of 1.0054 at NLO and 1.0073 at NNLO, again a small effect. Finally, we reinstate the hard evolution down to the resummation scale and find that the ratio of the one-step to the two-step (at $p_T^{\text{veto}} = 25$ GeV) is 1.0177 at NLO and 1.0125 at NNLO. The cumulative effect at this point is noticeable but still small. However, we note that we have so far kept $z = 0$ in the overall factor $F_0^H(z)$. The one-step procedure is recovered by re-instating $F_0^H(z)$. This implies that, in order to obtain the level of agreement quoted above between the two schemes, the overall factor of $F_0^H(z)$ must also be applied to give a modified version of the two-step scheme. Neglecting this step would result in a significant difference, since $|F_0^H(z)|^2 = 1.0653$ see Eq.(G.5).

Our overall conclusion on the two schemes is in line with the known result that Higgs boson production has substantial corrections. Accounting for the most important mass effects by

rescaling the two-step result by the exact result at leading order, the one-step procedure gives a larger result than the two-step procedure for $p_T^{\text{veto}} = 25$ GeV at the level of 1.3%. Any substantial difference between the two methods beyond this level is most likely due to uncontrolled higher order effects.

References

- [1] C.F. Berger, C. Marcantonini, I.W. Stewart, F.J. Tackmann and W.J. Waalewijn, *Higgs Production with a Central Jet Veto at NNLL+NNLO*, *JHEP* **04** (2011) 092 [[1012.4480](#)].
- [2] I.W. Stewart, F.J. Tackmann and W.J. Waalewijn, *N-Jettiness: An Inclusive Event Shape to Veto Jets*, *Phys. Rev. Lett.* **105** (2010) 092002 [[1004.2489](#)].
- [3] T. Becher and M. Neubert, *Factorization and NNLL Resummation for Higgs Production with a Jet Veto*, *JHEP* **07** (2012) 108 [[1205.3806](#)].
- [4] A. Banfi, G.P. Salam and G. Zanderighi, *NLL+NNLO predictions for jet-veto efficiencies in Higgs-boson and Drell-Yan production*, *JHEP* **06** (2012) 159 [[1203.5773](#)].
- [5] A. Banfi, P.F. Monni, G.P. Salam and G. Zanderighi, *Higgs and Z-boson production with a jet veto*, *Phys. Rev. Lett.* **109** (2012) 202001 [[1206.4998](#)].
- [6] S. Kallweit, E. Re, L. Rottoli and M. Wiesemann, *Accurate single- and double-differential resummation of colour-singlet processes with MATRIX+RADISH: W^+W^- production at the LHC*, *JHEP* **12** (2020) 147 [[2004.07720](#)].
- [7] E. Re, L. Rottoli and P. Torrielli, *Fiducial Higgs and Drell-Yan distributions at $N^3LL'+NNLO$ with RadISH*, [2104.07509](#).
- [8] T. Becher, R. Frederix, M. Neubert and L. Rothen, *Automated NNLL + NLO resummation for jet-veto cross sections*, *Eur. Phys. J. C* **75** (2015) 154 [[1412.8408](#)].
- [9] A. Banfi, P.F. Monni, G.P. Salam and G. Zanderighi, “JetVHeto.” <https://jetvheto.hepforge.org/>, 2016.
- [10] L. Arpino, A. Banfi, S. Jäger and N. Kauer, “MCFM-RE.” <https://github.com/lcarpino/MCFM-RE>, 2019.
- [11] L.R. Stefan Kallweit, Emanuele Re and M. Wiesemann, “MCFM-RE.” <https://matrix.hepforge.org/matrix+radish.html>, 2020.
- [12] T. Becher, M. Neubert and L. Rothen, *Factorization and N^3LL_p+NNLO predictions for the Higgs cross section with a jet veto*, *JHEP* **10** (2013) 125 [[1307.0025](#)].
- [13] I.W. Stewart, F.J. Tackmann, J.R. Walsh and S. Zuberi, *Jet p_T resummation in Higgs production at NNLL' + NNLO*, *Phys. Rev. D* **89** (2014) 054001 [[1307.1808](#)].
- [14] A. Banfi, F. Caola, F.A. Dreyer, P.F. Monni, G.P. Salam, G. Zanderighi et al., *Jet-vetoed Higgs cross section in gluon fusion at $N^3LO+NNLL$ with small- R resummation*, *JHEP* **04** (2016) 049 [[1511.02886](#)].
- [15] S. Dawson, P. Jaiswal, Y. Li, H. Ramani and M. Zeng, *Resummation of jet veto logarithms at $N^3LL_a + NNLO$ for W^+W^- production at the LHC*, *Phys. Rev. D* **94** (2016) 114014 [[1606.01034](#)].
- [16] L. Arpino, A. Banfi, S. Jäger and N. Kauer, *BSM WW production with a jet veto*, *JHEP* **08** (2019) 076 [[1905.06646](#)].

- [17] Y. Wang, C.S. Li and Z.L. Liu, *Resummation prediction on gauge boson pair production with a jet veto*, *Phys. Rev. D* **93** (2016) 094020 [[1504.00509](#)].
- [18] G.P. Salam, *Towards Jetography*, *Eur. Phys. J. C* **67** (2010) 637 [[0906.1833](#)].
- [19] M. Cacciari, G.P. Salam and G. Soyez, *The anti- k_t jet clustering algorithm*, *JHEP* **04** (2008) 063 [[0802.1189](#)].
- [20] Y.L. Dokshitzer, G.D. Leder, S. Moretti and B.R. Webber, *Better jet clustering algorithms*, *JHEP* **08** (1997) 001 [[hep-ph/9707323](#)].
- [21] M. Wobisch and T. Wengler, *Hadronization corrections to jet cross-sections in deep inelastic scattering*, in *Workshop on Monte Carlo Generators for HERA Physics (Plenary Starting Meeting)*, pp. 270–279, 4, 1998 [[hep-ph/9907280](#)].
- [22] S. Catani, Y.L. Dokshitzer, M.H. Seymour and B.R. Webber, *Longitudinally invariant K_t clustering algorithms for hadron hadron collisions*, *Nucl. Phys. B* **406** (1993) 187.
- [23] S.D. Ellis and D.E. Soper, *Successive combination jet algorithm for hadron collisions*, *Phys. Rev. D* **48** (1993) 3160 [[hep-ph/9305266](#)].
- [24] S. Abreu, J.R. Gaunt, P.F. Monni, L. Rottoli and R. Szafron, *Quark and gluon two-loop beam functions for leading-jet p_T and slicing at NNLO*, [2207.07037](#).
- [25] S. Abreu, J.R. Gaunt, P.F. Monni and R. Szafron, *The analytic two-loop soft function for leading-jet p_T* , [2204.02987](#).
- [26] T. Becher, M. Neubert and B.D. Pecjak, *Factorization and Momentum-Space Resummation in Deep-Inelastic Scattering*, *JHEP* **01** (2007) 076 [[hep-ph/0607228](#)].
- [27] Y. Li, D. Neill and H.X. Zhu, *An exponential regulator for rapidity divergences*, *Nucl. Phys. B* **960** (2020) 115193 [[1604.00392](#)].
- [28] A.A. Vladimirov, *Correspondence between Soft and Rapidity Anomalous Dimensions*, *Phys. Rev. Lett.* **118** (2017) 062001 [[1610.05791](#)].
- [29] Y. Li and H.X. Zhu, *Bootstrapping Rapidity Anomalous Dimensions for Transverse-Momentum Resummation*, *Phys. Rev. Lett.* **118** (2017) 022004 [[1604.01404](#)].
- [30] G. Billis, M.A. Ebert, J.K.L. Michel and F.J. Tackmann, *A toolbox for q_T and 0-jettiness subtractions at N^3LO* , *Eur. Phys. J. Plus* **136** (2021) 214 [[1909.00811](#)].
- [31] T. Becher and T. Neumann, *Fiducial q_T resummation of color-singlet processes at $N^3LL+NNLO$* , *JHEP* **03** (2021) 199 [[2009.11437](#)].
- [32] J.-Y. Chiu, A. Jain, D. Neill and I.Z. Rothstein, *A Formalism for the Systematic Treatment of Rapidity Logarithms in Quantum Field Theory*, *JHEP* **05** (2012) 084 [[1202.0814](#)].
- [33] J.-y. Chiu, A. Jain, D. Neill and I.Z. Rothstein, *The Rapidity Renormalization Group*, *Phys. Rev. Lett.* **108** (2012) 151601 [[1104.0881](#)].
- [34] S. Alioli and J.R. Walsh, *Jet Veto Clustering Logarithms Beyond Leading Order*, *JHEP* **03** (2014) 119 [[1311.5234](#)].
- [35] M. Dasgupta, F. Dreyer, G.P. Salam and G. Soyez, *Small-radius jets to all orders in QCD*, *JHEP* **04** (2015) 039 [[1411.5182](#)].
- [36] NNPDF collaboration, *Parton distributions from high-precision collider data*, *Eur. Phys. J. C* **77** (2017) 663 [[1706.00428](#)].
- [37] A. Banfi, P.F. Monni and G. Zanderighi, *Quark masses in Higgs production with a jet veto*, *JHEP* **01** (2014) 097 [[1308.4634](#)].

- [38] CMS collaboration, *Measurement of differential cross sections for the production of a Z boson in association with jets in proton-proton collisions at $\sqrt{s} = 13$ TeV*, [2205.02872](#).
- [39] CMS collaboration, *W^+W^- boson pair production in proton-proton collisions at $\sqrt{s} = 13$ TeV*, *Phys. Rev. D* **102** (2020) 092001 [[2009.00119](#)].
- [40] CMS collaboration, *Measurements of $pp \rightarrow ZZ$ production cross sections and constraints on anomalous triple gauge couplings at $\sqrt{s} = 13$ TeV*, *Eur. Phys. J. C* **81** (2021) 200 [[2009.01186](#)].
- [41] P. Jaiswal and T. Okui, *Reemergence of rapidity-scale uncertainty in soft-collinear effective theory*, *Phys. Rev. D* **92** (2015) 074035 [[1506.07529](#)].
- [42] J.K.L. Michel, P. Pietrulewicz and F.J. Tackmann, *Jet Veto Resummation with Jet Rapidity Cuts*, *JHEP* **04** (2019) 142 [[1810.12911](#)].
- [43] ATLAS collaboration, *Measurement of differential cross sections and W^+/W^- cross-section ratios for W boson production in association with jets at $\sqrt{s} = 8$ TeV with the ATLAS detector*, *JHEP* **05** (2018) 077 [[1711.03296](#)].
- [44] ATLAS collaboration, *Measurement of $W^\pm Z$ production cross sections and gauge boson polarisation in pp collisions at $\sqrt{s} = 13$ TeV with the ATLAS detector*, *Eur. Phys. J. C* **79** (2019) 535 [[1902.05759](#)].
- [45] CMS collaboration, *Measurement of the inclusive and differential WZ production cross sections, polarization angles, and triple gauge couplings in pp collisions at $\sqrt{s} = 13$ TeV*, *JHEP* **07** (2022) 032 [[2110.11231](#)].
- [46] A. Banfi, G.P. Salam and G. Zanderighi, *Principles of general final-state resummation and automated implementation*, *JHEP* **03** (2005) 073 [[hep-ph/0407286](#)].
- [47] P.F. Monni, L. Rottoli and P. Torrielli, *Higgs transverse momentum with a jet veto: a double-differential resummation*, *Phys. Rev. Lett.* **124** (2020) 252001 [[1909.04704](#)].
- [48] W. Bizon, P.F. Monni, E. Re, L. Rottoli and P. Torrielli, *Momentum-space resummation for transverse observables and the Higgs p_\perp at $N^3LL+NNLO$* , *JHEP* **02** (2018) 108 [[1705.09127](#)].
- [49] P.F. Monni, E. Re and P. Torrielli, *Higgs Transverse-Momentum Resummation in Direct Space*, *Phys. Rev. Lett.* **116** (2016) 242001 [[1604.02191](#)].
- [50] T. Becher, M. Neubert and D. Wilhelm, *Electroweak Gauge-Boson Production at Small q_T : Infrared Safety from the Collinear Anomaly*, *JHEP* **02** (2012) 124 [[1109.6027](#)].
- [51] V. Ahrens, T. Becher, M. Neubert and L.L. Yang, *Origin of the Large Perturbative Corrections to Higgs Production at Hadron Colliders*, *Phys. Rev. D* **79** (2009) 033013 [[0808.3008](#)].
- [52] ATLAS collaboration, *Measurement of the W^+W^- production cross section in pp collisions at a centre-of-mass energy of $\sqrt{s} = 13$ TeV with the ATLAS experiment*, *Phys. Lett. B* **773** (2017) 354 [[1702.04519](#)].
- [53] ATLAS collaboration, *Measurement of fiducial and differential W^+W^- production cross-sections at $\sqrt{s} = 13$ TeV with the ATLAS detector*, *Eur. Phys. J. C* **79** (2019) 884 [[1905.04242](#)].
- [54] CMS collaboration, *Search for anomalous triple gauge couplings in WW and WZ production in lepton + jet events in proton-proton collisions at $\sqrt{s} = 13$ TeV*, *JHEP* **12** (2019) 062 [[1907.08354](#)].
- [55] J.M. Campbell, R.K. Ellis, T. Neumann and S. Seth, *Transverse momentum resummation at $N^3LL+NNLO$ for diboson processes*, [2210.10724](#).
- [56] R. Bonciani, V. Del Duca, H. Frellesvig, M. Hidding, V. Hirschi, F. Moriello et al.,

Next-to-leading-order QCD Corrections to Higgs Production in association with a Jet, [2206.10490](#).

- [57] M. Czakon, R.V. Harlander, J. Klappert and M. Niggetiedt, *Exact Top-Quark Mass Dependence in Hadronic Higgs Production*, *Phys. Rev. Lett.* **127** (2021) 162002 [[2105.04436](#)].
- [58] T. Neumann and M. Wiesemann, *Finite top-mass effects in gluon-induced Higgs production with a jet-veto at NNLO*, *JHEP* **11** (2014) 150 [[1408.6836](#)].
- [59] A. Idilbi, X.-d. Ji and F. Yuan, *Transverse momentum distribution through soft-gluon resummation in effective field theory*, *Phys. Lett. B* **625** (2005) 253 [[hep-ph/0507196](#)].
- [60] A. Idilbi, X.-d. Ji, J.-P. Ma and F. Yuan, *Threshold resummation for Higgs production in effective field theory*, *Phys. Rev. D* **73** (2006) 077501 [[hep-ph/0509294](#)].
- [61] V. Ahrens, T. Becher, M. Neubert and L.L. Yang, *Renormalization-Group Improved Prediction for Higgs Production at Hadron Colliders*, *Eur. Phys. J. C* **62** (2009) 333 [[0809.4283](#)].
- [62] S. Mantry and F. Petriello, *Factorization and Resummation of Higgs Boson Differential Distributions in Soft-Collinear Effective Theory*, *Phys. Rev. D* **81** (2010) 093007 [[0911.4135](#)].
- [63] G. Bell, K. Brune, G. Das and M. Wald, *The NNLO quark beam function for jet-veto resummation*, [2207.05578](#).
- [64] M.-X. Luo, X. Wang, X. Xu, L.L. Yang, T.-Z. Yang and H.X. Zhu, *Transverse Parton Distribution and Fragmentation Functions at NNLO: the Quark Case*, *JHEP* **10** (2019) 083 [[1908.03831](#)].
- [65] M.-X. Luo, T.-Z. Yang, H.X. Zhu and Y.J. Zhu, *Transverse Parton Distribution and Fragmentation Functions at NNLO: the Gluon Case*, *JHEP* **01** (2020) 040 [[1909.13820](#)].
- [66] T. Becher and M. Neubert, *Drell-Yan Production at Small q_T , Transverse Parton Distributions and the Collinear Anomaly*, *Eur. Phys. J. C* **71** (2011) 1665 [[1007.4005](#)].
- [67] O.V. Tarasov, A.A. Vladimirov and A.Y. Zharkov, *The Gell-Mann-Low Function of QCD in the Three Loop Approximation*, *Phys. Lett. B* **93** (1980) 429.
- [68] S.A. Larin and J.A.M. Vermaseren, *The Three loop QCD Beta function and anomalous dimensions*, *Phys. Lett. B* **303** (1993) 334 [[hep-ph/9302208](#)].
- [69] T. van Ritbergen, J.A.M. Vermaseren and S.A. Larin, *The Four loop beta function in quantum chromodynamics*, *Phys. Lett. B* **400** (1997) 379 [[hep-ph/9701390](#)].
- [70] T. van Ritbergen, A.N. Schellekens and J.A.M. Vermaseren, *Group theory factors for Feynman diagrams*, *Int. J. Mod. Phys. A* **14** (1999) 41 [[hep-ph/9802376](#)].
- [71] J.M. Henn, G.P. Korchemsky and B. Mistlberger, *The full four-loop cusp anomalous dimension in $\mathcal{N} = 4$ super Yang-Mills and QCD*, *JHEP* **04** (2020) 018 [[1911.10174](#)].
- [72] A. von Manteuffel, E. Panzer and R.M. Schabinger, *Cusp and collinear anomalous dimensions in four-loop QCD from form factors*, *Phys. Rev. Lett.* **124** (2020) 162001 [[2002.04617](#)].
- [73] T. Becher, A. Broggio and A. Ferroglia, *Introduction to Soft-Collinear Effective Theory*, vol. 896, Springer (2015), [10.1007/978-3-319-14848-9](#), [[1410.1892](#)].
- [74] T. Becher and M. Neubert, *On the Structure of Infrared Singularities of Gauge-Theory Amplitudes*, *JHEP* **06** (2009) 081 [[0903.1126](#)].
- [75] G. Altarelli and G. Parisi, *Asymptotic Freedom in Parton Language*, *Nucl. Phys. B* **126** (1977) 298.

- [76] G. Curci, W. Furmanski and R. Petronzio, *Evolution of Parton Densities Beyond Leading Order: The Nonsinglet Case*, *Nucl. Phys. B* **175** (1980) 27.
- [77] W. Furmanski and R. Petronzio, *Singlet Parton Densities Beyond Leading Order*, *Phys. Lett. B* **97** (1980) 437.
- [78] R.K. Ellis, W.J. Stirling and B.R. Webber, *QCD and collider physics*, vol. 8, Cambridge University Press (2, 2011), [10.1017/CBO9780511628788](https://doi.org/10.1017/CBO9780511628788).
- [79] G. Kramer and B. Lampe, *Two Jet Cross-Section in $e^+ e^-$ Annihilation*, *Z. Phys. C* **34** (1987) 497.
- [80] T. Matsuura and W.L. van Neerven, *Second Order Logarithmic Corrections to the Drell-Yan Cross-section*, *Z. Phys. C* **38** (1988) 623.
- [81] T. Matsuura, S.C. van der Marck and W.L. van Neerven, *The Calculation of the Second Order Soft and Virtual Contributions to the Drell-Yan Cross-Section*, *Nucl. Phys. B* **319** (1989) 570.
- [82] S. Moch, J.A.M. Vermaseren and A. Vogt, *Three-loop results for quark and gluon form-factors*, *Phys. Lett. B* **625** (2005) 245 [[hep-ph/0508055](https://arxiv.org/abs/hep-ph/0508055)].
- [83] S. Moch, J.A.M. Vermaseren and A. Vogt, *The Quark form-factor at higher orders*, *JHEP* **08** (2005) 049 [[hep-ph/0507039](https://arxiv.org/abs/hep-ph/0507039)].
- [84] T. Gehrmann, E.W.N. Glover, T. Huber, N. Ikizlerli and C. Studerus, *Calculation of the quark and gluon form factors to three loops in QCD*, *JHEP* **06** (2010) 094 [[1004.3653](https://arxiv.org/abs/1004.3653)].
- [85] A. Idilbi and X.-d. Ji, *Threshold resummation for Drell-Yan process in soft-collinear effective theory*, *Phys. Rev. D* **72** (2005) 054016 [[hep-ph/0501006](https://arxiv.org/abs/hep-ph/0501006)].
- [86] A. Idilbi, X.-d. Ji and F. Yuan, *Resummation of threshold logarithms in effective field theory for DIS, Drell-Yan and Higgs production*, *Nucl. Phys. B* **753** (2006) 42 [[hep-ph/0605068](https://arxiv.org/abs/hep-ph/0605068)].
- [87] J.M. Campbell, R.K. Ellis and S. Seth, *Non-local slicing approaches for NNLO QCD in MCFM*, *JHEP* **06** (2022) 002 [[2202.07738](https://arxiv.org/abs/2202.07738)].
- [88] J. Davies, F. Herren and M. Steinhauser, *Top Quark Mass Effects in Higgs Boson Production at Four-Loop Order: Virtual Corrections*, *Phys. Rev. Lett.* **124** (2020) 112002 [[1911.10214](https://arxiv.org/abs/1911.10214)].
- [89] M. Spira, A. Djouadi, D. Graudenz and P.M. Zerwas, *Higgs boson production at the LHC*, *Nucl. Phys. B* **453** (1995) 17 [[hep-ph/9504378](https://arxiv.org/abs/hep-ph/9504378)].
- [90] R. Harlander and P. Kant, *Higgs production and decay: Analytic results at next-to-leading order QCD*, *JHEP* **12** (2005) 015 [[hep-ph/0509189](https://arxiv.org/abs/hep-ph/0509189)].
- [91] C. Anastasiou, S. Beerli, S. Bucherer, A. Daleo and Z. Kunszt, *Two-loop amplitudes and master integrals for the production of a Higgs boson via a massive quark and a scalar-quark loop*, *JHEP* **01** (2007) 082 [[hep-ph/0611236](https://arxiv.org/abs/hep-ph/0611236)].
- [92] R.V. Harlander and K.J. Ozeren, *Top mass effects in Higgs production at next-to-next-to-leading order QCD: Virtual corrections*, *Phys. Lett. B* **679** (2009) 467 [[0907.2997](https://arxiv.org/abs/0907.2997)].
- [93] A. Pak, M. Rogal and M. Steinhauser, *Virtual three-loop corrections to Higgs boson production in gluon fusion for finite top quark mass*, *Phys. Lett. B* **679** (2009) 473 [[0907.2998](https://arxiv.org/abs/0907.2998)].